

R-0 7/77 3/76
11-13-77
2/78
5-78
CR 135009
6-78
8-78



QUIET CLEAN SHORT-HAUL EXPERIMENTAL ENGINE (QCSEE)

The Aerodynamic and Mechanical Design of
the QCSEE Under-the-Wing Fan

MARCH, 1977

BY:

GENERAL ELECTRIC COMPANY
AIRCRAFT ENGINE GROUP
ADVANCED ENGRG. AND TECH. PROGRAMS DEPT.
CINCINNATI, OHIO 45215

(NASA-CR-135009) QUIET CLEAN SHORT-HAUL
EXPERIMENTAL ENGINE (QCSEE): THE
AERODYNAMIC AND MECHANICAL DESIGN OF THE
QCSEE UNDER-THE-WING FAN (General Electric
Co.) 144 p HC A07/MF A01 CACL 21E G3/07

N80-15109

Unclas
33491

PREPARED FOR:

NATIONAL AERONAUTICS AND SPACE ADMINISTRATION
LEWIS RESEARCH CENTER

CONTRACT NAS3-18021

1. Report No. NASA CR-135009		2. Government Accession No.		3. Recipient's Catalog No.	
4. Title and Subtitle QUIET CLEAN SHORT-HAUL EXPERIMENTAL ENGINE (QCSEE) AERODYNAMIC AND MECHANICAL DESIGN OF THE QCSEE UNDER-THE-WING FAN				5. Report Date March, 1977	
				6. Performing Organization Code	
7. Author(s) Advanced Engineering & Technology Programs Department Group Engineering Division				8. Performing Organization Report No. R75AEG484	
				10. Work Unit No.	
9. Performing Organization Name and Address General Electric Company Aircraft Engine Group 1 Jimson Road Cincinnati, Ohio 45215				11. Contract or Grant No. NAS3-18021	
				13. Type of Report and Period Covered Contractor Report	
12. Sponsoring Agency Name and Address National Aeronautics & Space Administration Washington, D.C. 20546				14. Sponsoring Agency Code	
15. Supplementary Notes Design Report, Project Manager, C.C. Ciepluch, QCSEE Project Office Technical Adviser, D.C. Reemsnyder NASA-Lewis Research Center, Cleveland, Ohio 44135					
16. Abstract The QCSEE Program provides for the design, fabrication, and testing of two experimental high-bypass geared turbofan engines and propulsion systems for short-haul passenger aircraft. This report covers the aerodynamic and mechanical design of a variable-pitch 1.34 pressure ratio fan for the under-the-wing (UTW) engine. The UTW fan was designed to permit rotation of the 18 composite fan blades into the reverse thrust mode of operation through both flat pitch and stall pitch directions.					
17. Key Words (Suggested by Author(s)) Aerodynamics Aircraft Propulsion and Power High-Bypass Fan					
18. Security Classif. (of this report) Unclassified		20. Security Classif. (of this report) Unclassified		22. PRICE 137	

TABLE OF CONTENTS

<u>Section</u>	<u>Page</u>
1.0 UTW FAN DESIGN	1
1.1 Summary	1
2.0 UTW FAN AERODYNAMIC DESIGN	2
2.1 Operating Requirements	2
2.2 Basic Design Features	2
2.3 Reverse Flow	5
2.4 Performance Representation with Variable Pitch	8
2.5 Detailed Configuration Design	8
2.6 Rotor Blade Design	17
2.7 Core OGV Design	42
2.8 Transition Duct Strut Design	42
2.9 Vane-Frame (Fan Bypass OGV) Design	47
2.10 Fan Performance Based on Scale Model Tests	54
3.0 UTW FAN ROTOR MECHANICAL DESIGN	75
3.1 Fan Rotor Summary	75
3.2 Composite Fan Blades	77
3.2.1 Design Requirements	77
3.2.2 Basic Design Features	78
3.2.3 Design Analysis	95
3.3 Fan Disk	119
3.4 Blade Support Bearing	119
3.5 Blade Trunnion	129
3.6 Fan Spinner	135
3.7 Fan Attachment Hardware	135

PRECEDING PAGE BLANK NOT FILMED

LIST OF ILLUSTRATIONS

<u>Figure</u>		<u>Page</u>
1.	UTW Variable-Pitch Fan Design Requirements.	3
2.	Cross Section of UTW Variable-Pitch Fan.	4
3.	UTW Fan Blade Geometry at Different Pitch Angle Settings.	7
4.	UTW Fan Stage Characteristics at 100% Speed for Various Pitch Settings.	9
5.	Radial Distribution of Rotor Total Pressure Ratio.	11
6.	Radial Distribution of Rotor Efficiency.	12
7.	Radial Distribution of Rotor Diffusion Factor.	13
8.	Radial Distribution of Rotor Relative Mach Numbers.	14
9.	Radial Distribution of Rotor Relative Air Angles.	15
10.	Radial Distribution of Design Parameters for Core OGV.	16
11.	Rotor Incidence, Deviation, and Empirical Adjustment Angles.	32
12.	Rotor Throat Margin Distribution.	33
13.	UTW Fan Rotor Blade Plane Sections.	34
14.	UTW Fan Rotor Camber and Stagger Angle Radial Distributions.	40
15.	UTW Fan Blade Thickness Distributions.	41
16.	Core OGV Aerodynamic Design Characteristics.	43
17.	Core OGV Geometry Parameters.	44
18.	Cylindrical Section of Core OGV at the Pitch Line Radius.	45
19.	Transition Duct Flowpath.	48
20.	Nominal and Modified Transition Duct Strut Cylindrical Sections.	49

LIST OF ILLUSTRATIONS (Cont'd)

<u>Figure</u>		<u>Page</u>
21.	Vane-Frame (Fan Bypass OGV) Aerodynamic Environment.	50
22.	Vane-Frame (Fan Bypass OGV) Diffusion Factor for Nominal Vanes.	52
23.	Vane-Frame (Fan Bypass OGV) Unwrapped Section at ID.	53
24.	Vane-Frame (Fan Bypass OGV) Unwrapped Section at ID - Detail Near Pylon LE Fairing.	55
25.	Vane-Frame (Fan Bypass OGV) Stagger and Camber Distributions.	62
26.	Vane-Frame (Fan Bypass OGV) Solidity and Chord Distributions.	63
27.	UTW Fan Bypass Stream Performance Map at Design Rotor Stagger Setting.	65
28.	UTW Fan Bypass Stream Performance Map at Cruise Rotor Stagger Setting.	66
29.	UTW Fan Bypass Stream Performance Map at Take-off Rotor Stagger Setting.	67
30.	Fan Hub Pressure Ratio Correlation (Forward Mode).	69
31.	Fan Hub Efficiency Correlation (Forward Mode).	70
32.	Reverse Mode Fan Performance.	71
33.	UTW Fan Scale Model Gross Reverse Thrust, Scaled to Engine Size.	72
34.	UTW Fan Reverse Mode Universal Characteristics.	73
35.	UTW Fan Reverse Mode Adiabatic Efficiency.	74
36.	UTW Fan Rotor Configuration.	76
37.	QCSEE UTW Composite Fan Blade and Platform.	79
38.	UTW Composite Fan Blade.	81

LIST OF ILLUSTRATIONS (Cont'd)

<u>Figure</u>		<u>Page</u>
39.	Molded Fan Blade.	82
40.	Blade Airfoil Sections.	83
41.	Radial Sections through the Molded Blade.	85
42.	Ply Lay-up and Material Arrangement.	87
43.	QCSEE UTW Composite Blade.	89
44.	Dovetail Molded Section.	93
45.	Platform Design.	94
46.	UTW Blade Resultant Radial Stress - 3326 rpm.	96
47.	Calculated Blade Radial Stress.	97
48.	Calculated Blade Chordal Stress.	98
49.	Calculated Blade Interlaminar Shear Stress.	99
50.	UTW Blade Displacements and Twist.	100
51.	Calculated Blade Relative Radial Stresses for First Flexural Mode.	101
52.	Calculated Blade Relative Radial Stresses for Second Flexural Mode.	102
53.	Calculated Blade Relative Radial Stresses for First Torsional Mode.	103
54.	Allowable Stress Range Diagram - Blade Radial Stress.	104
55.	Allowable Stress Range Diagram - Blade Radial Stress.	106
56.	Allowable Stress Range Diagram - Dovetail Shear Stress.	107
57.	Platform Cross Section.	108
58.	Limit Cycle Boundaries.	113
59.	Campbell Diagram - UTW Composite Blade.	114

LIST OF ILLUSTRATIONS (Cont'd)

<u>Figure</u>		<u>Page</u>
60.	UTW Blade Transferred Impact Energy for a 1.81-kg (4-1b) Bird.	116
61.	QCSEE Composite Blade Predicted Gross Impact Capability.	117
62.	UTW Blade Impact Momentum for a 0.68-kg (1-1/2-1b) Bird.	118
63.	UTW Fan Rotor.	120
64.	UTW Bearing and Disk Seat.	121
65.	UTW Fan Disk Stresses with Hamilton-Standard Actuator.	123
66.	Blade Thrust Bearing.	124
67.	UTW Mission Duty Cycle.	126
68.	Blade Trunnion.	130
69.	UTW Blade Trunnion Stresses.	131
70.	GE Ball Spline Actuation System.	133
71.	HS Variable Pitch Interface.	134
72.	Fan Flowpath Adapters.	136

LIST OF TABLES

<u>Table</u>		<u>Page</u>
1.	QCSEE UTW Variable-Pitch Fan Design Requirements.	2
2.	Design Blade Element Parameters for QCSEE UTW Fan.	18
3.	UTW Fan Rotor Blade Coordinates.	35
4.	UTW Fan Core OGV Coordinates at the Pitch Line Radius.	46
5.	Vane-Frame (Fan Bypass OGV) Coordinates.	56
6.	QCSEE UTW Composite Fan Blade Design Summary.	80
7.	PR288/AS Prepreg Properties.	90
8.	Composite Material Properties.	91
9.	Platform Stresses and Margins of Safety.	109
10.	Platform Natural Frequencies.	111
11.	UTW Fan Disk Design Data.	122
12.	QCSEE UTW Blade Support Bearing - Operating Conditions of Mission Duty Cycle.	127
13.	QCSEE UTW Blade Support Bearing Design.	128
14.	Trunnion Retainer (Nut).	132
15.	Disk Cone Flange Bolts.	137

SECTION 1.0

UTW FAN DESIGN

1.1 SUMMARY

An under-the-wing (UTW) and an over-the-wing (OTW) fan rotor will be built and tested as part of the NASA QCSEE Program. The UTW fan is a geared variable-pitch design with 18 composite fan blades. This concept, which includes full reverse thrust capability, is expected to offer significant advantages to a high-bypass fan system including:

- Lighter weight through the use of composite fan blades and by eliminating the heavy, large diameter thrust reverser
- Faster thrust response
- Improved off-design SFC
- Reduced off-design noise generation

At the major operating conditions of takeoff and maximum cruise, a corrected flow of 405.5 kg/sec (894 lb/sec) was selected for both fans which enables common inlet hardware to yield the desired 0.79 average throat Mach number at the critical take-off noise measurement condition. The aerodynamic design bypass pressure ratio is 1.34 for the UTW and 1.36 for the OTW which is intermediate between the take-off and maximum cruise power settings. Take-off pressure ratios are 1.27 for the UTW and 1.34 for the OTW. The take-off corrected tip speeds are 289 m/sec (950 ft/sec) for the UTW and 354 m/sec (1162 ft/sec) for the OTW. These pressure ratios and speeds were selected on the basis of minimum noise within the constraints of adequate stall margin and core engine supercharging.

The UTW fan was designed to permit rotation of the blades into the reverse thrust mode of operation through both flat pitch (like a propeller) and the stall pitch directions. The flowpath has been contoured to maintain tight blade tip and hub clearances throughout the blade actuation range.

The vane-frame, which is common to both engines, performs the dual function of an outlet guide vane for the bypass flow and a frame support for the engine components and nacelle. The UTW island configuration was selected specifically for the reverse thrust mode of operation.

Design practices and rotor material selections are consistent with flight-designed fan rotors for both the UTW and OTW. This includes consideration for fan CF life and for such FAA flight requirements as burst speed margin and bird strike capability. All rotor components for the UTW fan rotor are of a flight weight design.

SECTION 2.0

UTW FAN AERODYNAMIC DESIGN

2.1 OPERATING REQUIREMENTS

Major operating requirements for the under-the-wing (UTW) fan (Figure 1) are takeoff, where noise and thrust are of primary importance, and maximum cruise, where economy and thrust are of primary importance. At takeoff a low fan pressure ratio of 1.27 was selected to minimize the velocity of the bypass stream at nozzle exit. A corrected flow of 405.5 kg/sec (894 lbm/sec) at this pressure ratio yields the required engine thrust. The inlet throat is sized at this condition for an average Mach number of 0.79 to minimize the forward propagation of fan noise. This sizing of the inlet throat prohibits higher corrected flow at altitude cruise. Required maximum cruise thrust is obtained by raising the fan pressure ratio to 1.39. The aerodynamic design point was selected at an intermediate condition which is a pressure ratio of 1.34 and a corrected flow of 408 kg/sec (900 lb/sec). Table 1 summarizes the key parameters for these three conditions.

Parameter	Design Point	Takeoff	Maximum Cruise
Total fan flow	408 kg/sec (900 lb/sec)	405.5 kg/sec (894 lb/sec)	405.5 kg/sec (894 lb/sec)
Pressure ratio - bypass flow	1.34	1.27	1.39
Pressure ratio - core flow	1.23	1.20	1.21
Bypass ratio	11.3	11.8	11.4
Pitch setting	Nominal	Open 2°	Closed 2°
Corrected tip speed	306 m/sec (1005 ft/sec)	289 m/sec (950 ft/sec)	324 m/sec (1063 ft/sec)

2.2 BASIC DESIGN FEATURES

A cross section of the selected UTW fan configuration is shown in Figure 2. There are 18 variable-pitch composite rotor blades. The solidity of the blades is 0.95 at the OD and 0.98 at the ID. The chord is linear with radius. This permits rotation of the blades into the reverse thrust mode of operation through both the flat pitch and the stall pitch directions. The spherical casing radius over the rotor tip provides good blade tip clearances throughout the range of blade pitch angle settings. Circumferential grooved casing treatment is incorporated over the rotor tip to improve stall margin. Stall

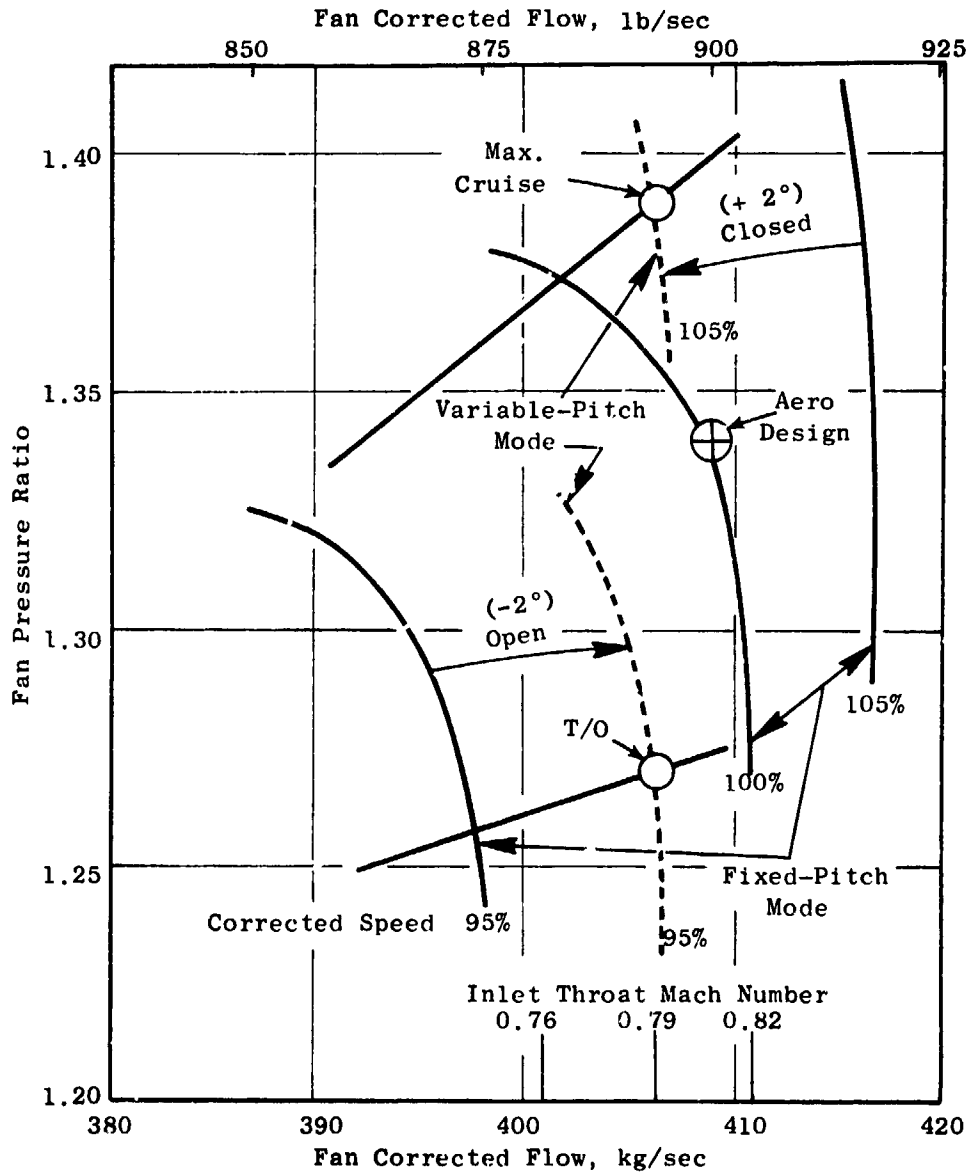


Figure 1. UTW Variable-Pitch Fan Design Requirements.

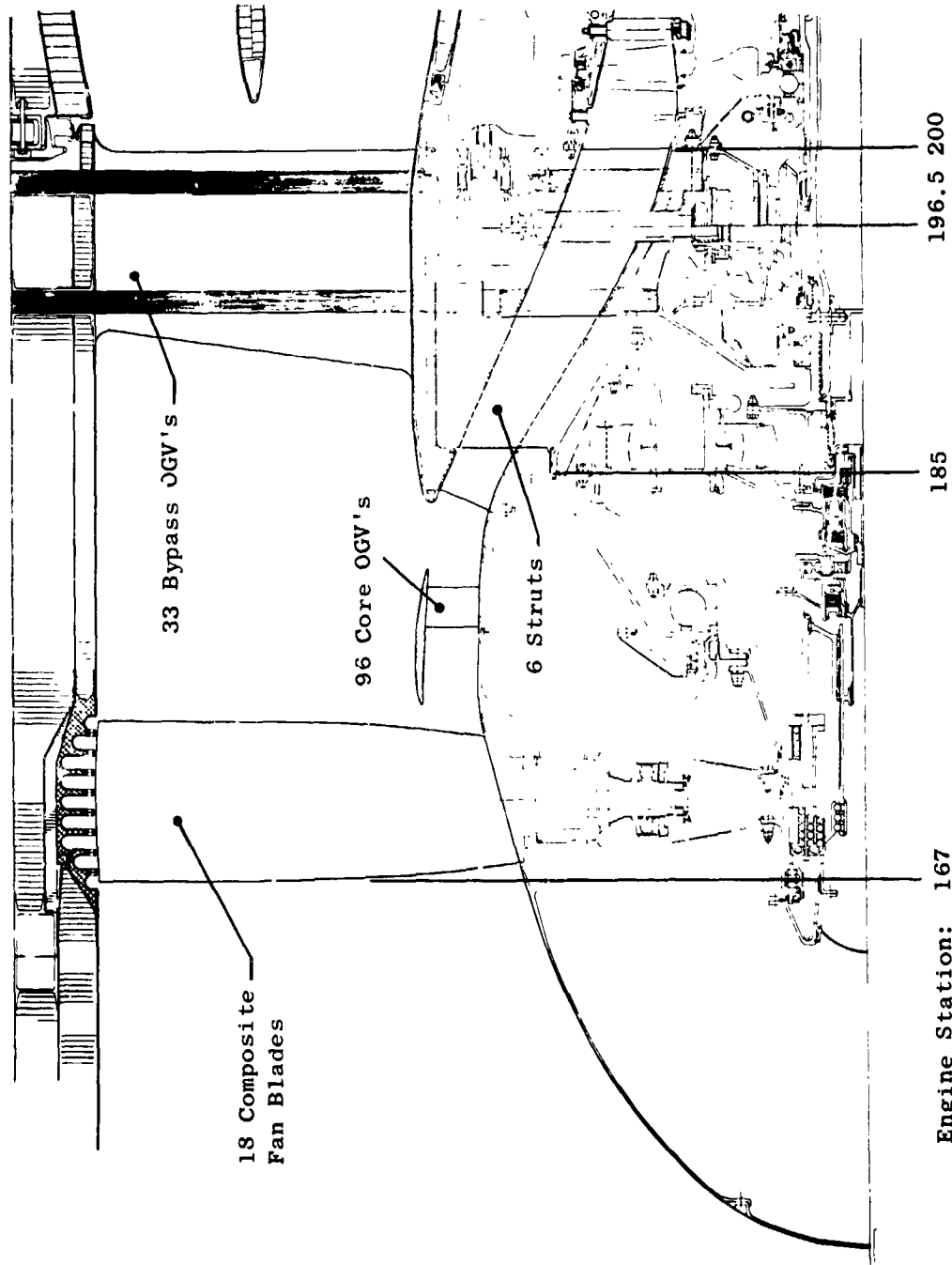


Figure 2. Cross Section of UTW Variable-Pitch Fan.

margins are significant because a minimum fan tip speed was selected to minimize noise generation. The circumferential grooved casing treatment type was selected since this type of treatment improves stall margin and has shown negligible adverse impact on overall fan efficiency. An additional benefit of the casing treatment is to reduce the material bulk over the blade tip, for a given clearance, which will reduce the severity of an inadvertent blade rub as might be encountered during a bird strike.

The vane-frame is positioned at an axial distance downstream of the rotor trailing edge equal to 1.5 true rotor tip chords. The vanes are nonaxisymmetric in that five vane geometries, each with a different camber and stagger, are employed around the annulus. This nonaxisymmetric geometry is required to conform the vane-frame downstream flow field to the geometry of the pylon, which protrudes forward into the vane-frame, and simultaneously maintain a condition of minimum circumferential static pressure distortion upstream of the vane-frame. There are 33 vanes in the vane-frame which yields a vane-blade ratio of 1.83. Immediately following the rotor, in the hub region, is an annular ring or island. The 96 OGV's for the fan hub, or core portion flow, are in the annular space between the under side of the island and the hub. A full-circumference axial gap separates the island trailing edge from the splitter leading edge. The splitter divides the flow into the bypass portion and core portion. There are six struts in the gooseneck which guide the fan hub flow into the core compressor.

The island configuration was selected specifically to permit the attainment of a high hub supercharging pressure ratio for forward pitch operation without causing a large core flow induction pressure drop during reverse pitch operation, see Section 2.3. In the forward mode of operation, a vortex sheet is shed from the trailing edge of the island in the form of a swirl angle discontinuity since most of the swirl in the flow under the island is removed by the core OGV. Total pressure on top of the island differs from that under the island only by the losses in the core OGV, hence the Mach numbers of the two streams are nearly the same. The General Electric CF6-6 fan incorporates a similar island configuration, except that the bypass OGV's are on top of the island and there is no swirl in the bypass flow at the island trailing edge. A vortex sheet is shed from the trailing edge of this island configuration also. This vortex sheet is in the form of a velocity magnitude discontinuity. The swirl angle is zero both on top of and under the island but the total pressures differ by the work input in the tip region of the 1/4 stage. Numerically, the strength of the QCSEE UTW island shed vortex is approximately the same as the strength of the CF6-6 island shed vortex. Orientation of the vortex vectors is rotated approximately 70°, however.

2.3 REVERSE FLOW

A major feature of the UTW fan is its ability to change the direction of fan thrust by reversing the direction of flow through the fan. This flow reversal affects the pressure level into the core engine (and, hence, the core engine's ability to produce power) in two ways. First, there is the direct

loss of the fan hub supercharging pressure; and, second, there is the loss associated with inducting the flow into the core engine such as the recoveries of the exlet, vane frame, turn around the splitter leading edge, core OGV's, and gooseneck struts. The hub supercharging pressure loss is obviously related to the magnitude of the design (forward mode) fan hub pressure ratio, but the flow losses are also related to this magnitude. When operating in the reverse thrust mode, camber on the core OGV's is in the wrong direction and high hub supercharging in forward operation increases the camber of both bypass and core OGV's. Concern over this matter because of relatively high hub pressure ratio of the UTW fan was the primary reason for selecting the island approach. The major advantage to this configuration is that flow can enter the core compressor duct through the axial gap between the island and splitter and thereby avoid the problem of adversely oriented camber on the core OGV's. The swirling flow, of course, must still pass through the six axially oriented struts in the core inlet gooseneck. Relatively, this path for the flow is much less restrictive. A second benefit is that the bluntness of the splitter leading edge compared to the island leading edge (which would be the splitter leading edge if the axial gap were filled), is conducive to minimizing losses associated with reversing the axial component of the core portion flow from its forward direction in the bypass duct to its aft direction in the core transition duct.

Reverse fan thrust can be achieved by rotating the blades through the flat pitch (like a propeller) or the stall pitch directions. Rotation of the blades into the reverse thrust condition puts a constraint on selection of blade solidity. This depends primarily on the direction in which the blades are rotated and the blade twist. The constraint is on those blade sections which pass through a tangential orientation, e.g., the leading edge of each blade must be able to pass the trailing edge of the adjacent blade, or physical interference will result. Therefore, those sections must have a solidity less than unity.

Figure 3 shows a tip and hub section of two adjacent blades in nominal, reverse through stall, and reverse through flat pitch orientations. The 45° tip stagger for both reverse through flat and reverse through stall was selected based on experimental reverse thrust performance. For blade rotation through the flat pitch direction, the entire blade span is constrained to a solidity less than one. For rotation through the stall pitch direction, the outer portion of the blade is not constrained. However, because of the 44° twist in the blade, the chord of the hub region cannot be increased significantly without interference. The assumed orientation of the tip section would have to be in error on the order of 5° before significant hub region chord increase could be accommodated. Even if a hub region chord increase could be accommodated, a significant increase in supercharging potential is probably not available because the implied increase in blade twist would probably cause a physical interference.

Therefore, it was concluded that a hub solidity less than unity was a design requirement for reverse through stall pitch rather than a compromise to permit reverse through flat pitch.

ORIGINAL PAGE IS
OF POOR QUALITY

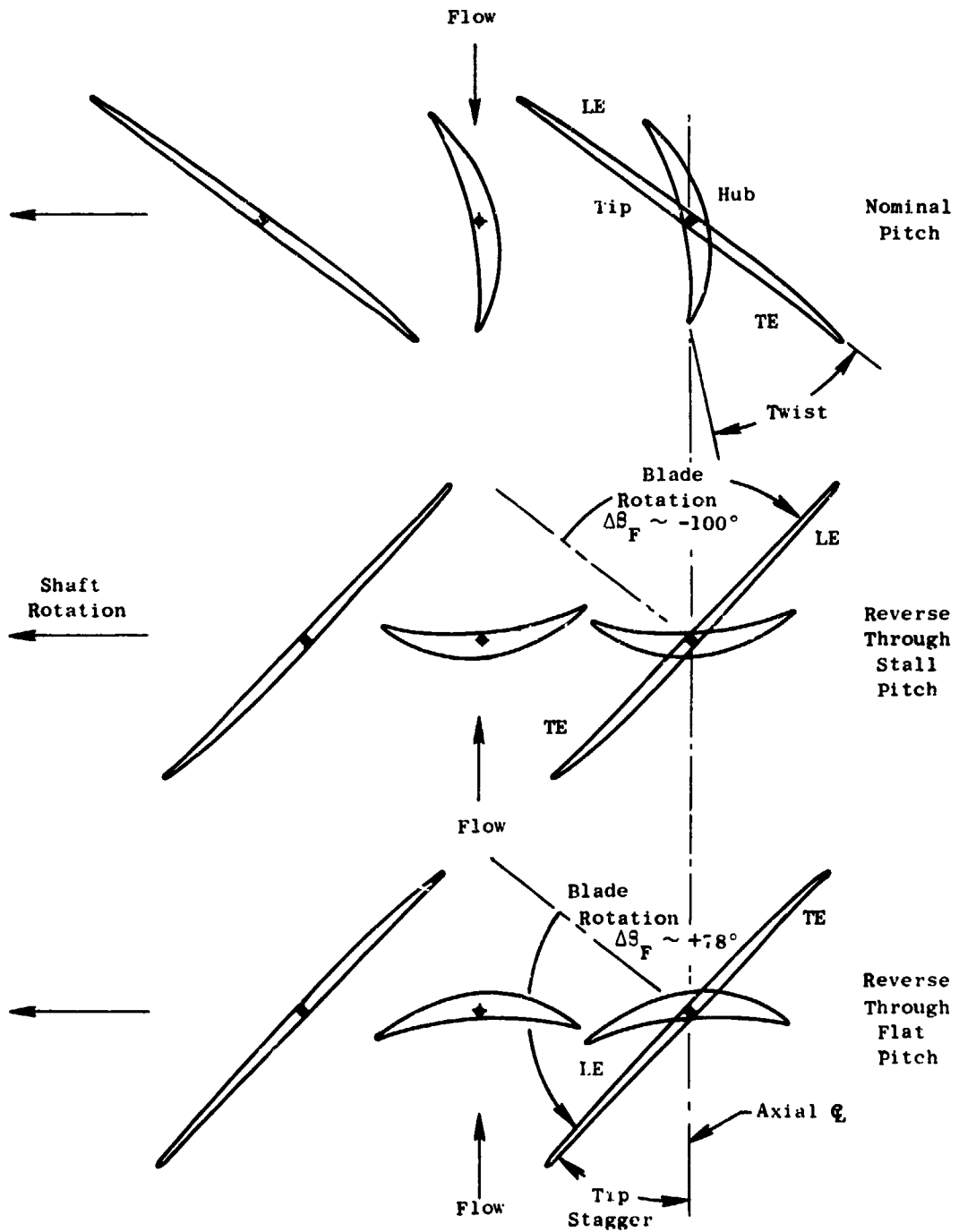


Figure 3. UTW Fan Blade Geometry at Different Pitch Angle Settings.

2.4 PERFORMANCE REPRESENTATION WITH VARIABLE PITCH

The variable-pitch feature of the UTW fan adds a third independent variable to the representation of fan performance in that, in addition to normal independent variables of speed and operating line, the blade pitch angle is also required. It has been found, however, that experimental stage characteristics at different rotor pitch angle settings can be collapsed into a nearly universal characteristic applicable for all blade angle settings. The method used to collapse the characteristics was to deduce the rotor incidence and deviation angle from the test data and then calculate the performance of the stage at nominal blade angle with the rotor operating at this incidence and deviation angle and the test efficiency. A separate correlation of aerodynamic loading is used to identify a stall limit, as the collapsing technique breaks down due to the change in aerodynamic loading inherent in the transformation. Figure 4 shows the stage characteristics assumed for the UTW fan at 100% corrected speed for a range of pitch angles. In the reverse flow mode of operation a similar, but simplified, form of the universal characteristic approach is used to represent fan performance. The same collapsing technique is incorporated to include the effect of blade angle setting.

2.5 DETAILED CONFIGURATION DESIGN

The corrected tip speed at the aerodynamic design point was selected at 306 m/sec (1005 ft/sec). This selection is a compromise for design purposes between 289 m/sec (950 ft/sec) at takeoff and the 324 m/sec (1063 ft/sec) at maximum cruise. The objective design point adiabatic efficiency is 88% for the bypass portion and 78% for the core portion. A stall margin of 16% is projected at takeoff. This stall margin is provided at minimum tip speed by incorporating circumferential grooved casing treatment over the rotor tip. Minimum tip speed is important because of the favorable impact of low tip speed on fan generated noise, fan efficiency in the transonic region, and the mechanical design of the variable-pitch system. An inlet radius ratio of 0.44 balances the desire to minimize fan diameter within the physical constraints of the variable-pitch mechanism and gear box and good fan hub supercharging for the core engine. A fan inlet flow per annulus area of 199 kg/sec-m² (40.8 lb/sec-ft²) at the design point results in a tip diameter of 1.803 m (71.0 in.).

The standard General Electric axisymmetric flow computation procedure was employed in calculating the velocity diagrams. Several calculation stations were included internal to the rotor blade to improve the overall accuracy of the solution in this region. The physical island geometry is represented in the calculations. Forward of the island and in the axial space between the island and the splitter, calculation stations span the radial distance from OD to ID. Within the axial space of the island, calculation stations span the radial distance between the OD and the topside of the island and between the underside of the island and the hub contour. In the bypass and core inlet ducts, calculation stations are also included. At each calculation station, effective area coefficients consistent with established design practice were assumed.

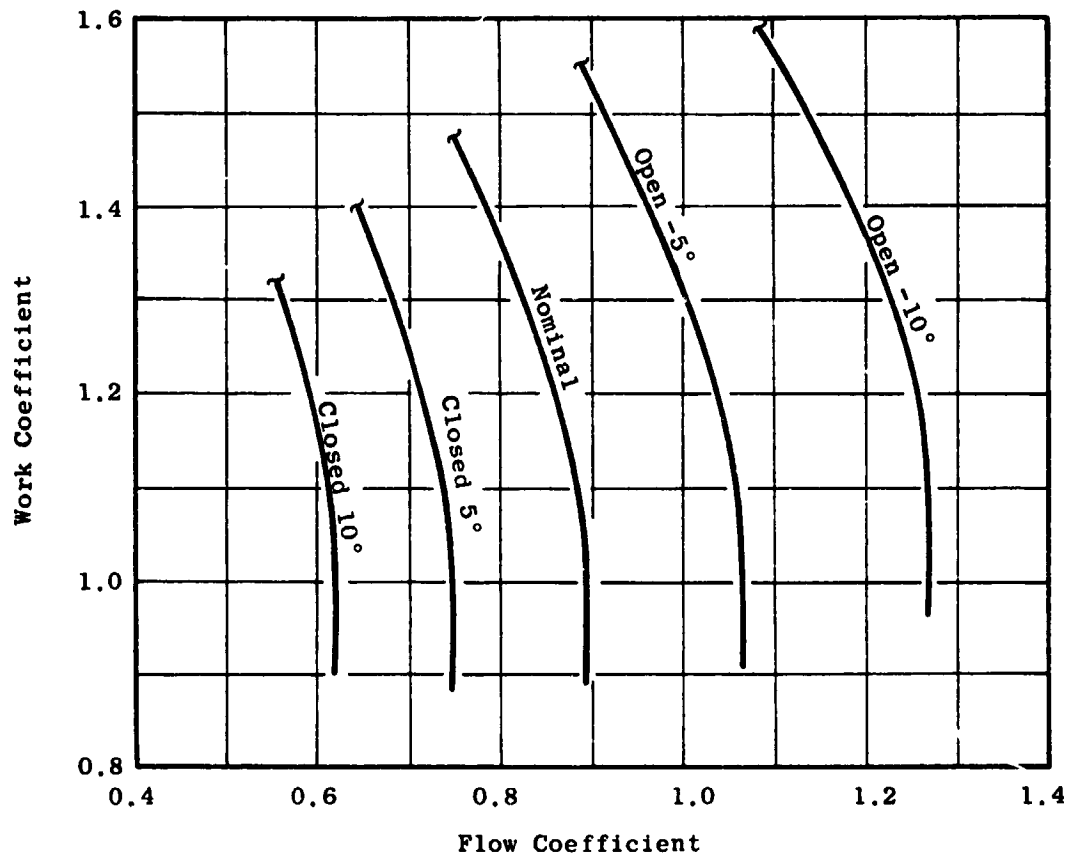


Figure 4. UTW Fan Stage Characteristics at 100% Speed for Various Pitch Settings.

A special constraint is necessary in the aerodynamic design of the island geometry in that a smooth flow or Kutta condition must be satisfied at the trailing edge of the island. The technique employed in this design was to specify a calculation station at the axial location of the island trailing edge which spanned the total flowpath height from OD to ID. Using this technique, a continuous radial distribution of static pressure results which was assumed to be consistent with matching the Kutta condition. The radial location of the island stream function of this calculation station was determined, and the upstream geometry of the island was then adjusted to provide a smooth continuous contour blending into this point. Iteration was obviously necessary because of the interaction of the assumed geometry with the calculated radial location of the island stream function. Convergence was found to be quite rapid. An artificial radial displacement was incorporated between the island upper surface streamline and the island lower surface streamline in order to avoid problems in calculating the streamline curvatures. This displacement was assumed equal to the island thickness at the trailing edge and was smoothly blended to zero at an axial distance of approximately 10 edge thicknesses downstream.

The design radial distribution of rotor total pressure ratio is shown in Figure 5. This distribution is consistent with a stage average pressure ratio of 1.34 in the bypass region. Despite the lower-than-average pressure ratio in the hub region, it has been maximized to the extent possible subject to the constraint of acceptable rotor diffusion factors so as to provide maximum core engine supercharging. A stage average pressure ratio of 1.23 results at the core OGV exit. The radial distribution of rotor efficiency assumed for the design is shown in Figure 6. The assumption of efficiency, rather than total pressure loss coefficient, is a General Electric design practice for rotors of this type. This distribution was based on the measured results from similar configurations with adjustments to account for recognized differences. The radial distribution of rotor diffusion factor which results from these assumptions is shown in Figure 7. The moderately high diffusion factor in the tip region of the blade, where stall generally initiates, confirms the need for casing treatment to obtain adequate margin. The radial distributions of rotor relative Mach number and air angle are shown in Figures 8 and 9, respectively.

The assumed radial distribution of total-pressure-loss coefficient for the core portion OGV is shown in Figure 10. The relatively high level, (~ 0.2) particularly in the ID region, is in recognition of the very high bypass ratio of the UTW engine and, accordingly, the small size of the core OGV compared to the rotor. The annulus height of the core OGV is approximately one-half of the rotor staggered spacing, a significant dimension when analyzing secondary flow phenomena. It is anticipated that the core OGV will be influenced by the rotor secondary flow over the entire annulus height. The diffusion factor, Mach number, and air angle radial distributions which result from the design assumptions are also shown in Figure 10. An average swirl of 0.104 radial (6°) is retained in the fluid at exit from the core OGV. This was done to lower its aerodynamic loading and the magnitude of the vortex sheet shed from the island. The transition duct (core inlet) struts (6) are cambered to accept this swirl and remove it prior to entrance into the core engine.

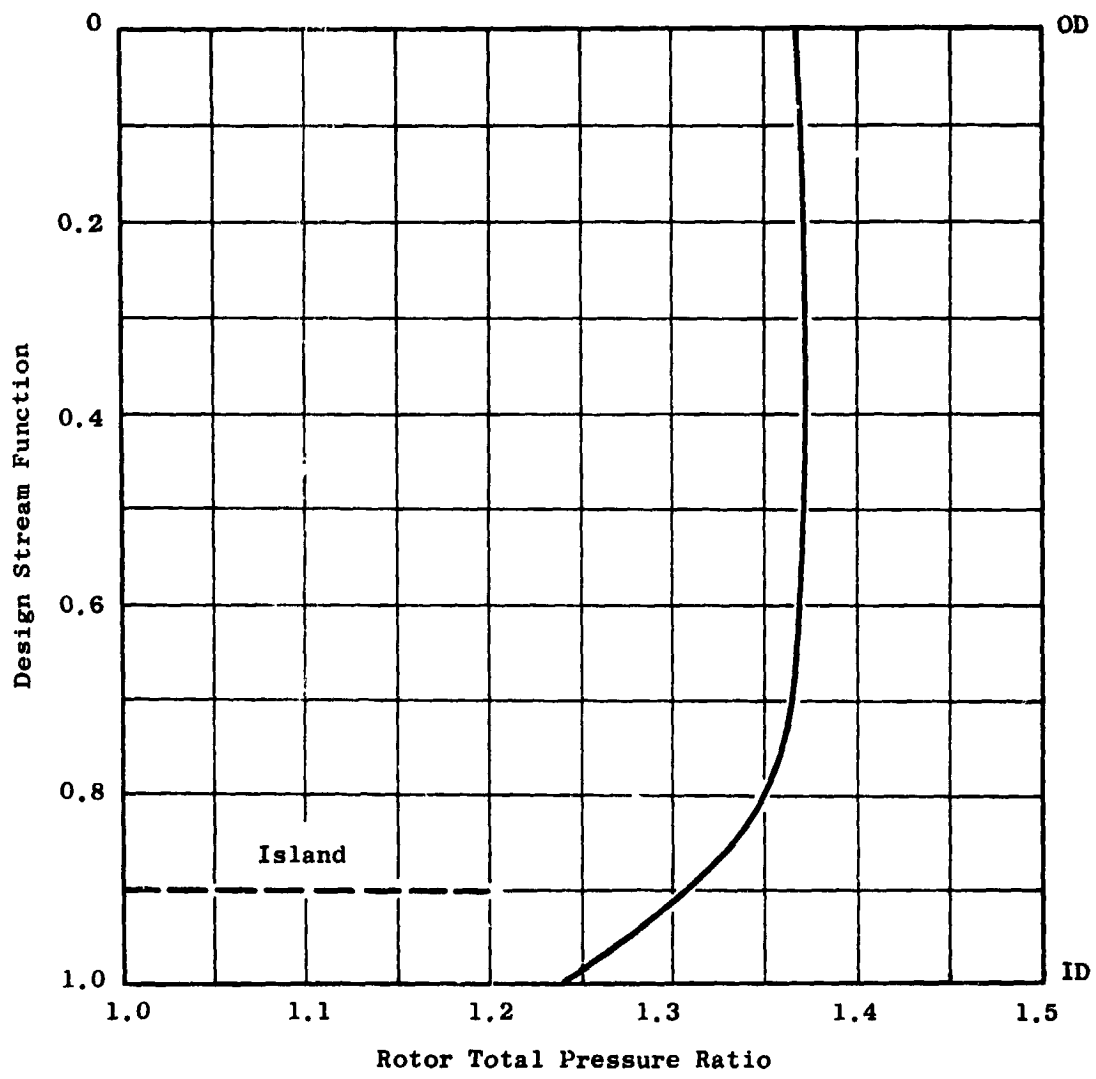


Figure 5. Radial Distribution of Rotor Total Pressure Ratio.

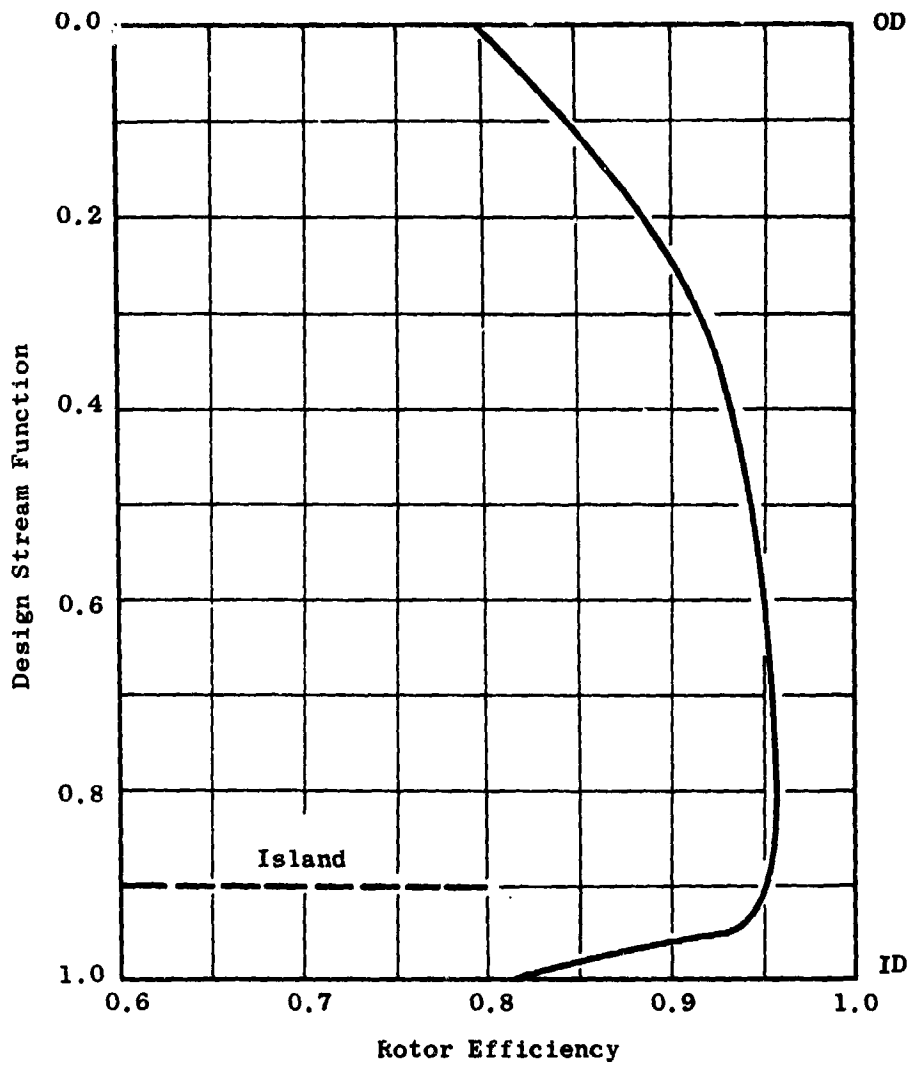


Figure 6. Radial Distribution of Rotor Efficiency.

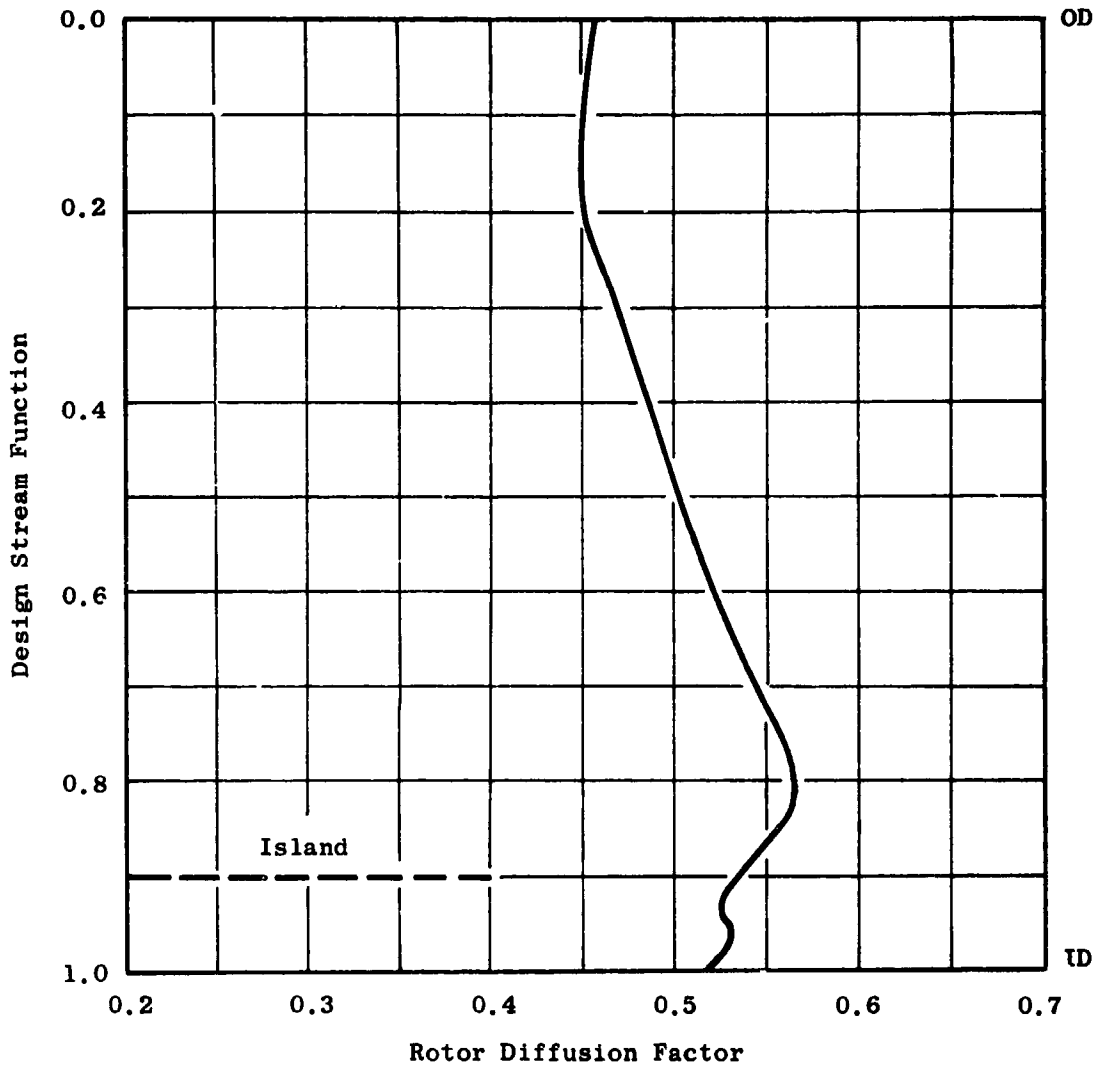


Figure 7. Radial Distribution of Rotor Diffusion Factor.

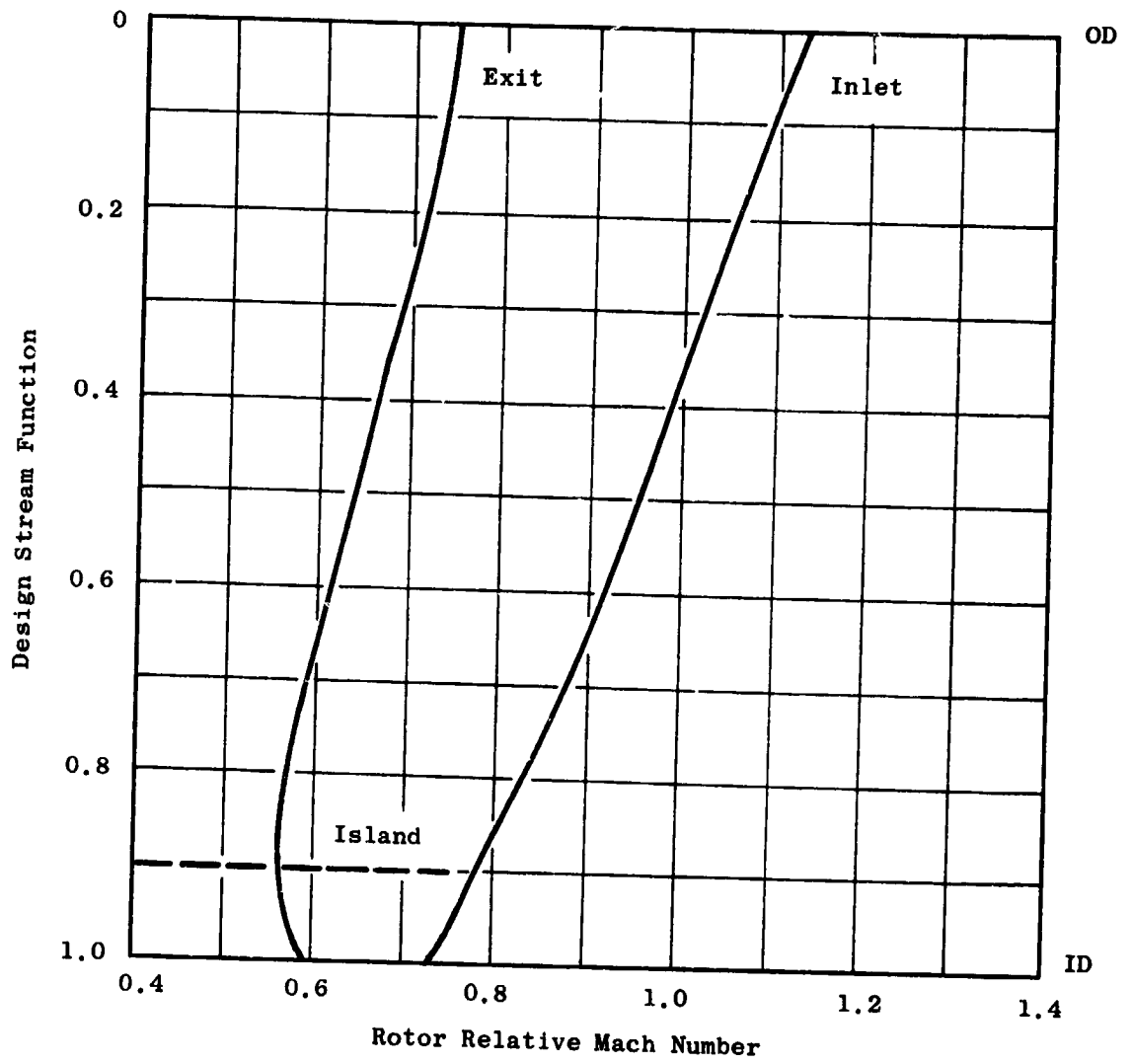


Figure 8. Radial Distribution of Rotor Relative Mach Numbers.

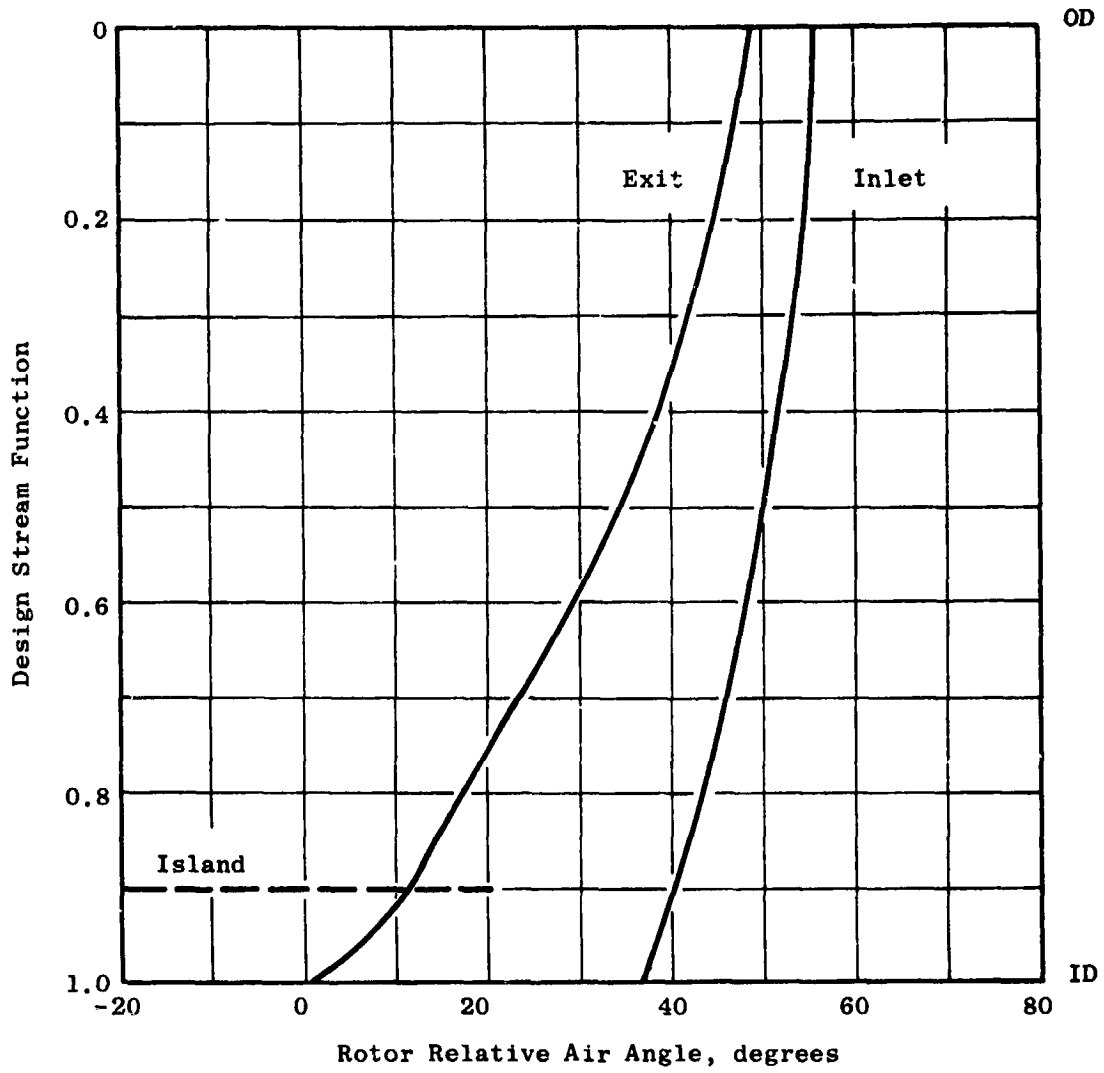


Figure 9. Radial Distribution of Rotor Relative Air Angles.

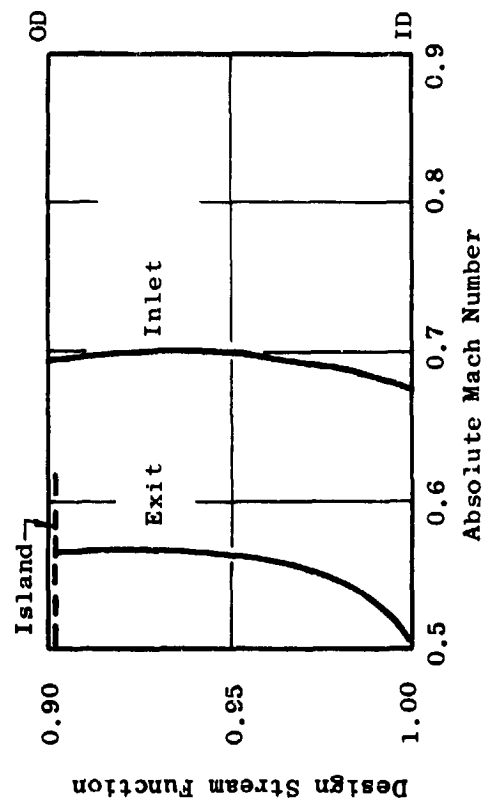
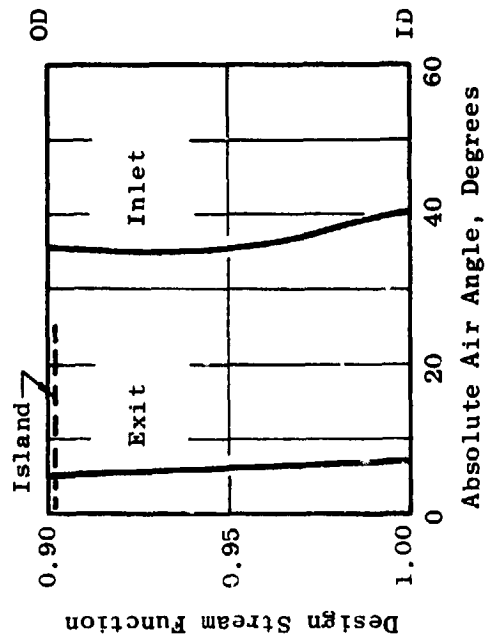
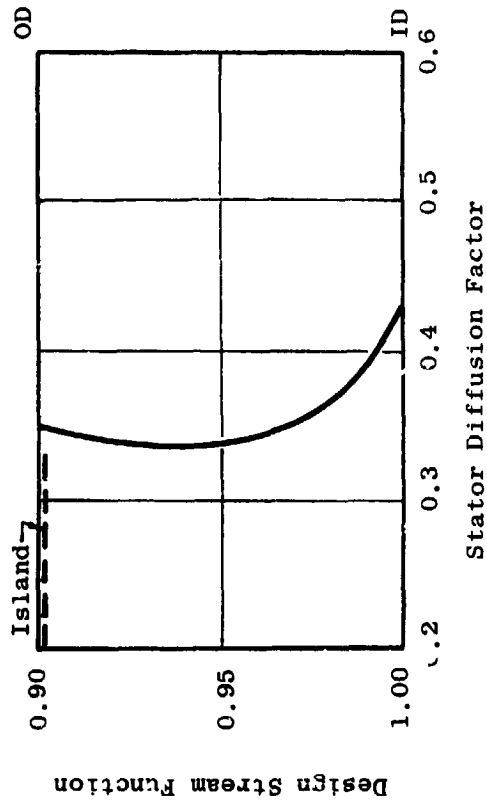
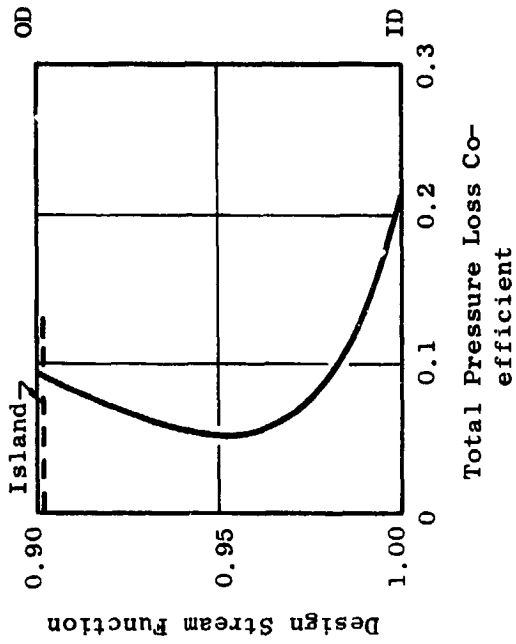


Figure 10. Radial Distribution of Design Parameters for Core CGV.

A tabulation of significant blade element parameters for the UTW design is presented in Table 2 for both metric (2-A) and English (2-B) units.

2.6 ROTOR BLADE DESIGN

Detailed layout procedures employed in design of the fan blade generally paralleled established design procedures. In the tip region of the blade, where the inlet relative flow is supersonic, the uncovered portion of the suction surface was set to ensure that the maximum flow-passing capacity is consistent with the design flow requirement. Incidence angles in the tip region were selected according to transonic blade design practice which has yielded good overall performance for previous designs. In the hub region, where inlet flow is subsonic, incidence angles were selected from NASA cascade data correlations.

The blade trailing edge angle was established by the deviation angle which was obtained from Carter's Rule applied to the camber of an equivalent two-dimensional cascade with an additive empirical adjustment, X. This adjustment is derived from aerodynamic design and performance synthesis for this general type of rotor. Incidence and deviation angles and the empirical adjustment angle employed in the design are shown in Figure 11.

Over the entire blade span, the minimum passage area, or throat, must be sufficient to pass the design flow including allowances for boundary layer, losses, and flow nonuniformities. In the transonic and supersonic region, the smallest throat area (consistent with permitting design flow to pass) is desirable, since this minimizes overexpansions on the suction surface. A further consideration was to minimize disturbances to the flow along the forward portion of the suction surface to minimize forward-propagating waves that might provide an additional noise source. Design experience guided the degree to which each of these desires was applied to individual section layouts. The percent throat margin, that percentage by which the ratio of the effective throat area to the capture area exceeds the critical area ratio, is shown in Figure 12. Values employed are generally consistent with past experience. The blade shapes that result are generally similar to multiple circular arc sections in the tip region, with a small percentage of the overall camber occurring in the forward portion. In the hub region, the blade shapes are similar to double circular arc sections.

Figure 13 shows plane sections of the blade at several radial locations. Table 3 is a tabulation of the fan rotor blade coordinates (in inches) for the sections shown in this figure. The coordinate center is at the stacking axis. Figure 14 shows the resulting camber and stagger angle radial distributions. The radial thickness distributions employed, which were dictated primarily by aeromechanical considerations, are shown in Figure 15. The 0.13 thickness-to-chord ratio at the hub is larger than conventional practice because of the composite blade requirements; a small performance penalty will result. The additional profile loss created by this thickness, however, is believed smaller than the system penalties associated with altering the

Table 2-A. Design Blade Element Parameters for QCSEE UTW Fan.

NOMENCLATURE FOR TABULATION

HEADING	IDENTIFICATION	METRIC UNITS
GENERAL		
SL	STREAMLINE NUMBER	-
PSI	STREAM FUNCTION	-
RADIUS	STREAMLINE RADIUS	CM.
X IMM	PERCENT IMMERSION FROM OUTER WALL	%
Z	AXIAL DIMENSION	CM.
BLKAGE	ANNULUS BLOCKAGE FACTOR	-
FLOW	WEIGHT FLOW	KG/SEC
ANGLES AND MACH NUMBERS		
PHI	MERIDIONAL FLOW ANGLE	DEG.
ALPHA	ABSOLUTE FLOW ANGLE = ARCTAN (CU/CZ)	DEG.
BETA	RELATIVE FLOW ANGLE = ARCTAN (-WU/CZ)	DEG.
M=ABS	ABSOLUTE MACH NUMBER	-
M=REL	RELATIVE MACH NUMBER	-
VELOCITIES		
C	ABSOLUTE VELOCITY	M/SEC
W	RELATIVE VELOCITY	M/SEC
CZ	AXIAL VELOCITY	M/SEC
U	BLADE SPEED	M/SEC
CU	TANGENTIAL COMPONENT OF C	M/SEC
WU	TANGENTIAL COMPONENT OF W	M/SEC
FLUID PROPERTIES		
PT	ABSOLUTE TOTAL PRESSURE	N/SQ.CM.
TI	ABSOLUTE TOTAL TEMPERATURE	DEG-K
TT=REL	RELATIVE TOTAL TEMPERATURE	DEG-K
PS	STATIC PRESSURE	N/SQ.CM.
TS	STATIC TEMPERATURE	DEG-K
RHO	STATIC DENSITY	KG/CM ³
EFF	CUMULATIVE ADIABATIC EFFICIENCY REFERENCED TO PTI, TII	-
PTI	INLET ABSOLUTE TOTAL PRESSURE	N/SQ.CM.
TII	INLET ABSOLUTE TOTAL TEMPERATURE	DEG-K
AERODYNAMIC BLADING PARAMETERS		
TPLC	TOTAL PRESSURE LOSS COEFFICIENT	-
PK=ROW	TOTAL PRESSURE RATIO ACROSS BLADE ROW	-
DEL-T	TOTAL TEMPERATURE RISE ACROSS ROTOR	DEG-K
D	DIFFUSION FACTOR	-
DP/W	STATIC PRESSURE RISE COEFFICIENT	-
CZ/CZ	AXIAL VELOCITY RATIO ACROSS BLADE ROW	-
SOLDTY	SOLIDITY	-
R=AVG	AVERAGE STREAMLINE RADIUS ACROSS BLADE ROW	CM.
F=TAN	TANGENTIAL BLADE FORCE PER UNIT BLADE LENGTH	N/CM
F=AXL	AXIAL BLADE FORCE PER UNIT BLADE LENGTH	N/CM
F=COEF	FLOW COEFFICIENT = CZ/U1	-
T=COEF	WORK COEFFICIENT = (2*G*J*CP*DEL-T)/(U2*U2)	-

Table 2-A. Design Blade Element Parameters for QCSEE UTW Fan (Continued).

SL	PSI	RADIUS	Z	IMM	PHI	ALPHA	BETA	M-ABS	M-REL	L	N	CZ	U	CU	MU	SL	MEINIC UNITS
1	0.1000	90.1702	0.	0.	0.	0.	56.03	0.630	1.128	206.4	369.4	206.4	306.3	0.	-506.3	1	
2	0.2500	80.5671	7.2	2.31	0.	0.	45.35	0.620	1.091	203.5	357.6	203.5	294.1	0.	-294.1	2	
3	0.4000	64.7672	16.7	5.55	0.	0.	51.97	0.609	1.034	199.9	339.5	199.5	274.4	0.	-274.4	3	
4	0.4000	74.5029	31.2	5.45	0.	0.	51.68	0.612	0.985	201.0	323.2	200.1	255.1	0.	-253.1	4	
5	0.6900	64.5384	59.1	10.26	0.	0.	46.06	0.614	0.877	201.4	287.8	198.2	205.7	0.	-205.7	5	
6	0.8000	54.2263	71.7	12.60	0.	0.	43.31	0.610	0.829	200.3	272.1	195.4	184.2	0.	-184.2	6	
7	0.9420	44.6160	90.8	15.73	0.	0.	34.32	0.607	0.752	199.3	250.3	191.8	151.6	0.	-151.6	7	
8	0.9810	43.1544	93.7	15.97	0.	0.	37.39	0.608	0.754	199.5	247.6	191.8	146.6	0.	-146.6	8	
9	0.9810	41.5660	96.9	16.09	0.	0.	36.24	0.611	0.747	200.5	245.2	192.7	141.2	0.	-141.2	9	
10	1.0000	40.0051	100.0	15.80	0.	0.	34.85	0.610	0.745	202.9	244.2	195.2	135.9	0.	-135.9	10	

STATION 1.0000C Z 423.926830 ROTOR INLET

SL	PSI	RADIUS	PT	PTI	TI	TI-REL	PS	TS	MMD	PI/PTI	TI/TII	EFF	BLKAGE
1	0.1000	90.1702	10.132	288.16	334.86	334.86	7.755	266.97	1.01199	1.0000	1.00000	0.58000	
2	0.2500	80.5671	10.132	288.16	331.20	331.20	7.616	267.56	1.01763	1.0000	1.00000	0.98000	
3	0.4000	64.7672	10.132	288.16	325.63	325.63	7.488	268.27	1.02437	1.0000	1.00000	0.98000	
4	0.4000	74.5029	10.132	288.16	320.04	320.04	7.467	268.06	1.02239	1.0000	1.00000	0.98000	
5	0.6900	64.5384	10.132	288.16	309.21	309.21	7.658	267.97	1.02157	1.0000	1.00000	0.98000	
6	0.8000	54.2263	10.132	288.16	305.05	305.05	7.681	268.20	1.02374	1.0000	1.00000	0.98000	
7	0.9420	44.6160	10.132	288.16	299.59	299.59	7.902	268.40	1.02565	1.0000	1.00000	0.98000	
8	0.9810	43.1544	10.132	288.16	298.84	298.84	7.697	268.35	1.02517	1.0000	1.00000	0.98000	
9	0.9810	41.5660	10.132	288.16	298.08	298.08	7.676	268.5	1.02326	1.0000	1.00000	0.98000	
10	1.0000	40.0051	10.132	288.16	297.35	297.35	7.628	267.68	1.01876	1.0000	1.00000	0.98000	

ORIGINAL PAGE IS
OF POOR QUALITY

MASS AVERAGED VALUE:

PT, PTI 1.0000 EFF CORR. FLOW 408.233 PT 10.132 TI 288.16 TI/TII 1.0000 CZ 198.76
 CORR. RPM 3248.1 CORR. U-TIP 306.3

PTI 10.152
 TII 288.161
 GAMMA 1.4000

Table 2-A. Design Blade Element Parameters for QCSEE UTW Fan (Continued).

SL	PSI	RADIUS	Z	IMM	FMI	ALPHA	BETA	M-ABS	M-REL	C	N	CZ	U	CU	MU	SL
1	0.	90.1102	0.	0.	-4.54	53.17	49.01	0.584	0.745	203.5	259.2	169.8	308.3	111.0	-195.3	1
2	0.1000	86.6954	7.7	0.84	-0.84	57.05	46.75	0.593	0.734	205.7	254.5	174.4	294.5	109.2	-185.3	2
3	0.2500	81.2467	19.8	0.37	32.12	45.62	0.597	0.698	206.2	241.2	241.2	174.6	276.0	109.6	-166.4	3
4	0.5000	75.4725	32.6	1.42	52.90	38.71	0.612	0.659	210.9	228.9	177.0	170.4	258.4	114.5	-141.9	4
5	0.6900	62.8425	40.6	4.66	55.64	23.96	0.603	0.590	220.7	201.7	183.8	183.8	215.5	131.4	-81.7	5
6	0.8000	57.5360	72.8	7.83	37.25	16.97	0.678	0.566	231.0	192.8	182.8	194.8	159.0	159.0	-55.8	6
7	0.9420	44.9809	91.4	8.21	35.96	8.89	0.695	0.572	234.7	192.9	188.7	169.4	169.9	156.9	-29.5	7
8	0.9810	47.7524	94.1	8.14	36.60	6.58	0.703	0.570	237.0	192.2	189.0	162.2	140.4	140.4	-21.8	8
9	0.9810	46.4111	97.1	8.34	36.68	4.04	0.719	0.579	241.8	194.6	192.1	157.7	144.1	144.1	-13.6	9
10	1.0000	45.0952	100.0	8.74	37.02	1.53	0.738	0.592	247.6	198.6	196.2	153.2	148.0	148.0	-5.2	10

STATION	Z	442.722866	ROTOR	EXT.	MEIKIL UNITS
1.50000	2	442.722866	ROTOR	EXT.	

SL	PSI	RADIUS	PI	TT	TT-REL	PS	TS	KMU	PI/PTI	TT/TTI	EFF	BLKAGE
1	0.	90.1102	13.861	322.00	350.86	11.002	301.44	1.27154	1.3680	1.11743	0.7475	0.96000
2	0.1000	86.6954	13.671	320.17	331.33	10.931	299.10	1.27319	1.3690	1.11107	0.6453	0.96000
3	0.2500	81.2467	13.491	318.28	316.08	10.919	297.12	1.27026	1.3710	1.10451	0.9027	0.96000
4	0.5000	75.4725	13.902	317.39	320.88	10.794	295.25	1.27358	1.3720	1.10143	0.9324	0.96000
5	0.6900	62.8425	13.620	316.17	310.84	10.287	290.59	1.25329	1.3640	1.09719	0.9542	0.96000
6	0.8000	57.5360	13.678	315.11	307.04	10.050	288.55	1.21340	1.3500	1.09352	0.9572	0.96000
7	0.9420	44.9809	13.000	310.83	301.94	9.411	283.43	1.15674	1.2830	1.07868	0.9379	0.96000
8	0.9810	47.7524	12.684	310.63	301.26	9.257	282.87	1.13762	1.2680	1.07868	0.8921	0.96000
9	0.9810	46.4111	12.706	310.78	300.53	9.007	281.68	1.11396	1.2540	1.07849	0.8512	0.96000
10	1.0000	45.0952	12.564	310.72	299.84	8.751	280.22	1.08799	1.2400	1.07829	0.8096	0.96000

SL	PSI	TPLC	PR-RUM	DEL-T	U	DP/W	CZ/CZ	SULUTY	M-AVG	T-TAN.	P-AXL	T-CUEF
1	0.	0.13282	1.3660	33.64	0.456	0.346	0.823	0.9300	90.1702	1294.99	1412.76	0.745
2	0.1000	0.10102	1.3690	32.01	0.449	0.359	0.858	0.9306	86.6313	1235.64	1369.50	0.741
3	0.2500	0.06502	1.3710	30.12	0.460	0.396	0.875	0.9322	81.0070	1157.63	1281.53	0.794
4	0.5000	0.08720	1.3720	29.23	0.485	0.433	0.885	0.9341	74.9877	1124.84	1154.99	0.893
5	0.6900	0.05651	1.3640	28.01	0.542	0.475	0.928	0.9395	61.6904	1062.73	827.45	1.235
6	0.8000	0.03600	1.3500	26.45	0.564	0.483	0.935	0.9628	55.7812	996.37	670.86	1.427
7	0.9420	0.05069	1.2830	22.67	0.524	0.407	0.984	0.9701	46.7985	809.62	425.88	1.645
8	0.9810	0.06938	1.2680	22.67	0.530	0.371	0.986	0.9716	45.4544	800.34	387.47	1.731
9	0.9810	0.12430	1.2540	22.62	0.525	0.320	0.997	0.9735	43.9885	793.93	309.41	1.864
10	1.0000	0.15903	1.2400	22.56	0.516	0.265	1.005	0.9757	42.5502	790.72	252.53	1.932

PT/PTI	EFF	0.9123	PT	13.718	TT	316.72	TT/TTI	1.09911	CZ	170.20	MIN	PI2/PT1	1.5339	
PT/PTI	1.5339	EFF	0.9123	PT	13.718	TT	316.72	TT/TTI	1.09911	CZ	170.20	MIN	PI2/PT1	1.5339
		COMB. FLOW				COMB. RPM								

ORIGINAL PAGE IS
OF POOR QUALITY

Table 2-A. Design Blade Element Parameters for QCSEE UTW Fan (Continued).

STATION 11.90000 Z 50R.000999 BYPASS OGV EXIT															METRIC UNITS		
SL	PSI	RADIUS	X IMM	PM1	ALPHA	BETA	M-ABS	M-REL	L	N	CZ	U	CU	MU	SL		
1	0.1000	90.1702*	0.	0.24	0.	59.31	0.519	1.017	181.8	356.2	181.8	306.3	0.	-306.3	1		
2	0.2500	86.8872	8.6	-0.21	0.	57.62	0.537	1.002	187.2	349.5	187.2	295.2	0.	-295.2	2		
3	0.4000	81.6571	22.4	-0.07	0.	55.87	0.542	0.987	188.5	335.9	188.5	276.1	0.	-276.1	3		
4	0.6900	76.5508	36.6	0.44	0.	54.06	0.543	0.926	188.5	321.2	188.5	260.1	0.	-260.1	4		
5	0.8000	64.9958	67.7	0.93	0.	49.98	0.545	0.832	185.4	288.3	185.4	220.0	0.	-220.0	5		
6	0.9021	54.2126	96.7	0.13	0.	48.39	0.522	0.786	180.8	272.3	180.8	203.6	0.	-203.6	6		
7	0.9022	54.2056	96.7	0.13	0.	50.58	0.436	0.686	151.4	238.4	151.4	184.2	0.	-184.2	7		
9	0.9184	52.9921*	100.0	0.	0.	54.09	0.374	0.637	130.4	222.3	130.4	180.0	0.	-180.0	9		

STATION 11.90000 Z 50R.000999 BYPASS OGV EXIT															METRIC UNITS		
SL	PSI	RADIUS	PT	TI	TI-REL	PS	IS	RMU	PT/PTI	TI/TII	EFF	BLKAGE	SL				
1	0.1000	90.1702	15.515	322.00	368.70	11.248	303.55	1.28250	1.3338	1.11743	0.7304	0.94000	1				
2	0.2500	86.8872	13.691	320.17	363.53	11.254	302.73	1.29509	1.3512	1.11107	0.8086	0.94000	2				
3	0.4000	81.6571	13.766	318.28	356.76	11.271	300.60	1.30618	1.3586	1.10951	0.8756	0.94000	3				
4	0.6900	76.5508	13.791	317.39	351.05	11.283	299.70	1.31152	1.3610	1.10143	0.9077	0.94000	4				
5	0.8000	64.9958	13.696	316.17	340.43	11.272	299.05	1.31310	1.3517	1.09719	0.9252	0.94000	5				
6	0.9021	54.2126	13.528	315.11	335.74	11.236	298.84	1.30990	1.3551	1.09352	0.9204	0.94000	6				
7	0.9022	54.2056	12.766	312.04	328.92	11.206	300.65	1.29858	1.2559	1.08285	0.8236	0.94000	7				
8	0.9022	54.2056	12.475	312.04	328.91	11.206	302.62	1.29005	1.2512	1.08285	0.7390	0.94000	8				
9	0.9184	52.9921	12.339	311.54	327.67	11.206	303.09	1.28800	1.2718	1.08115	0.7156	0.94000	9				

STATION 11.90000 Z 50R.000999 BYPASS OGV EXIT															METRIC UNITS		
SL	PSI	TPLC	PRENUM	DEL-T	C	DP/D	CZ/CZ	SOLIDTY	M-AVG	F-TAN	F-AXL	F-CUET	1-CUET	SL			
1	0.1000	0.10933	0.9750	0.366	0.176	0.987	1.2233	90.1702	1374.50	283.46	283.46	0.94000	1				
2	0.2500	0.05574	0.9870	0.330	0.191	0.999	1.2974	86.8615	1339.12	334.45	334.45	0.94000	2				
3	0.4000	0.03740	0.9910	0.317	0.216	0.987	1.4236	81.7700	1283.06	341.47	341.47	0.94000	3				
4	0.6900	0.03216	0.9920	0.318	0.243	0.978	1.5750	76.4012	1252.39	355.51	355.51	0.94000	4				
5	0.8000	0.03350	0.9910	0.342	0.314	0.955	1.9934	64.6934	1185.91	392.18	392.18	0.94000	5				
6	0.8000	0.03974	0.9890	0.362	0.354	0.930	2.2276	54.5648	1119.04	389.13	389.13	0.94000	6				
7	0.9021	0.11991	0.9680	0.454	0.437	0.798	2.5745	54.0076	884.81	263.87	263.87	0.94000	7				
8	0.9022	0.12085	0.9700	0.393	0.482	0.623	2.5761	54.0076	113.20	-42.19	-42.19	0.94000	8				
9	0.9184	0.15785	0.9610	0.424	0.485	0.592	2.8676	52.9921	114.76	-64.87	-64.87	0.94000	9				

MASS AVERAGED VALUES															
PT/PTI	1.3445	EFF	0.8748	PT	13.623	TI	317.24	TI/TII	1.10090	CZ	183.37	MUM	P12/P11	0.9879	
		CURR. FLOW		CORR. MPH		3091.8									

* Bypass OGV exit tip and hub radii listed in this table were changed to 90.2843 cm and 52.2986 cm, respectively, after the aero design was completed in order to improve transition of the fan flow-path into the bypass exhaust duct contours. The impact of these changes on OGV blade element parameters was estimated to be small, and the design data were not recomputed.

Table 2-B. Design Blade Element Parameters for QCSEE UTW Fan
(Continued).

NOMENCLATURE FOR TABULATION

HEADING	IDENTIFICATION	ENGLISH UNITS
GENERAL		
SL	STREAMLINE NUMBER	-
PSI	STREAM FUNCTION	-
RADIUS	STREAMLINE RADIUS	IN.
Z IMM	PERCENT IMMERSION FROM OUTER WALL	%
Z	AXIAL DIMENSION	IN.
BLKAGE	ANNULUS BLOCKAGE FACTOR	-
FLOW	WEIGHT FLOW	LBM/SEC
ANGLES AND MACH NUMBERS		
PHI	MERIDIONAL FLOW ANGLE	DEG.
ALPHA	ABSOLUTE FLOW ANGLE $=\text{ARCTAN}(CU/CZ)$	DEG.
BETA	RELATIVE FLOW ANGLE $=\text{ARCTAN}(-WU/CZ)$	DEG.
M=ABS	ABSOLUTE MACH NUMBER	-
M=REL	RELATIVE MACH NUMBER	-
VELOCITIES		
C	ABSOLUTE VELOCITY	FT/SEC
W	RELATIVE VELOCITY	FT/SEC
CZ	AXIAL VELOCITY	FT/SEC
U	BLADE SPEED	FT/SEC
CU	TANGENTIAL COMPONENT OF C	FT/SEC
WU	TANGENTIAL COMPONENT OF W	FT/SEC
FLUID PROPERTIES		
PT	ABSOLUTE TOTAL PRESSURE	LBF/SQ. IN.
TT	ABSOLUTE TOTAL TEMPERATURE	DEG-R
TT=REL	RELATIVE TOTAL TEMPERATURE	DEG-R
PS	STATIC PRESSURE	LBF/SQ. IN.
TS	STATIC TEMPERATURE	DEG-R
RHO	STATIC DENSITY	LBM/CU. FT.
EFF	CUMULATIVE ADIABATIC EFFICIENCY REFERENCED TO PTI, TII	-
PTI	INLET ABSOLUTE TOTAL PRESSURE	LBF/SQ. IN.
TII	INLET ABSOLUTE TOTAL TEMPERATURE	DEG-R
AERODYNAMIC BLADING PARAMETERS		
TPLC	TOTAL PRESSURE LOSS COEFFICIENT	-
PH=ROM	TOTAL PRESSURE RATIO ACROSS BLADE ROW	-
DEL-T	TOTAL TEMPERATURE RISE ACROSS ROTOR	DEG-R
D	DIFFUSION FACTOR	-
DP/Q	STATIC PRESSURE RISE COEFFICIENT	-
CZ/CZ	AXIAL VELOCITY RATIO ACROSS BLADE ROW	-
SOLIDTY	SOLIDITY	-
R-AVG	AVERAGE STREAMLINE RADIUS ACROSS BLADE ROW	IN.
F-TAN	TANGENTIAL BLADE FORCE PER UNIT BLADE LENGTH	LBF/IN
F-AXL	AXIAL BLADE FORCE PER UNIT BLADE LENGTH	LBF/IN
F-COEF	FLOW COEFFICIENT $=CZ/U1$	-
T-COEF	WORK COEFFICIENT $=(2*G*J*CP*DEL-T)/(U2*U2)$	-

Table 2-B. Design Blade Element Parameters for QCSEE UTW Fan (Continued).

STATION 1.00000 Z 166.900000 ROTOR INLET										ENGLISH UNITS						
SL	PSI	RADIUS	Z	IMM	PHI	ALPHA	BT1A	M-AKS	M-REL	C	M	CZ	U	CU	RU	SL
1	0.	35.5000	0.	0.	0.	0.	59.03	0.630	1.126	677.1	1211.8	677.1	1005.0	0.	-1005.0	1
2	0.1000	34.0815	7.2	2.31	2.31	0.	55.35	0.620	1.091	667.5	1173.2	667.0	964.8	0.	-964.8	2
3	0.2500	31.7981	18.7	3.55	3.55	0.	53.97	0.609	1.034	655.9	1115.8	654.7	900.2	0.	-900.2	3
4	0.4000	29.5318	31.2	5.45	5.45	0.	51.68	0.612	0.985	659.4	1060.5	656.4	830.4	0.	-830.4	4
5	0.6900	25.8340	59.1	10.26	10.26	0.	46.06	0.614	0.877	660.8	944.4	650.2	674.7	0.	-674.7	5
6	0.8000	23.7489	71.7	12.60	12.60	0.	43.31	0.610	0.829	657.0	892.7	641.2	604.4	0.	-604.4	6
7	0.9420	17.5653	90.8	15.73	15.73	0.	38.32	0.607	0.762	653.7	821.4	629.2	497.5	0.	-497.5	7
8	0.9810	16.9907	93.7	15.97	15.97	0.	37.39	0.608	0.754	654.6	812.5	629.5	481.0	0.	-481.0	8
9	0.9810	16.3645	96.9	16.09	16.09	0.	36.24	0.611	0.747	657.8	804.6	632.1	463.3	0.	-463.3	9
10	1.0000	15.7500	100.0	15.80	15.80	0.	36.85	0.619	0.745	665.6	801.1	640.4	445.9	0.	-445.9	10

STATION 1.00000 Z 166.900000 ROTOR INLET										ENGLISH UNITS						
SL	PSI	RADIUS	Z	IMM	PHI	ALPHA	BT1A	M-AKS	M-REL	C	M	CZ	U	CU	RU	SL
1	0.	35.5000	0.	0.	0.	0.	59.03	0.630	1.126	677.1	1211.8	677.1	1005.0	0.	-1005.0	1
2	0.1000	34.0815	7.2	2.31	2.31	0.	55.35	0.620	1.091	667.5	1173.2	667.0	964.8	0.	-964.8	2
3	0.2500	31.7981	18.7	3.55	3.55	0.	53.97	0.609	1.034	655.9	1115.8	654.7	900.2	0.	-900.2	3
4	0.4000	29.5318	31.2	5.45	5.45	0.	51.68	0.612	0.985	659.4	1060.5	656.4	830.4	0.	-830.4	4
5	0.6900	25.8340	59.1	10.26	10.26	0.	46.06	0.614	0.877	660.8	944.4	650.2	674.7	0.	-674.7	5
6	0.8000	23.7489	71.7	12.60	12.60	0.	43.31	0.610	0.829	657.0	892.7	641.2	604.4	0.	-604.4	6
7	0.9420	17.5653	90.8	15.73	15.73	0.	38.32	0.607	0.762	653.7	821.4	629.2	497.5	0.	-497.5	7
8	0.9810	16.9907	93.7	15.97	15.97	0.	37.39	0.608	0.754	654.6	812.5	629.5	481.0	0.	-481.0	8
9	0.9810	16.3645	96.9	16.09	16.09	0.	36.24	0.611	0.747	657.8	804.6	632.1	463.3	0.	-463.3	9
10	1.0000	15.7500	100.0	15.80	15.80	0.	36.85	0.619	0.745	665.6	801.1	640.4	445.9	0.	-445.9	10

PT/PTI 1.0000 EFF CLMK. FLOW 900.000 PT 14.696 TT 518.69 CURR. RPM 5244.1 1.00000 CZ 652.10
 CURR. RPM 5244.1 COMP. U-IIP 1005.0

PTI 14.696
 TTI 518.690
 GAMMA 1.4000

MASS AVERAGED VALUES

Table 2-B. Design Blade Element Parameters for QCSEE UTW Fan (Continued).

		STATION 1.70000 Z 178.450001 CORE OGV INLET										ENGLISH UNITS				
SL	PSI	RADIUS	X	Y	PHI	ALPHA	BETA	M-ANS	M-KEL	C	W	CZ	U	CU	RU	SL
1	0.9021	20.3020	0.	0.	-3.04	55.59	11.25	0.700	0.582	776.3	645.4	632.2	574.7	449.2	-125.5	1
2	0.9420	19.5566	57.4	57.4	-2.42	55.31	9.04	0.700	0.579	774.6	640.3	631.7	548.0	447.4	-100.6	2
3	0.9610	18.8797	56.4	56.4	-2.21	56.64	7.00	0.694	0.562	769.0	621.9	616.8	534.5	456.7	-75.8	3
4	0.9810	18.5464	7.2	7.2	-2.02	38.20	4.63	0.687	0.542	761.7	600.7	598.3	519.4	470.4	-48.5	4
5	1.0000	17.6010	10.0	10.0	-2.41	40.48	2.00	0.672	0.512	746.2	568.2	567.5	503.9	484.1	-19.8	5

SL	PSI	RADIUS	PI	TI	TI-KEL	PS	IS	RMQ	PI/PTI	TI/TII	EFF	BLKAGE	SL
1	0.9021	20.3020	19.128	561.66	546.18	15.788	511.51	0.07276	1.5016	1.08285	0.9440	0.96000	1
2	0.9420	19.5566	18.855	559.50	543.68	15.593	509.56	0.07200	1.2830	1.07868	0.9379	0.96000	2
3	0.9610	18.8797	18.634	559.50	542.47	15.500	510.28	0.07141	1.2680	1.07868	0.8921	0.96000	3
4	0.9810	18.5464	18.429	559.40	541.14	15.436	511.11	0.07096	1.2540	1.07849	0.8512	0.96000	4
5	1.0000	17.6010	18.223	559.30	539.83	13.463	512.96	0.07084	1.2400	1.07829	0.8096	0.96000	5

PI/PTI 1.2737 EFF 0.9009 PT 18.719 MASS AVERAGED VALUES
 CORR. FLOW 71.870 CORR. RPM 5122.4
 TI 559.90 TI/TII 1.07945 CZ 616.24

Table 2-B. Design Blade Element Parameters for QCSEE UTW Fan (Continued).

STATION		1.90000		Z		180.250000		CORE		OGV		EXIT		ENGLISH UNITS				
SL	PSI	RADIUS	X	IMP	PHI	ALPHA	BETA	M-ABS	M-REL	C	M	CZ	U	CU	MU	SL		
1	0.9021	20.2070	0.	0.	-3.02	4.97	39.75	0.555	0.719	626.0	810.6	622.6	572.1	54.2	-217.9	1		
2	0.9420	19.2823	37.9	0.	-2.92	5.77	37.65	0.560	0.703	629.5	790.7	625.5	545.9	65.2	-482.6	2		
3	0.9810	18.8254	56.8	0.	-2.11	6.16	36.98	0.553	0.689	627.9	775.1	618.9	532.9	66.8	-466.1	3		
4	0.9810	18.5114	77.8	0.	-1.45	6.56	46.85	0.535	0.665	603.7	749.5	595.6	518.4	69.0	-449.4	4		
5	1.0000	17.7700	100.0	0.	-1.46	6.97	38.76	0.484	0.616	548.0	697.5	543.6	503.1	66.5	-476.6	5		
SL	PSI	RADIUS	FI	TT-REL	PS	IS	RMU	PT/PTI	TT/TTI	EFF	BLRAGE	SL						
1	0.9021	20.2070	18.653	583.74	15.150	529.05	0.07719	1.2693	1.08285	0.8510	0.98000	1						
2	0.9420	19.2823	18.578	576.55	15.014	526.52	0.07699	1.2681	1.07868	0.8803	0.98000	2						
3	0.9610	18.8234	18.347	577.21	14.900	527.20	0.07628	1.2484	1.07868	0.8319	0.98000	3						
4	0.9810	18.5114	17.941	575.82	14.760	529.06	0.07550	1.2206	1.07849	0.7473	0.98000	4						
5	1.0000	17.7700	17.186	574.80	14.645	534.31	0.07596	1.1694	1.07829	0.5842	0.98000	5						
SL	PSI	TRLC	PR-NUM	DFL-T	PP/W	CZ/CZ	SOLIDTY	F-TAN	F-AXL	F-LUEF	T-CUEF	SL						
1	0.9021	0.08864	0.9752	0.371	0.251	0.985	1.4411	484.71	159.20			1						
2	0.9420	0.05267	0.9853	0.352	0.271	0.990	1.5087	447.62	165.87			2						
3	0.9610	0.05590	0.9846	0.555	0.273	1.003	1.5436	434.15	168.32			3						
4	0.9810	0.09782	0.9735	0.374	0.265	1.002	1.5847	415.62	155.81			4						
5	1.0000	0.21166	0.9431	0.436	0.248	0.956	1.6445	384.81	110.57			5						
PT/PTI	1.2440	EFF	0.8101	PT	18.281	TT	559.90	TT/TTI	1.07945	CZ	610.07	ROM	PTZ/PTI	0.9766				
		COMR.	FLO.		73.589	CORR.	KPH		3122.4									

ORIGINAL PAGE IS
OF POOR QUALITY

Table 2-B. Design Blade Element Parameters for QCSEE UTW Fan (Concluded).

STATION 11.90000 Z 200.000000 BYPASS OGV EXIT										ENGLISH UNITS									
SL	PSI	RADIUS	Z	IMM	PHI	ALPHA	BETA	M-ABS	M-REL	C	M	CZ	U	CU	MU	SL			
1	0.	35.5000*	0.	0.	0.	0.	59.31	0.519	1.017	596.5	1168.7	596.5	1005.0	0.	-1005.0	1			
2	0.1000	34.2075	6.8	0.	-0.23	0.	57.62	0.537	1.002	614.1	1146.7	614.1	968.4	0.	-968.4	2			
3	0.2500	32.2271	22.4	0.	-0.21	0.	55.87	0.542	0.967	618.4	1102.2	618.4	912.3	0.	-912.3	3			
4	0.4000	30.1381	36.6	0.	-0.07	0.	54.06	0.543	0.926	618.5	1053.6	618.5	853.2	0.	-853.2	4			
5	0.6000	25.5089	67.7	0.	0.44	0.	49.98	0.535	0.832	608.4	946.0	608.4	724.4	0.	-724.4	5			
6	0.8000	23.5917	81.4	0.	0.93	0.	48.39	0.522	0.786	593.3	893.3	593.3	667.9	0.	-667.9	6			
7	0.9021	21.3435	96.7	0.	0.13	0.	50.58	0.456	0.686	490.7	782.1	490.7	604.2	0.	-604.2	7			
8	0.9022	21.3607	96.7	0.	0.13	0.	53.24	0.394	0.659	451.3	754.1	451.3	604.2	0.	-604.2	8			
9	0.9184	20.8630*	100.0	0.	0.	0.	54.09	0.374	0.637	427.7	729.2	427.7	590.6	0.	-590.6	9			

SL	PSI	RADIUS	PI	TI	TI=REL	PS	TS	RMU	PT/PTI	TI/TII	EFF	BLKAGE
1	0.	35.5000	19.601	579.60	663.66	16.315	549.99	0.08007	1.5336	1.11763	0.7304	0.94000
2	0.1000	34.2075	19.857	576.30	654.35	16.323	544.91	0.08085	1.3312	1.11107	0.8086	0.94000
3	0.2500	32.2271	19.967	572.90	642.18	16.347	541.07	0.08154	1.3586	1.10451	0.8756	0.94000
4	0.4000	30.1381	20.002	571.30	631.89	16.368	539.46	0.08188	1.3616	1.10143	0.9077	0.94000
5	0.6000	25.5089	19.665	569.10	617.76	16.369	538.29	0.08198	1.3517	1.09719	0.9252	0.94000
6	0.8000	23.5917	19.621	567.20	604.32	16.297	537.91	0.08178	1.3351	1.09352	0.9204	0.94000
7	0.9021	21.3435	18.516	561.66	592.05	16.253	541.13	0.08107	1.2399	1.08265	0.8246	0.94000
8	0.9022	21.3607	18.094	561.66	592.04	16.253	544.71	0.08054	1.2312	1.08285	0.7390	0.94000
9	0.9184	20.8630	17.896	560.78	589.81	16.253	545.55	0.08041	1.2176	1.08115	0.7136	0.94000

SL	PSI	TPLC	PR=RMU	DFL=1	U	DP/U	CZ/CZ	SOLIDTY	M=AVG	F=IAN	F=AXL	F=CUET	T=CUET
1	0.	0.10935	0.9750	0.366	0.176	0.987	1.2233	35.5000	784.67	163.01			
2	0.1000	0.04574	0.9870	0.330	0.191	0.999	1.2974	34.1914	764.66	190.98			
3	0.2500	0.03740	0.9910	0.317	0.216	0.987	1.4236	32.1929	732.65	194.99			
4	0.4000	0.03216	0.9920	0.318	0.243	0.976	1.5750	30.0792	715.14	203.00			
5	0.6000	0.03350	0.9910	0.342	0.314	0.955	1.9934	25.4698	677.18	223.94			
6	0.8000	0.03978	0.9890	0.362	0.354	0.930	2.2276	23.4505	636.99	222.20			
7	0.9021	0.11991	0.9680	0.454	0.437	0.798	2.5745	21.2628	505.24	151.81			
8	0.9022	0.12085	0.9700	0.393	0.482	0.625	2.5761	21.2604	60.64	-24.09			
9	0.9184	0.15785	0.9610	0.423	0.485	0.592	2.8676	20.4630	65.53	-37.04			

PI/PTI	1.3445	EFF	0.8746	PI	19.759	MASS AVERAGED VALUES	11	571.03	11/111	1.10090	LL	601.60	RUM	PI2/PTI	0.9879
COMM, FLOW	605.028	COMM, RPM	3091.8												

* Bypass OGV exit tip and hub radii listed in this table were changed to 35.5450 inches and 20.5900 inches, respectively, after the aero design was completed in order to improve transition of the fan flowpath into the bypass exhaust duct contours. The impact of these changes on OGV blade element parameters was estimated to be small, and the design data were not recomputed.

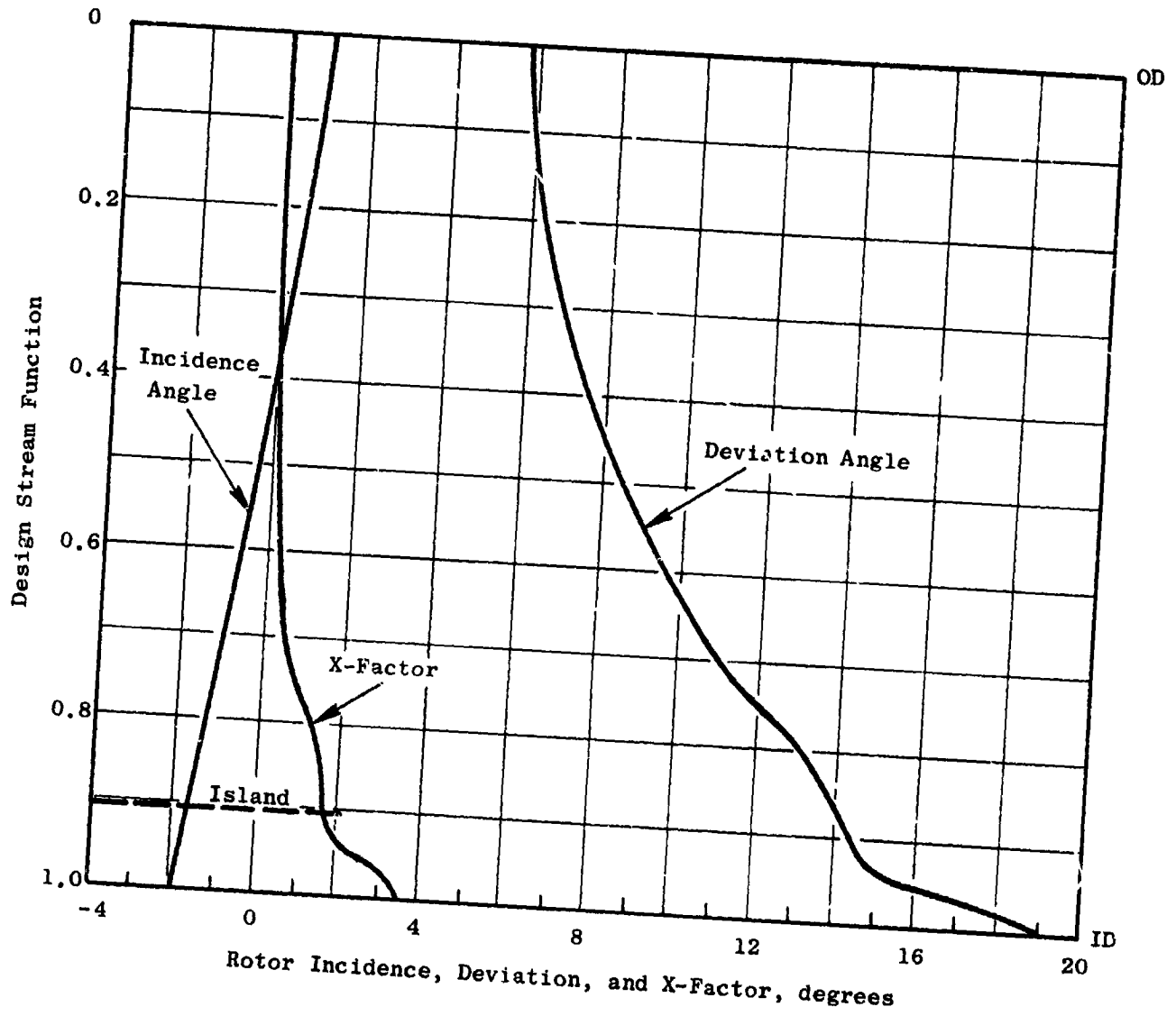


Figure 11. Rotor Incidence, Deviation, and Empirical Adjustment Angles.

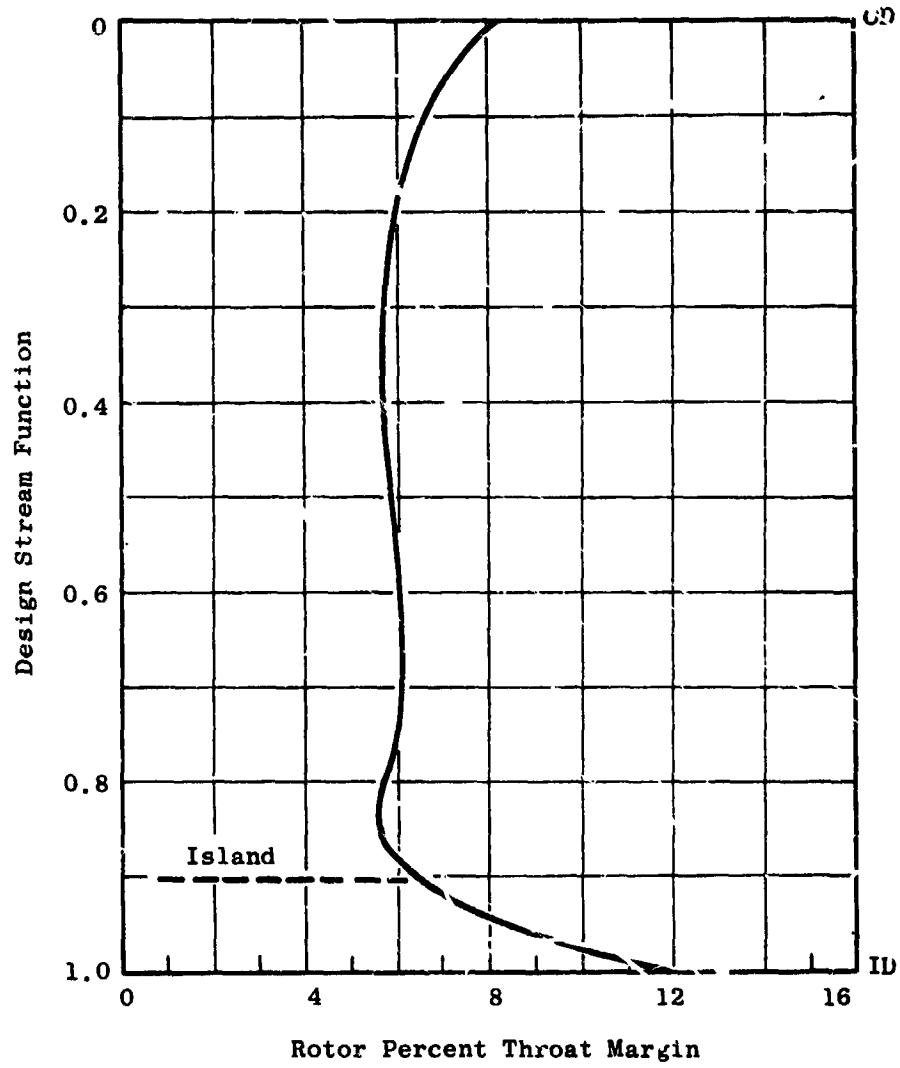


Figure 12. Rotor Throat Margin Distribution.

Section	Radius	
	(cm)	(in.)
1	85.8	33.8
2	76.2	30.0
3	66.8	26.3
4	57.2	22.5
5	47.7	18.8

Tip L.E. Radius = 90.2 cm (35.5 in.)
 Hub L.E. Radius = 0.1 cm (0.039 in.)

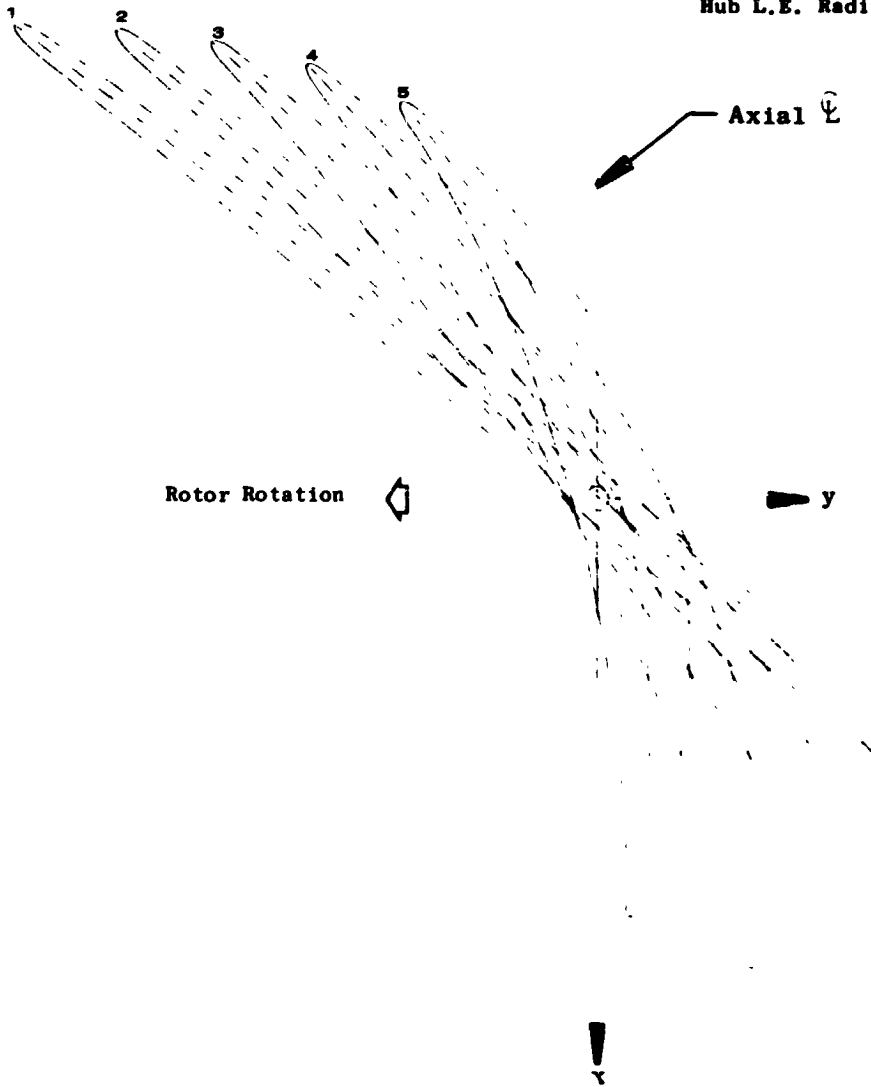


Figure 13. UTW Fan Rotor Blade Plane Sections.

ORIGINAL PAGE IS
OF POOR QUALITY

Table 3. UTW Fan Rotor Blade Coordinates.

SECTION 1 RADIUS 85.8 cm (33.8 in.)

Convex		Concave	
X (Axial)	Y	X (Axial)	Y
-3.57088	-4.59391	-3.57088	-4.59391
-3.58047	-4.57843	-3.55304	-4.59755
-3.58149	-4.55132	-3.52725	-4.58914
-3.57322	-4.51309	-3.49418	-4.56819
-3.55468	-4.46442	-3.45477	-4.53407
-3.52497	-4.40594	-3.40985	-4.48620
-3.48372	-4.33791	-3.35965	-4.42440
-3.43173	-4.25976	-3.30327	-4.34931
-3.28197	-4.03998	-3.14552	-4.13796
-3.10837	-3.78879	-2.96199	-3.89548
-2.93466	-3.54118	-2.77855	-3.65661
-2.76085	-3.29697	-2.59523	-3.42110
-2.58691	-3.05594	-2.41203	-3.18870
-2.41283	-2.81788	-2.22897	-2.95911
-2.23861	-2.58255	-2.04606	-2.73207
-2.02933	-2.30343	-1.82678	-2.46255
-1.81981	-2.02749	-1.60773	-2.19574
-1.61005	-1.75422	-1.38893	-1.93102
-1.40004	-1.48309	-1.17038	-1.66776
-1.18976	-1.21357	-0.95209	-1.40535
-0.97919	-0.94512	-0.73410	-1.14321
-0.76830	-0.67730	-0.51643	-0.88090
-0.55706	-0.40974	-0.29910	-0.61801
-0.34544	-0.14216	-0.08216	-0.35428
-0.13341	0.12568	0.13438	-0.08948
0.07905	0.39390	0.35048	0.17649
0.29200	0.66258	0.56610	0.44367
0.50541	0.93165	0.78125	0.71187
0.71939	1.20090	0.99583	0.98088
0.93446	1.46953	1.20933	1.25060
1.15118	1.73661	1.42117	1.52080
1.36959	2.00127	1.63132	1.79057
1.58962	2.26258	1.83985	2.05873
1.81122	2.51919	2.04682	2.32380
2.03423	2.76958	2.25237	2.58435
2.25847	3.01244	2.45670	2.83912
2.48369	3.24657	2.66004	3.08697
2.70963	3.47109	2.86266	3.32710
2.93604	3.68531	3.06482	3.55877
3.16264	3.88877	3.26679	3.78150
3.35143	4.04988	3.43513	3.99992
3.50232	4.17313	3.56998	4.09777
3.53436	4.18426	3.58462	4.13010
3.57185	4.16733	3.57185	4.16733

Table 3. UTW Fan Rotor Blade Coordinates (Continued).

SECTION 2 RADIUS 76.2 cm (30.0 in.)			
Convex		Concave	
X (Axial)	Y	X (Axial)	Y
-3.53096	-3.78711	-3.53096	-3.78711
-3.53951	-3.77219	-3.51429	-3.79124
-3.53964	-3.74671	-3.48973	-3.78440
-3.53068	-3.71117	-3.45787	-3.76615
-3.51173	-3.66625	-3.41950	-3.73590
-3.48194	-3.61259	-3.37527	-3.69315
-3.44093	-3.55049	-3.32533	-3.63779
-3.38936	-3.47948	-3.26875	-3.57053
-3.23593	-3.27533	-3.10711	-3.37975
-3.06179	-3.05086	-2.92182	-3.16812
-2.88750	-2.83311	-2.73667	-2.96328
-2.71310	-2.62119	-2.55163	-2.76416
-2.53857	-2.41421	-2.36672	-2.56974
-2.36391	-2.21141	-2.18195	-2.37919
-2.18911	-2.01213	-1.99731	-2.19170
-1.97915	-1.77680	-1.77595	-1.96984
-1.76893	-1.54478	-1.55484	-1.75039
-1.55840	-1.31538	-1.33404	-1.53261
-1.34752	-1.08803	-1.11360	-1.31584
-1.13622	-0.86234	-0.89358	-1.09966
-0.92445	-0.63802	-0.67403	-0.88369
-0.71217	-0.41484	-0.45498	-0.66769
-0.49933	-0.19267	-0.23650	-0.45148
-0.28588	0.02855	-0.01862	-0.23502
-0.07178	0.24883	0.19860	-0.01830
0.14300	0.46807	0.41515	0.19855
0.35854	0.68608	0.63093	0.41533
0.57513	0.90231	0.84567	0.63193
0.79303	1.11612	1.05909	0.84814
1.01230	1.32693	1.27115	1.06331
1.23284	1.53411	1.48193	1.27675
1.45459	1.73698	1.69151	1.48777
1.67745	1.93487	1.89997	1.69568
1.90130	2.12710	2.10745	1.89976
2.12599	2.31301	2.31408	2.09936
2.35136	2.49202	2.52003	2.29388
2.57722	2.66361	2.72549	2.48276
2.80339	2.82735	2.93065	2.66553
3.02965	2.98287	3.13571	2.84173
3.25581	3.12995	3.34088	3.01103
3.44407	3.24594	3.51206	3.14659
3.59086	3.33233	3.64598	3.24884
3.62375	3.33841	3.66485	3.27823
3.65778	3.31641	3.65778	3.31641

ORIGINAL PAGE IS
OF POOR QUALITY

Table 3. UTW Fan Rotor Blade Coordinates (Continued).

SECTION 3 RADIUS 66.8 cm (26.3 in.)

Convex		Concave	
X (Axial)	Y	X (Axial)	Y
-3.44902	-3.03130	-3.44902	-3.03130
-3.45631	-3.01728	-3.43399	-3.03624
-3.45564	-2.99433	-3.41140	-3.03192
-3.44652	-2.96289	-3.38170	-3.01797
-3.42827	-2.92354	-3.34544	-2.99392
-3.40027	-2.87680	-3.30309	-2.95936
-3.36226	-2.82288	-3.25468	-2.91428
-3.31482	-2.76130	-3.19940	-2.85937
-3.15984	-2.56706	-3.02637	-2.68941
-2.99245	-2.36411	-2.83784	-2.51105
-2.82463	-2.16755	-2.64974	-2.33963
-2.65638	-1.97693	-2.46207	-2.17435
-2.48767	-1.79173	-2.27486	-2.01442
-2.31848	-1.61151	-2.08814	-1.85914
-2.14878	-1.43584	-1.90191	-1.70781
-1.94447	-1.23052	-1.67912	-1.53056
-1.73937	-1.03059	-1.45712	-1.35712
-1.53340	-0.83559	-1.23598	-1.18674
-1.32651	-0.64513	-1.01577	-1.01875
-1.11859	-0.45896	-0.79658	-0.85271
-0.90958	-0.27691	-0.57850	-0.68827
-0.69938	-0.09890	-0.36159	-0.52522
-0.48796	0.07507	-0.14590	-0.36339
-0.27532	0.24498	0.06856	-0.20265
-0.06144	0.41083	0.28178	-0.04291
0.15371	0.57254	0.49373	0.11595
0.37024	0.73003	0.70431	0.27396
0.58823	0.88309	0.91342	0.43096
0.80777	1.03142	1.12098	0.58671
1.02884	1.17467	1.32702	0.74066
1.25131	1.31237	1.53166	0.89227
1.47503	1.44402	1.73504	1.04101
1.69984	1.56905	1.93733	1.18636
1.92553	1.68698	2.13875	1.32781
2.15181	1.79732	2.33957	1.46492
2.37838	1.89976	2.54010	1.59735
2.60492	1.99412	2.74067	1.72484
2.83111	2.08047	2.94158	1.84731
3.05681	2.15904	3.14299	1.96460
3.28185	2.22986	3.34505	2.07641
3.46864	2.28300	3.51417	2.16531
3.61268	2.32088	3.64570	2.23165
3.64345	2.31843	3.66807	2.25485
3.66937	2.29101	3.66937	2.29101

Table 3. UTW Fan Rotor Blade Coordinates (Continued).

SECTION 4 RADIUS 57.2 cm (22.5 in.)

Convex		Concave	
X (Axial)	Y	X (Axial)	Y
-3,27656	-2,27702	-3,27656	-2,27702
-3,28322	-2,26279	-3,26204	-2,28303
-3,28186	-2,24050	-3,23980	-2,28070
-3,27207	-2,21053	-3,21017	-2,26971
-3,25332	-2,17341	-3,17355	-2,24967
-3,22513	-2,12958	-3,13024	-2,22029
-3,18733	-2,07922	-3,08018	-2,18164
-3,14041	-2,02184	-3,02260	-2,13446
-3,00531	-1,86253	-2,86579	-2,00785
-2,84845	-1,68435	-2,68165	-1,86527
-2,69081	-1,51211	-2,49829	-1,72907
-2,53231	-1,34548	-2,31578	-1,59863
-2,37289	-1,18419	-2,13420	-1,47341
-2,21244	-1,02809	-1,95364	-1,35305
-2,05092	-0,87713	-1,77416	-1,23720
-1,85563	-0,70271	-1,56025	-1,10369
-1,65868	-0,53560	-1,34800	-0,97568
-1,46005	-0,37578	-1,13742	-0,85268
-1,25975	-0,22324	-0,92852	-0,73420
-1,05776	-0,07797	-0,72130	-0,61984
-0,85414	0,06003	-0,51571	-0,50917
-0,64895	0,19075	-0,31170	-0,40182
-0,44225	0,31420	-0,10920	-0,29746
-0,23413	0,43043	0,09188	-0,19578
-0,02466	0,53944	0,29162	-0,09654
0,18612	0,64122	0,49005	0,00047
0,39814	0,73569	0,68723	0,09543
0,61134	0,82282	0,88324	0,18838
0,82557	0,90254	1,07821	0,27929
1,04070	0,97480	1,27229	0,36809
1,25652	1,03950	1,46567	0,45467
1,47281	1,09659	1,65858	0,53892
1,68933	1,14604	1,85126	0,62070
1,90583	1,18789	2,04397	0,69984
2,12215	1,22220	2,23685	0,77609
2,33818	1,24891	2,43003	0,84904
2,55368	1,26786	2,62373	0,91817
2,76842	1,27875	2,81820	0,98277
2,98190	1,28127	3,01392	1,04212
3,19369	1,27534	3,21134	1,09559
3,36866	1,26400	3,37737	1,13521
3,50345	1,25130	3,50742	1,16266
3,52868	1,24005	3,53283	1,17758
3,54352	1,20850	3,54352	1,20850

Table 3. UTW Fan Rotor Blade Coordinates (Concluded).

SECTION 5 RADIUS 44.7 cm (18.8 in.)			
Convex		Concave	
X (Axial)	Y	X (Axial)	Y
-2,99111	-1,53332	-2,99111	-1,53332
-2,99661	-1,51937	-2,97778	-1,54019
-2,99415	-1,49848	-2,95672	-1,53986
-2,98342	-1,47101	-2,92817	-1,53206
-2,96398	-1,43741	-2,89242	-1,51649
-2,93547	-1,39809	-2,84966	-1,49292
-2,89777	-1,35321	-2,79978	-1,46149
-2,85128	-1,30229	-2,74206	-1,42298
-2,74616	-1,19129	-2,62085	-1,34350
-2,60488	-1,04793	-2,45456	-1,23970
-2,46249	-0,91015	-2,28934	-1,14224
-2,31901	-0,77783	-2,12523	-1,05062
-2,17438	-0,65084	-1,96226	-0,96435
-2,02861	-0,52907	-1,80043	-0,88293
-1,88167	-0,41240	-1,63979	-0,80592
-1,70357	-0,27903	-1,44876	-0,71897
-1,52347	-0,15302	-1,25975	-0,63765
-1,34115	-0,03456	-1,07296	-0,56178
-1,15662	0,07596	-0,88837	-0,49114
-0,97013	0,17822	-0,70574	-0,42527
-0,78186	0,27207	-0,52490	-0,36372
-0,59214	0,35744	-0,34551	-0,30593
-0,40109	0,43439	-0,16744	-0,25140
-0,20852	0,50299	0,00911	-0,19998
-0,01449	0,56305	0,18419	-0,15156
0,18120	0,61427	0,35762	-0,10623
0,37827	0,65609	0,52966	-0,06403
0,57603	0,68809	0,70102	-0,02487
0,77398	0,71018	0,87218	0,01129
0,97134	0,72250	1,04394	0,04463
1,16778	0,72543	1,21662	0,07529
1,36313	0,71937	1,39038	0,10335
1,55717	0,70473	1,56546	0,12878
1,74974	0,68192	1,74201	0,15152
1,94060	0,65140	1,92026	0,17148
2,12950	0,61378	2,10047	0,18861
2,31654	0,56974	2,28255	0,20292
2,50190	0,51979	2,46631	0,21426
2,68565	0,46433	2,65167	0,22235
2,86787	0,40358	2,83857	0,22666
3,01856	0,34896	2,99548	0,22686
3,13513	0,30368	3,10630	0,22470
3,15489	0,28737	3,13939	0,22758
3,16082	0,25675	3,16082	0,25675

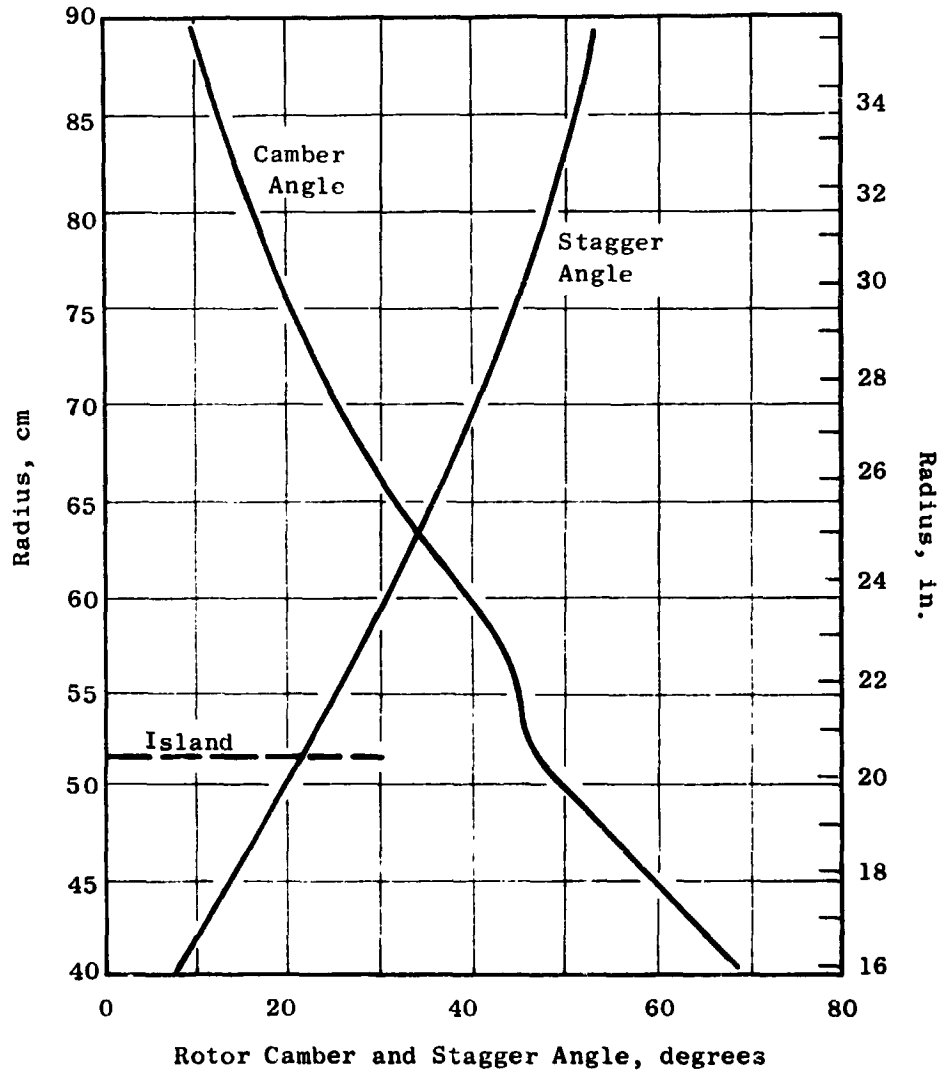


Figure 14. UTW Fan Rotor Camber and Stagger Angle Radial Distributions.

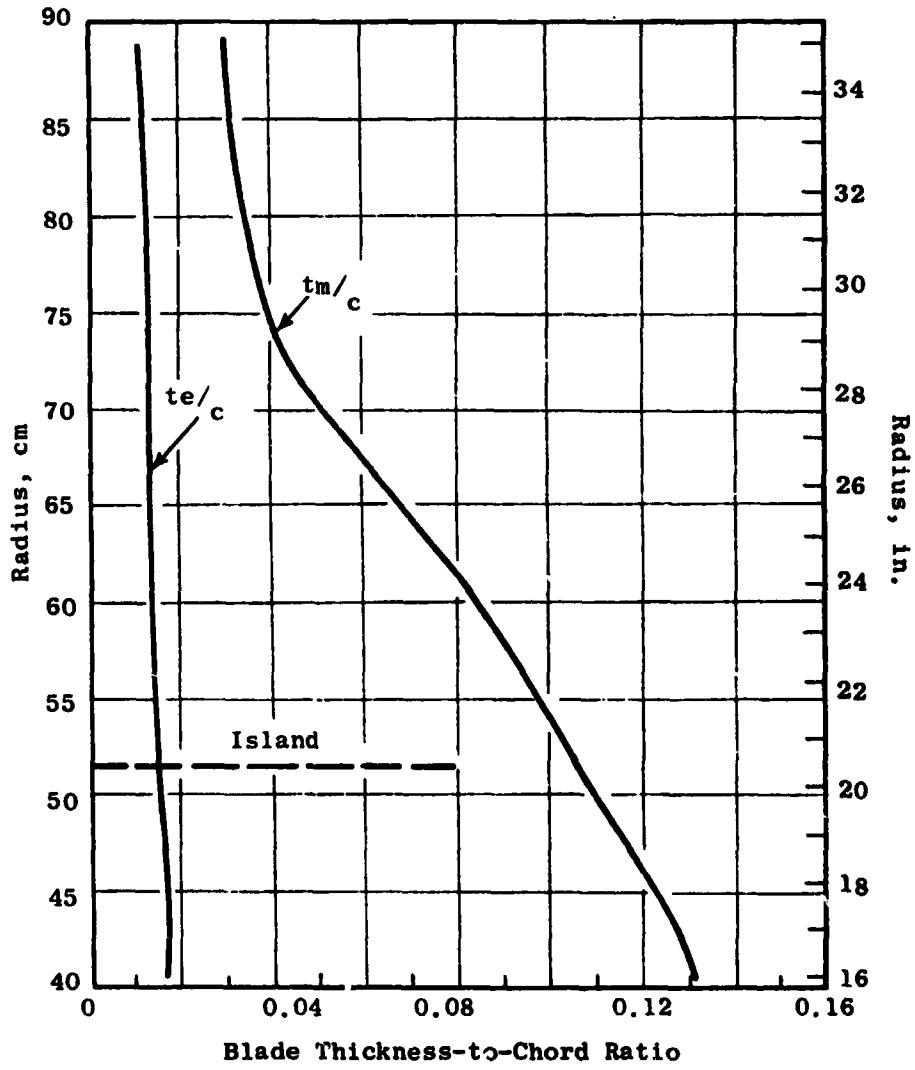


Figure 15. UTW Fan Blade Thickness Distributions.

configuration (such as reduction in the tip chord or a reduction in blade number) to reduce the hub thickness-to-chord ratio to 0.10, a value more representative of past experience.

2.7 CORE OGV DESIGN

A moderately low aspect ratio of 1.3 was selected for the core portion OGV to provide a rugged mechanical system. This selection was in recognition of the potentially severe aeromechanical environment (i.e., large rotor wakes) of the core OGV because of its small size in relationship to that of the rotor blade. A solidity at the ID of 1.65 was selected to yield reasonable levels of diffusion factor, Figure 10. The number of vanes which resulted is 96. Radial distribution of total pressure loss coefficient, diffusion factor, Mach number, and air angle are presented in Figure 10.

Profiles for the core portion OGV are a modified NASA 65-series thickness distribution on a circular-arc meanline. The incidence angle over the outer portion of the span was selected from a correlation of NASA low-speed cascade data. Locally, in the ID region, the incidence angle was reduced 0.07 radian (4°). This local reduction in incidence was in recognition of traverse data results on other high-bypass fan configurations which show core stator inlet air angles several degrees higher than the axisymmetric calculated values. The deviation angle was obtained from Carter's Rule as was described for the rotor blade, but no empirical adjustment was made. The resulting incidence and deviation angles and throat margin are shown in Figure 16. The throat area for the selected geometry was checked to ensure sufficient margin to pass the design flow. The minimum margin relative to the critical contraction ratio was 6%, which is sufficient to avoid choke. Resulting geometric parameters for the core OGV are presented in Figure 17. Figure 18 is a cylindrical section of the core OGV at the pitch line radius. A tabulation of the coordinates for this core OGV is given in Table 4.

2.8 TRANSITION DUCT STRUT DESIGN

The transition duct flowpath is shown in Figure 19. The ratio of duct exit to duct inlet flow area is 1.02. There are six struts in the transition duct which are aerodynamically configured to remove the 0.105 radian (6°) of swirl left in the air by the core OGV's and to house the structural spokes of the composite wheels (see Figure 2). In addition, at engine station 196.5 (Figure 2), the 6 and 12 o'clock strut positions must house radial accessory drive shafts. The number of struts and axial position of the strut trailing edge were selected identical with the F101 engine to minimize unknowns in the operation of the core engine system. Axial position and thickness requirements of the composite wheel spokes were dictated by mechanical considerations. The axial location of the strut leading edge at the OD was determined by its proximity to the splitter leading edge. At the OD flowpath, the strut leading edge is 17.8 mm (0.7 in.) forward of the wheel spoke. A relatively blunt strut leading edge results from the 26.7 mm (1.05 in.) wheel spoke

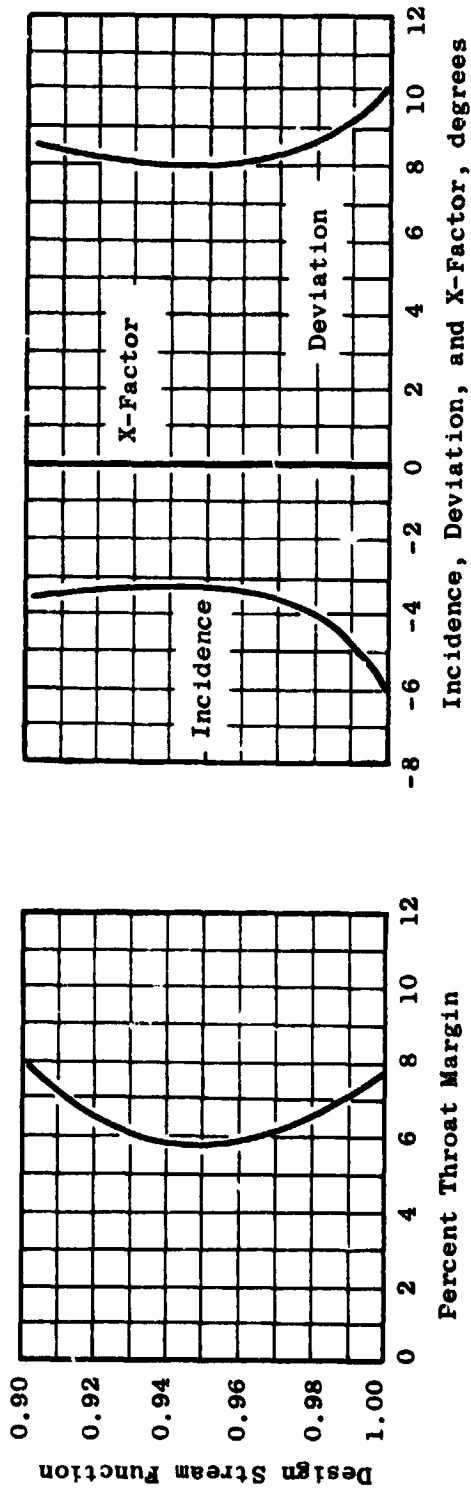


Figure 16. Core OGV Aerodynamic Design Characteristics.

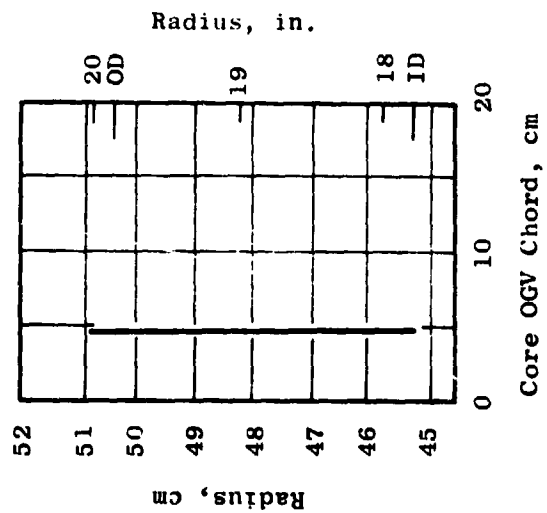
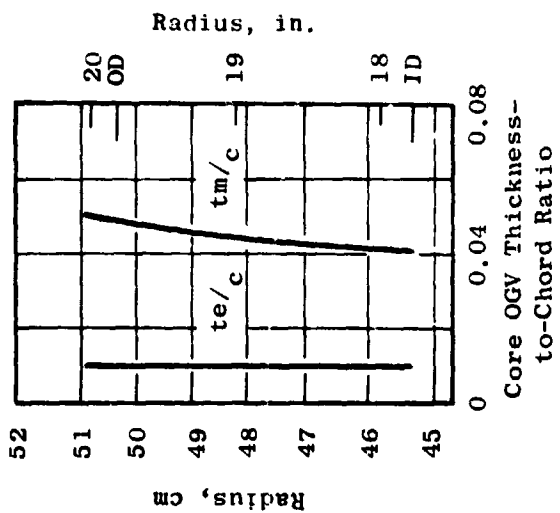
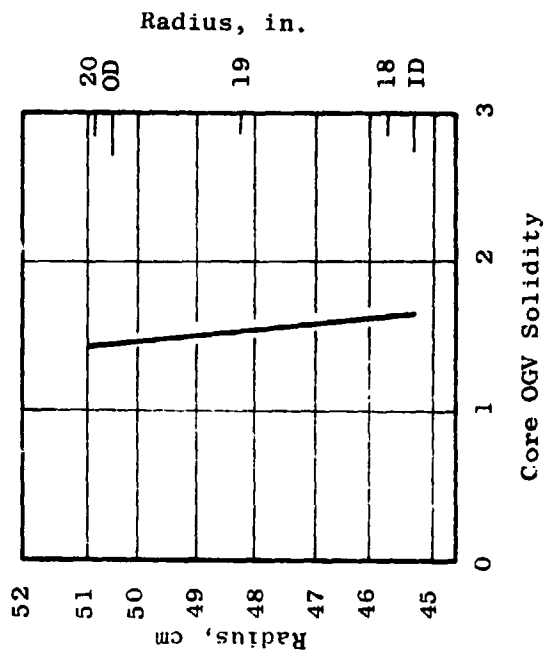
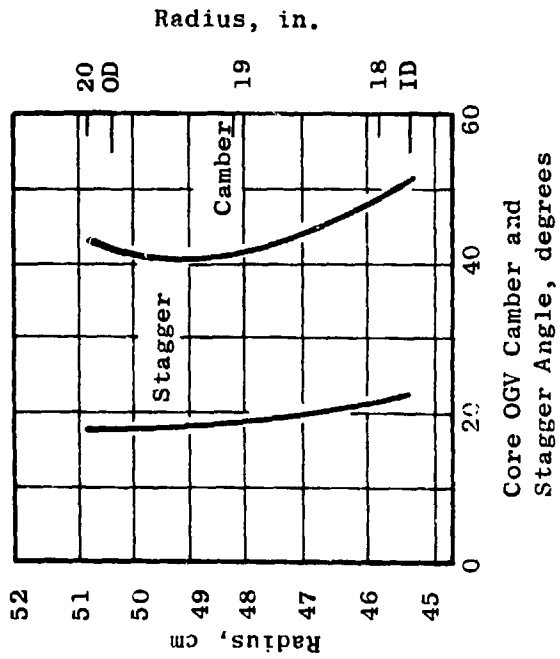


Figure 17. Core OGV Geometry Parameters.

ORIGINAL PAGE IS
OF POOR QUALITY

ORIGINAL PAGE IS
OF POOR QUALITY

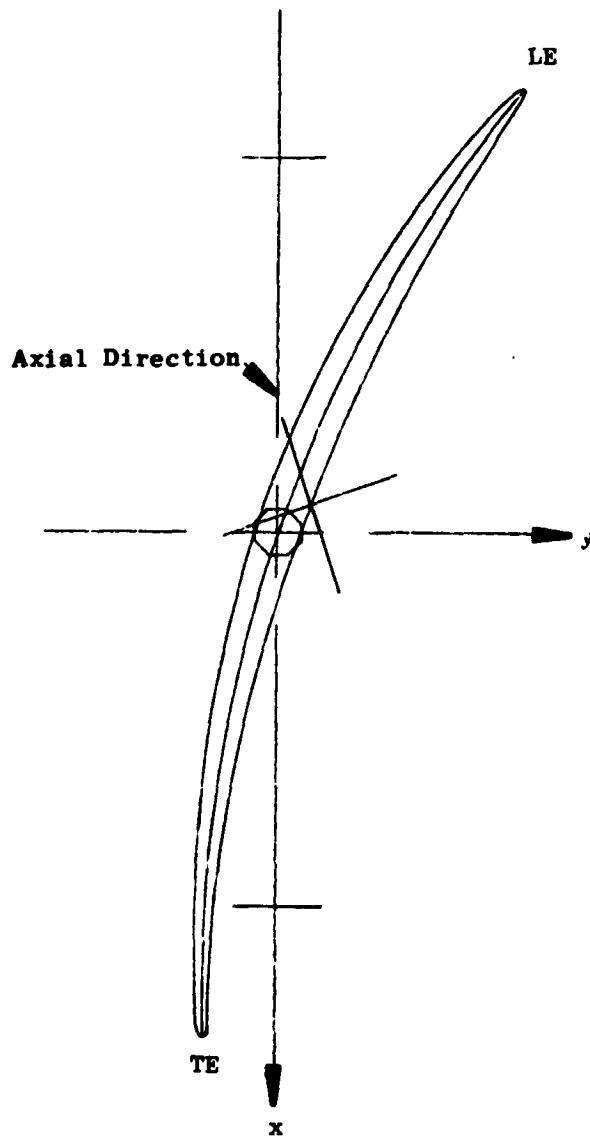


Figure 18. Cylindrical Section of Core
OGV at the Pitch Line Radius.

Table 4. UTW Fan Core OGV Coordinates at the Pitch Line Radius.

Convex		Concave	
X (Axial)	Y	X (Axial)	Y
-0.842769	0.477539	-0.842769	0.477539
-0.842102	0.478085	-0.843193	0.476788
-0.841193	0.478426	-0.843371	0.475831
-0.840041	0.478562	-0.843303	0.474671
-0.838648	0.478489	-0.842988	0.473308
-0.837016	0.478207	-0.842422	0.471747
-0.835148	0.477713	-0.841604	0.469990
-0.833043	0.477005	-0.840531	0.468041
-0.830706	0.476081	-0.839199	0.465902
-0.825930	0.473879	-0.836147	0.461586
-0.816825	0.468976	-0.829578	0.453512
-0.795126	0.455609	-0.811971	0.434780
-0.752668	0.428386	-0.775318	0.399261
-0.710699	0.401338	-0.737517	0.365474
-0.668893	0.374802	-0.698908	0.333049
-0.585404	0.323526	-0.619675	0.271892
-0.501676	0.274929	-0.538221	0.215193
-0.417507	0.229049	-0.454815	0.162726
-0.332770	0.185866	-0.369635	0.114358
-0.247368	0.145345	-0.282819	0.070005
-0.161246	0.107397	-0.194455	0.029661
-0.074357	0.071905	-0.104611	-0.006417
0.013395	0.038873	-0.013395	-0.038873
0.102065	0.008204	0.079131	-0.067022
0.191787	-0.019959	0.172840	-0.091196
0.282669	-0.045471	0.267634	-0.111499
0.374803	-0.068200	0.363446	-0.128002
0.468270	-0.087992	0.460225	-0.140766
0.563146	-0.104640	0.557937	-0.149878
0.659491	-0.117933	0.656874	-0.155395
0.757358	-0.127551	0.756149	-0.157452
0.856774	-0.133069	0.856712	-0.156245
0.876843	-0.133602	0.876951	-0.155667
0.896972	-0.133921	0.897236	-0.154995
0.917161	-0.134016	0.917569	-0.154238
0.937408	-0.133872	0.937951	-0.153407
0.948266	-0.133695	0.948850	-0.152936
0.954694	-0.136013	0.955078	-0.150279
0.958048	-0.142994	0.958048	-0.142994

thickness requirement. The wheel spoke is radial. The axial lean of the strut leading edge provides relief from the LE bluntness at lower radii and makes the LE approximately normal to the incoming flow. Since the inlet Mach number in the OD region is less than 0.5, and since the boundary layer along the outer wall initiates at the splitter LE, no significant aerodynamic penalty was assessed because of the bluntness. A NASA 65-series thickness distribution was selected for the basic profile thickness which was modified for the special considerations required in this design. The strut thickness is the same for all radii aft of the forward wheel spoke LE (Figure 19) to facilitate fabrication. A cylindrically cut cross section showing the nominal strut geometry at three radii is shown in Figure 20. The thickness distribution for the 6 and 12 o'clock struts was modified for the envelope of the radial drive shaft. Cylindrically cut cross sections of these struts are also shown in Figure 20. The forward 40% chord of these modified sections is identical to that of the nominal strut geometry. Aft of the forward wheel spoke LE, the strut thickness is the same for all radii. The core engine has demonstrated operation in the presence of a similar thick strut in the F101 application without duress.

2.9 VANE-FRAME (FAN BYPASS OGV) DESIGN

The vane-frame performs the dual function of an outlet guide vane for the bypass flow and a frame support for the engine components and nacelle. It is a common piece of hardware for both the UTW and OTW engine fans. It is integrated with the pylon which houses the radial drive shaft at engine station 195.5 (see Figure 2), houses the engine mount at approximately engine station 210, provides an interface between the propulsion system and the aircraft system, and houses the forward thrust links. Furthermore, the vane-frame acts as an inlet guide vane for the UTW fan when in the reverse mode of operation.

A conventional OGV system turns the incoming flow to axial. Housing requirements of the pylon dictate a geometry which requires the OGV's to underturn approximately 0.174 radian (10°) on one side and to overturn approximately 0.174 radian (10°) on the other side. The vane must be tailored to downstream vector diagrams which conform to the natural flow field around the pylon to avoid creating velocity distortions in the upstream flow. Ideally each vane would be individually tailored. However, to avoid excessive costs, five vane geometry groups were selected as adequate.

The Mach number and air angle at the inlet to the vane-frame (far bypass OGV) are shown in Figure 21 for both the UTW and OTW fans. In the outer portion of the bypass duct annulus, the larger air angle in the UTW environment results in a less negative incidence angle than for the OTW environment. Mach number in the outer portion of the annulus is also higher in the UTW environment. When selecting incidence angles, a higher Mach number environment naturally leads to the desire to select a less negative incidence angle. The amount by which the incidence angle would naturally be increased due to the higher Mach number UTW environment is approximately equal to the increase in the inlet air angle of the UTW environment. In the inner portion of the annulus, the inlet Mach number and air angle are higher for the OTW environment.

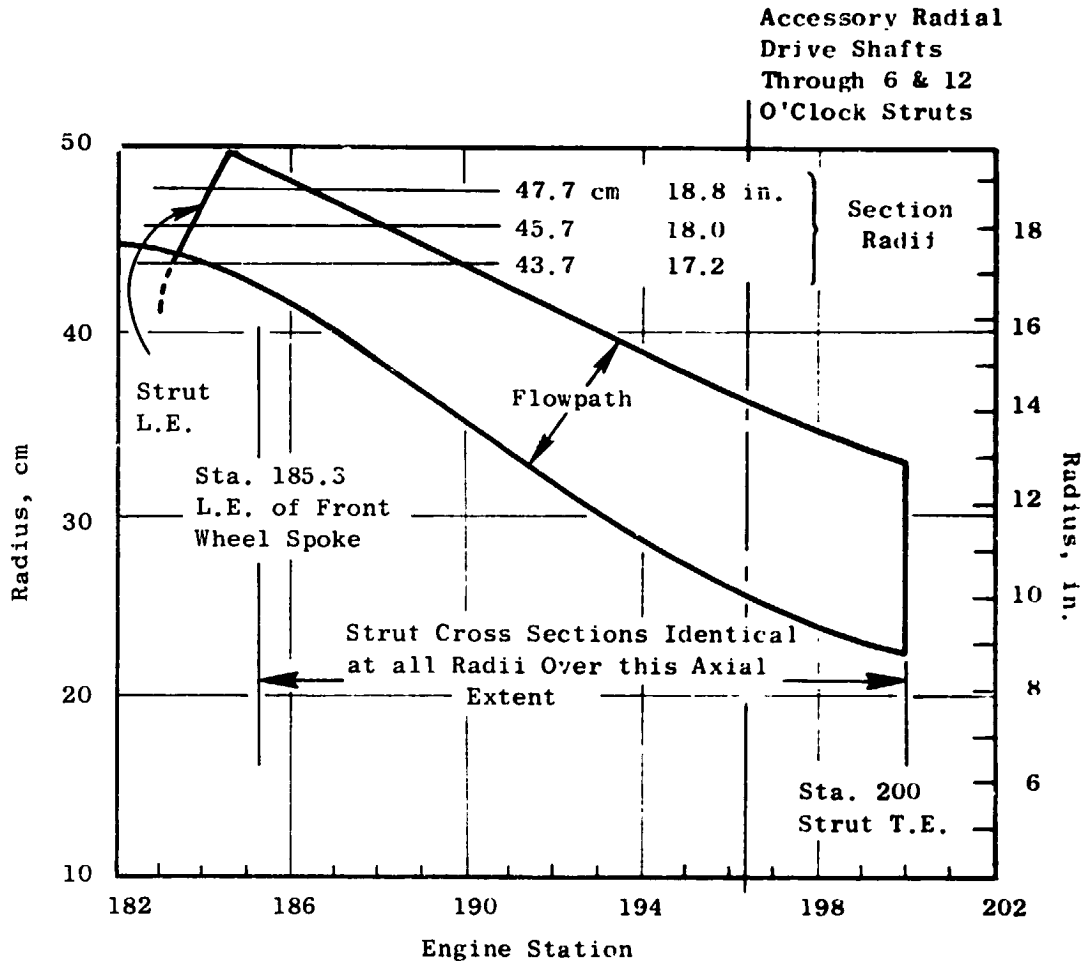


Figure 19. Transition Duct Flowpath.

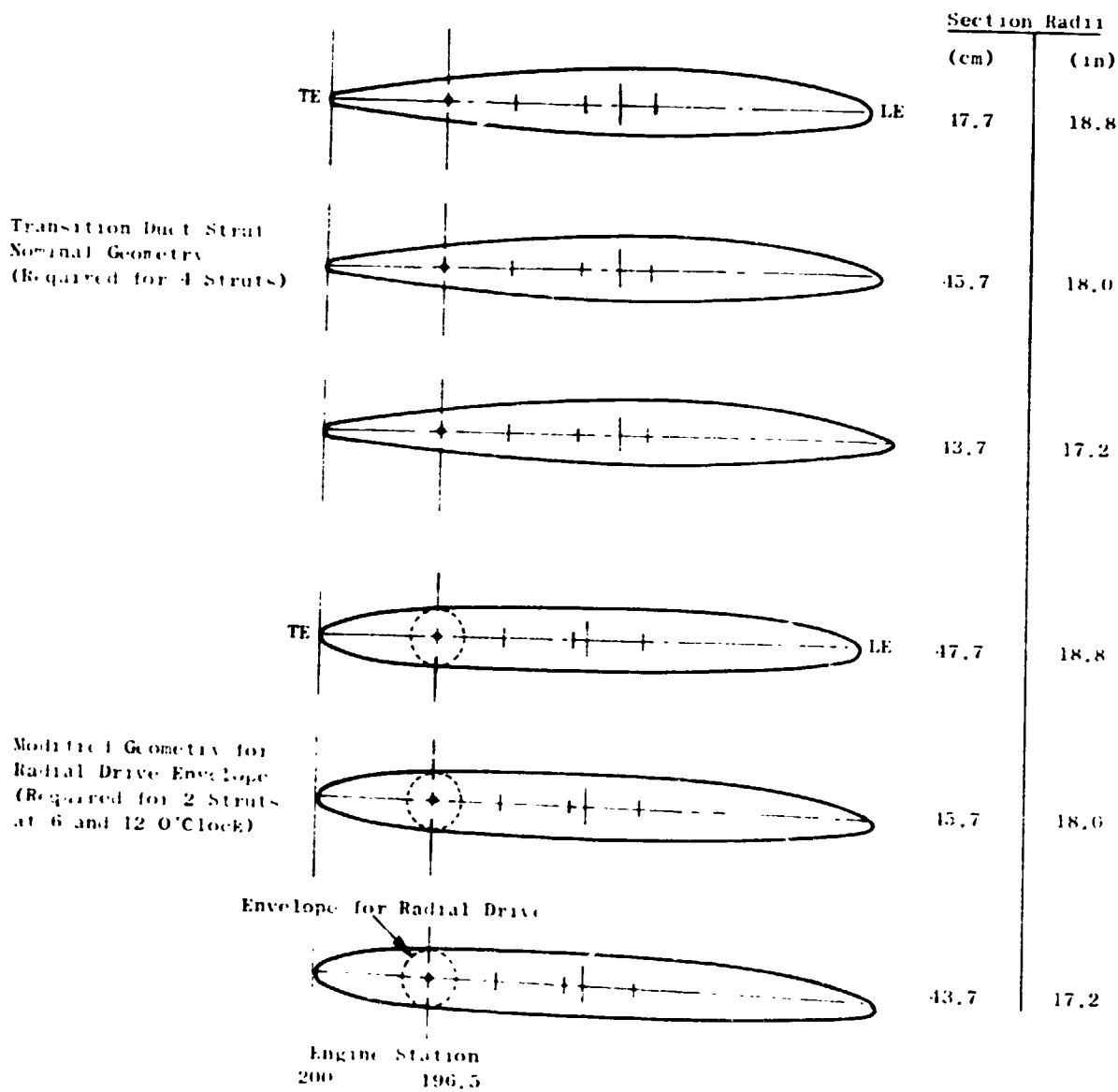


Figure 20. Nominal and Modified Transition Duct Strut Cylindrical Sections.

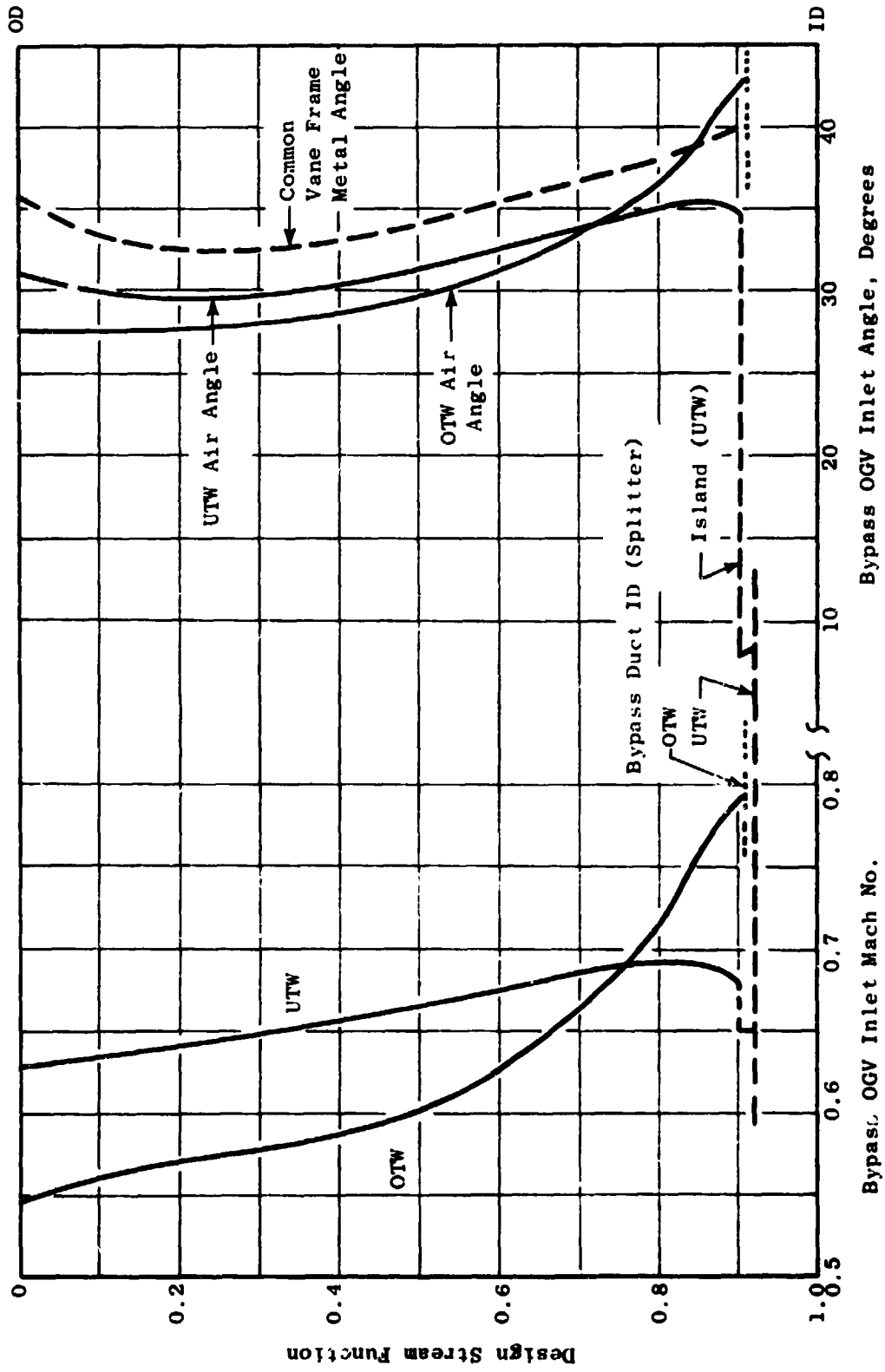


Figure 21. Vane-Frame (Fan Bypass OGV) Aerodynamic Environment.

The natural increase in incidence angle desired because of the higher Mach number is approximately the same as the increase in the inlet air angle. As a result of these considerations, no significant aerodynamic performance penalty is assessed to using common hardware for both the UTW and OTW fans.

Locally, near the bypass duct ID, there is a discontinuity in the aerodynamic environment of the UTW configuration. This discontinuity represents that portion of the flow which passes under the island but bypasses the splitter. The calculation ignored mixing across the vortex sheet. In the design of the vane geometry, no special considerations were incorporated because of this discontinuity, since it is believed that in a real fluid the mixing process will greatly diminish the vortex strength.

The vane chord at the OD was selected largely by the mechanical requirement of axial spacing between the composite frame spokes. At the ID, the vane leading edge was lengthened primarily to obtain an aerodynamically reasonable leading edge fairing on the pylon compatible with the envelope requirements of the radial drive shaft. The ID region is significantly more restrictive in this regard because of choking considerations, particularly for the OTW environment, with the reduced circumferential spacing between vanes. The solidity resulting from 33 vanes, an acoustic requirement, was acceptable from an aerodynamic loading viewpoint as shown in Figure 22. The two diffusion factor curves are a result of the two aerodynamic environments, UTW and OTW, to which the common vane frame geometry is exposed. The thickness is a modified NASA 65-series distribution. Maximum-thickness and trailing-edge thickness-to-chord ratios of 0.08 and 0.02, respectively, were selected at the OD. The same maximum thickness and trailing edge thickness were used at all other radii which results in maximum-thickness and trailing edge thickness-to-chord ratios of 0.064 and 0.016, respectively, at the ID.

As a guide in the selection of the overall vector diagram requirements of the vane-frame, a circumferential analysis of an approximate vane geometry (including the pylon) was performed. This analysis indicated, for uniform flow at vane inlet, that the vane discharge Mach number was approximately constant circumferentially and that the discharge air angle was nearly linear circumferentially between the pylon wall angles. Figure 23, an unwrapped cross section at the ID, shows the flow field calculated by this analysis. The specific design criteria selected for the layout of the five vane geometry groups were to change the average discharge vector diagram with zero swirl to vector diagrams with $\pm 5^\circ$ of swirl and $\pm 10^\circ$ of swirl.

The meanline shapes for each of the five vane groups vary. For the vane group which overturns the flow by $+10^\circ$, the meanline is approximately a circular arc. As a result of passage area distribution and choking considerations, the meanline shape employed in the forward 25% chord region of this vane group was retained for the other four groups.

The incidence angle for all vane groups was the same and was selected for the group with the highest camber. A correlation of NASA low-speed cascade data was the starting point for the incidence selection. Over the outer portion of the vane, where the inlet Mach number is lower, the incidence

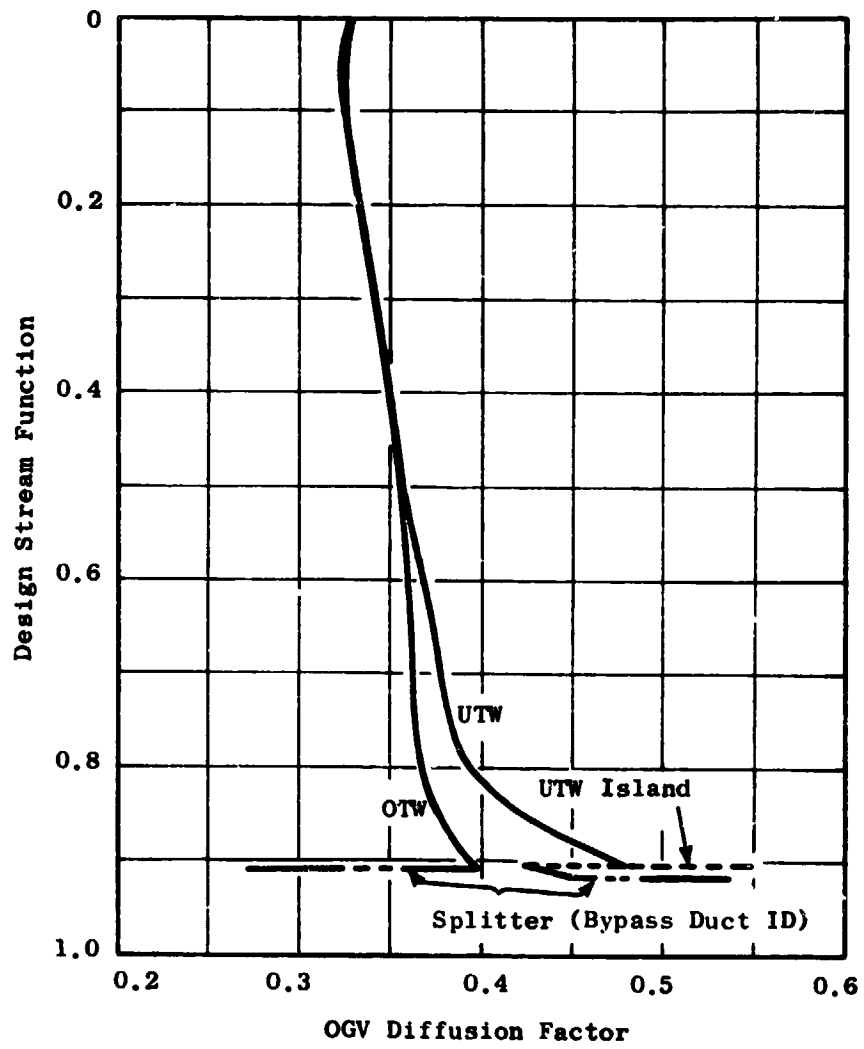


Figure 22. Vane-Frame (Fan Bypass OGV) Diffusion Factor for Nominal Vanes.

ORIGINAL PAGE IS
OF POOR QUALITY

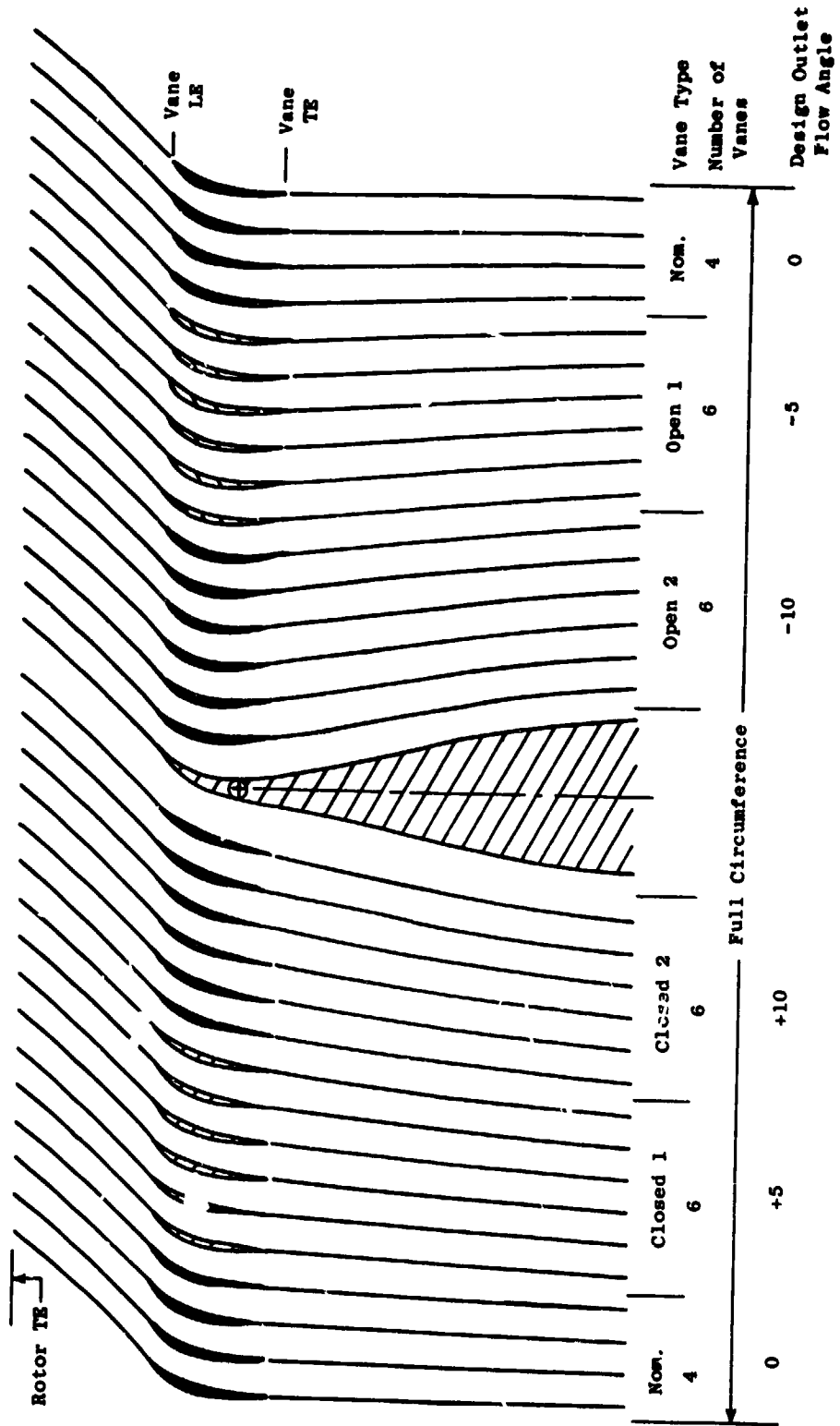


Figure 23. Vane-Frame (Fan Bypass OGV) Unwrapped Section at ID.

angles were slanted to the low side of the correlation. This was done in consideration of the reverse thrust mode of operation for the UTW fan. In this mode, the OGV's impart a swirl counter to the direction of rotor rotation. Additional vane leading edge camber tends to increase the counterswirl and therefore increase the pumping capacity of the fan in reverse. In the inner portion of the vane, the incidence angles are higher than suggested by the correlation because of the higher inlet Mach number. Also, in the reverse mode of operation, this reduction in vane leading edge camber in the ID region reduces the swirl for that portion of the fluid which enters the core engine and tends to reduce its pressure drop.

The deviation angle for each of the five vane groups was calculated from Carter's Rule as described for the rotor. The portion of the meanline aft of the 25% chord point approximates a circular arc blending between the front circular arc and the required trailing edge angle. For the vane group which underturns the flow by 10° , the aft portion of the blade has little camber. Figure 24 shows an unwrapped cross section at the ID of two of the 10° over-cambered vanes and two of the 10° under cambered vanes adjacent to the pylon. Note that the spacing between the pylon and the first under cambered vane is 50% larger than averages. This increased spacing was required to open the passage internal area, relative to the capture area, to retrieve the area blocked by the radial drive shaft envelope requirements.

Table 5 gives the detailed coordinate data for the two vane geometries and the pylon leading edge geometry shown in Figure 24. The coordinate data for the nominal vane geometry at three radial locations are also given in this table. The vane coordinate data are in inches.

Radial distributions of camber and stagger for the nominal and two extreme vane geometries are shown in Figure 25. Radial distributions of chord and solidity for the nominal vane are shown in Figure 26. The design held the leading and trailing edge axial projection common for all five groups which results in slightly different chord lengths for the other four vane types.

2.10 FAN PERFORMANCE BASED ON SCALE MODEL TESTS

Aerodynamic performance data in forward and reverse thrust modes were obtained from a 50.8-cm (20-inch)-diameter scale model of the UTW engine fan. This simulator had adjustable-rotor blades, allowing forward fan performance to be measured at the design stagger angle and with the blades opened 5° and closed 5° from the design forward value. Complete results of these tests are described by Giffin, et. al.,* and key results relating to the adequacy of the fan design for use in the UTW engine are presented in this section.

*Giffin, R.G.; McFalls, R.A.; and Beacher, B.F.; "Fan Aerodynamic and Aero-mechanical Performance of a 50.8-cm (20-inch)-Diameter 1.34PR Variable Pitch Fan with Core Flow," NASA CR-135017, 1975 (to be published).

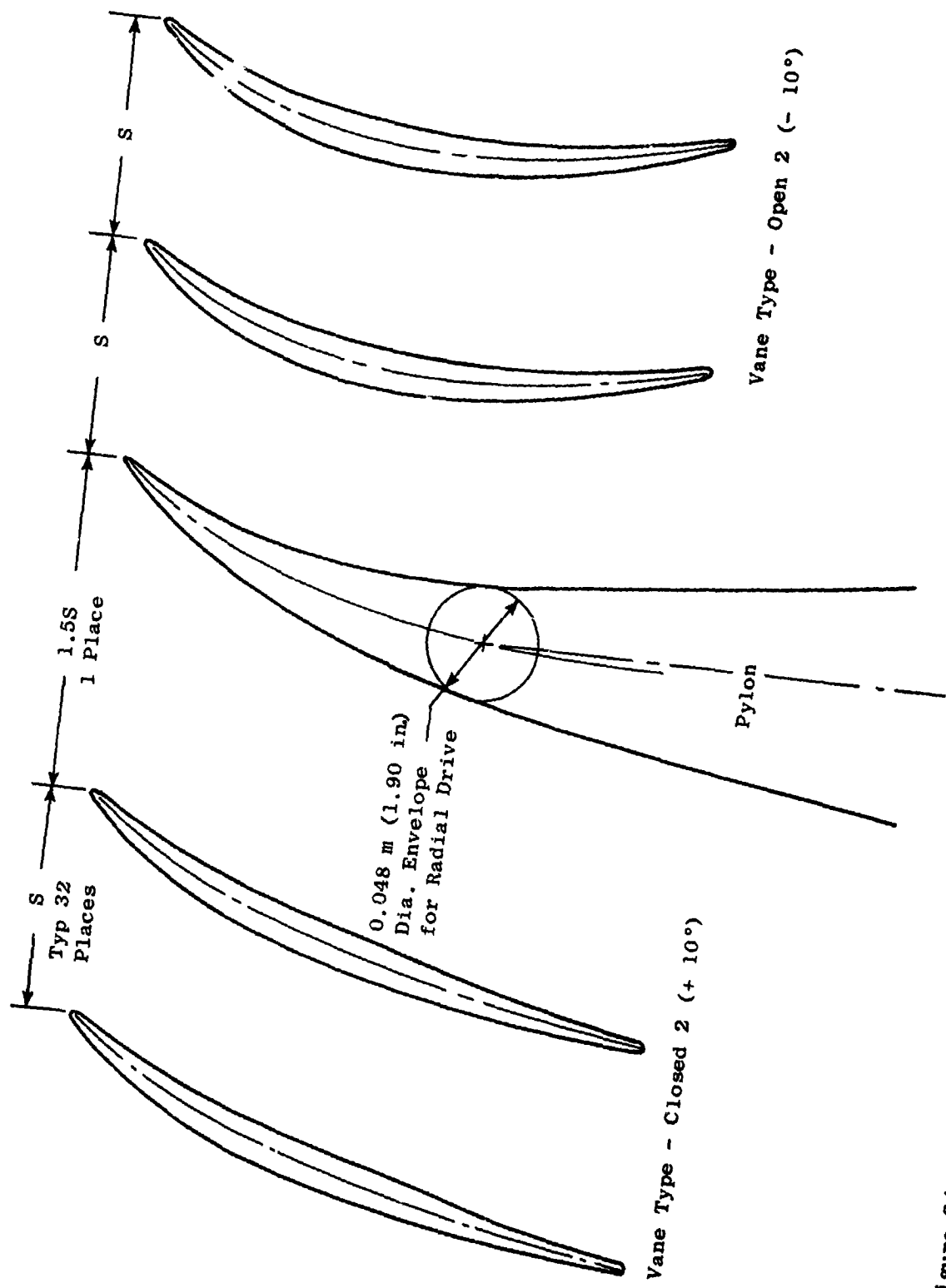


Figure 24. Vane-Frame (Fan Bypass OGV) Unwrapped Section at IL - Detail Near Pylon LE Fairing.

Table 5. Vane-Frame (Fan Bypass OGV) Coordinates.

Vane Type: Closed 2 (~ +10°)
 Radius 53.0 cm (20.86 in.)

Convex		Concave	
X (Axial)	Y	X (Axial)	Y
-6.48210	2.34116	-6.48210	2.34116
-6.48759	2.32790	-6.47014	2.34917
-6.48654	2.30949	-6.45181	2.35181
-6.47875	2.28616	-6.42730	2.34886
-6.46396	2.25823	-6.39677	2.34011
-6.44206	2.22584	-6.36025	2.32555
-6.41331	2.18867	-6.31735	2.30561
-6.29919	2.05618	-6.16591	2.22947
-6.07119	1.83449	-5.89480	2.07990
-5.83097	1.63835	-5.63592	1.92961
-5.58939	1.45347	-5.37839	1.79199
-5.34632	1.27982	-5.12236	1.66526
-5.10018	1.11977	-4.86939	1.54502
-4.85192	0.97171	-4.61855	1.43098
-4.60258	0.83339	-4.36878	1.32361
-4.30233	0.67897	-4.07011	1.20263
-4.00106	0.53619	-3.77245	1.08890
-3.69886	0.40428	-3.47572	0.98129
-3.39590	0.28251	-3.17976	0.87882
-3.09242	0.16986	-2.88431	0.78108
-2.78889	0.06546	-2.58892	0.68742
-2.48547	-0.03115	-2.29341	0.59624
-2.18202	-0.12056	-1.99793	0.50613
-1.87857	-0.20389	-1.70246	0.41663
-1.57498	-0.28229	-1.40712	0.32765
-1.27110	-0.35637	-1.11208	0.23941
-0.96707	-0.42655	-0.81718	0.15212
-0.66307	-0.49346	-0.52225	0.06612
-0.35916	-0.55754	-0.22724	-0.01841
-0.05521	-0.61845	0.06774	-0.10206
0.24894	-0.67585	0.36251	-0.18531
0.55329	-0.73002	0.65709	-0.26774
0.85774	-0.78128	0.95157	-0.34873
1.16223	-0.82964	1.24600	-0.42780
1.46682	-0.87488	1.54034	-0.50454
1.77161	-0.91602	1.83448	-0.57877
2.07653	-0.95211	2.12848	-0.65013
2.38133	-0.98311	2.42260	-0.71727
2.68567	-1.00936	2.71719	-0.77845
2.98924	-1.03206	3.01255	-0.83151
3.29155	-1.04887	3.25934	-0.86832
3.41111	-1.05853	3.42574	-0.88974
3.46658	-1.04155	3.47884	-0.91753
3.50000	-0.98095	3.50000	-0.98095

Table 5. Vane-Frame (Fan Bypass OGV) Coordinates (Continued).

Vane Type: Pylon Leading Edge
Radius 53.0 cm (20.86 in.)

Convex		Concave	
X (Axial)	Y	X (Axial)	Y
-6.48132	2.39154	-6.48132	2.39154
-6.48473	2.38081	-6.47148	2.39700
-6.48161	2.36491	-6.45525	2.39712
-6.47179	2.34406	-6.43279	2.39173
-6.45509	2.31849	-6.40420	2.38068
-6.43144	2.28828	-6.36944	2.36404
-6.40114	2.25305	-6.32808	2.34232
-6.28510	2.12434	-6.17848	2.26374
-6.06174	1.89820	-5.90277	2.12120
-5.82801	1.69438	-5.63744	1.98182
-5.58938	1.50620	-5.37700	1.85097
-5.35069	1.32592	-5.11662	1.73488
-5.11131	1.15379	-4.85694	1.63146
-4.86999	0.99135	-4.59920	1.53737
-4.62695	0.83784	-4.34317	1.45194
-4.33354	0.66380	-4.03770	1.36062
-4.03838	0.49997	-3.73397	1.28070
-3.74142	0.34566	-3.43206	1.21133
-3.44249	0.20051	-3.13211	1.15184
-3.14194	0.06430	-2.83378	1.10152
-2.84029	-0.06372	-2.53655	1.05974
-2.53811	-0.18441	-2.23985	1.02584
-2.23601	-0.29875	-1.94307	0.99894
-1.93375	-0.40770	-1.64646	0.97830
-1.63088	-0.51145	-1.35045	0.96310
-1.32713	-0.60978	-1.05531	0.95241
-1.02219	-0.70205	-0.76138	0.94519
-0.71617	-0.78789	-0.46851	0.94075
-0.40945	-0.86865	-0.17635	0.94005
-0.10190	-0.94573	0.11497	0.94418
0.20685	-1.01906	0.40510	0.95304
0.51627	-1.08827	0.69456	0.96621
0.82574	-1.15361	0.98398	0.98345
1.13505	-1.21546	1.27354	1.00450
1.44405	-1.27381	1.56343	1.02871
1.73876	-1.32623	2.14355	1.08453
2.03355	-1.37574	2.44720	1.11734
3.50000	-1.64800	3.50000	1.20800

Table 5. Vane-Frame (Fan Bypass OGV) Coordinates (Continued).

Vane Type: Open 2 (~ -10°)
 Radius 53.0 cm (20.86 in.)

Convex		Concave	
X (Axial)	Y	X (Axial)	Y
-6.48210	2.34116	-6.48210	2.34116
-6.48759	2.32791	-6.47013	2.34918
-6.48653	2.30950	-6.45180	2.35183
-6.47873	2.28619	-6.42726	2.34891
-6.46391	2.25830	-6.39669	2.34021
-6.44195	2.22597	-6.36068	2.32574
-6.41309	2.18893	-6.31705	2.30598
-6.29837	2.05743	-6.16673	2.23191
-6.06881	1.84013	-5.89719	2.08881
-5.82663	1.65165	-5.64026	1.94846
-5.58259	1.47746	-5.38519	1.82404
-5.33663	1.31730	-5.13205	1.71340
-5.08740	1.17343	-4.88217	1.61171
-4.83591	1.04408	-4.63456	1.51847
-4.58317	0.92682	-4.38619	1.43400
-4.27866	0.80069	-4.09378	1.34319
-3.97293	0.68941	-3.80058	1.26249
-3.66610	0.59230	-3.50849	1.19083
-3.35833	0.50871	-3.21733	1.12737
-3.04985	0.43788	-2.92688	1.07194
-2.74105	0.37917	-2.63676	1.02425
-2.43218	0.33258	-2.34670	0.98319
-2.12344	0.29797	-2.05652	0.94770
-1.81511	0.27447	-1.76592	0.91756
-1.50737	0.26103	-1.47473	0.89269
-1.20033	0.25681	-1.18284	0.87302
-0.89392	0.26100	-0.89033	0.85854
-0.58804	0.27293	-0.59728	0.84962
-0.28271	0.29217	-0.30369	0.84652
0.02205	0.31915	-0.00952	0.84873
0.32598	0.35420	0.28547	0.85578
0.62892	0.39664	0.58146	0.86776
0.93104	0.44568	0.87827	0.88487
1.23245	0.50099	1.17578	0.90731
1.53315	0.56243	1.47401	0.93516
1.83305	0.63035	1.77304	0.96799
2.13206	0.70496	2.07295	1.00552
2.43030	0.78549	2.37364	1.04842
2.72800	0.87086	2.67486	1.09772
3.02565	0.95941	2.97614	1.15510
3.27398	1.03479	3.22691	1.20994
3.44400	1.08772	3.39850	1.25063
3.49006	1.12317	3.45780	1.24339
3.50000	1.149138	3.50000	1.19138

ORIGINAL PAGE IS
OF POOR QUALITY

Table 5. Vane-Frame (Fan Bypass OGV) Coordinates (Continued).

Vane Type: Nominal (0°)
Radius 53.0 cm (20.85 in.)

Convex		Concave	
X (Axial)	Y	X (Axial)	Y
-6.48210	2.34116	-6.48210	2.34116
-6.48159	2.32791	-6.47013	2.34918
-6.48654	2.30949	-6.45181	2.35182
-6.47874	2.28617	-6.42729	2.34888
-6.46394	2.25825	-6.39675	2.34014
-6.44203	2.22588	-6.36020	2.32561
-6.41324	2.18874	-6.31726	2.30572
-6.29896	2.05654	-6.16614	2.23018
-6.07054	1.83608	-5.89545	2.08244
-5.82980	1.64205	-5.63708	1.93498
-5.58753	1.46015	-5.38025	1.80119
-5.34355	1.29036	-5.12513	1.67933
-5.09631	1.13518	-4.87326	1.56502
-4.84677	0.99309	-4.62370	1.45801
-4.59597	0.86190	-4.37539	1.35882
-4.29378	0.71764	-4.07866	1.24915
-3.99047	0.58679	-3.78304	1.14834
-3.68627	0.46852	-3.48832	1.05511
-3.38139	0.36194	-3.19426	0.96836
-3.07616	0.26589	-2.90057	0.88755
-2.77084	0.17937	-2.60697	0.81205
-2.46549	0.10210	-2.31339	0.74054
-2.16009	0.03377	-2.01986	0.67182
-1.85478	-0.02657	-1.72625	0.60556
-1.54964	-0.07997	-1.43246	0.54168
-1.24470	-0.12720	-1.13847	0.48014
-0.93983	-0.16894	-0.84442	0.42105
-0.63494	-0.20568	-0.55038	0.36497
-0.33012	-0.23761	-0.25628	0.31230
0.02535	-0.26417	0.03788	0.26268
0.27916	-0.28484	0.33230	0.21567
0.58316	-0.30022	0.62722	0.17134
0.88725	-0.31091	0.92205	0.13018
1.19188	-0.31606	1.21636	0.09358
1.49640	-0.31452	1.51076	0.06272
1.80035	-0.30547	1.80573	0.03755
2.10352	-0.28852	2.10149	0.01793
2.40575	-0.26457	2.39819	0.00441
2.70721	-0.23490	2.69565	-0.00204
3.00816	-0.20101	2.99363	0.00047
3.25869	-0.17029	3.24220	0.01049
3.42732	-0.14778	3.40980	0.02082
3.47856	-0.12068	3.46729	0.00351
3.50000	-0.05474	3.50000	-0.05474

Table 5. Vane-Frame (Fan Bypass OGV) Coordinates (Continued).

Vane Type: Nominal (0°)
 Radius 69.8 cm (27.48 in.)

Convex		Concave	
X (Axial)	Y	X (Axial)	Y
-5.58734	1.85159	-5.58734	1.85159
-5.59204	1.83581	-5.57482	1.86239
-5.58888	1.81511	-5.55459	1.86805
-5.57767	1.78979	-5.52679	1.86834
-5.55820	1.76017	-5.49156	1.86305
-5.53036	1.72642	-5.44892	1.85215
-5.49435	1.68825	-5.39858	1.83610
-5.41795	1.61418	-5.30236	1.80216
-5.20924	1.44123	-5.05671	1.70308
-4.99074	1.28915	-4.82084	1.59775
-4.77087	1.14424	-4.58634	1.49967
-4.54950	1.00677	-4.35334	1.40820
-4.32535	0.87963	-4.12313	1.32006
-4.09911	0.76188	-3.89500	1.23567
-3.87166	0.65193	-3.66808	1.15607
-3.59755	0.52960	-3.39695	1.06657
-3.32237	0.41733	-3.12689	0.98287
-3.04629	0.31473	-2.85773	0.90412
-2.76943	0.22135	-2.58935	0.82965
-2.49196	0.13645	-2.32158	0.75933
-2.21403	0.05948	-2.05428	0.69304
-1.93557	-0.00932	-1.78749	0.62999
-1.65657	-0.06966	-1.52125	0.56948
-1.37718	-0.12194	-1.25540	0.51166
-1.09766	-0.16670	-0.98968	0.45683
-0.81820	-0.20440	-0.72390	0.40517
-0.53899	-0.23556	-0.45787	0.35687
-0.26019	-0.26089	-0.19143	0.31220
0.01826	-0.28092	0.07536	0.27132
0.29653	-0.29522	0.34234	0.23382
0.57458	-0.30326	0.60952	0.19928
0.85232	-0.30529	0.87702	0.16812
1.12961	-0.30174	1.14497	0.14089
1.40634	-0.29289	1.41349	0.11784
1.68247	-0.27890	1.68260	0.09902
1.95797	-0.25944	1.95234	0.08394
2.23282	-0.23433	2.22272	0.07231
2.50703	-0.20433	2.49376	0.06473
2.78065	-0.17056	2.76537	0.06229
3.05389	-0.13473	3.03738	0.06670
3.28146	-0.10422	3.26418	0.07653
3.42738	-0.08386	3.40977	0.08530
3.47882	-0.05633	3.46701	0.06804
3.50000	0.00941	3.50000	0.00941

Table 5. Vane-Frame (Fan Bypass OGV) Coordinates (Concluded)

Vane Type: Nominal (C°)
 Radius 90.1 cm (35.5 in.)

Convex		Concave	
X (Axial)	Y	X (Axial)	Y
-4.49480	1.64519	-4.49480	1.64519
-4.50141	1.62777	-4.48003	1.65611
-4.49961	1.60423	-4.45704	1.66064
-4.48913	1.57488	-4.42607	1.65851
-4.46969	1.54012	-4.38715	1.64946
-4.44110	1.50020	-4.34056	1.63344
-4.40352	1.45490	-4.28574	1.61098
-4.36001	1.40641	-4.22984	1.58666
-4.17865	1.23208	-4.0114	1.48459
-3.98730	1.08043	-3.80307	1.38218
-3.79412	0.93890	-3.59652	1.28894
-3.59889	0.80698	-3.39201	1.20396
-3.40085	0.68675	-3.19030	1.12394
-3.20110	0.57686	-2.99032	1.04840
-3.00038	0.47518	-2.79129	0.97765
-2.75845	0.36283	-2.55353	0.89860
-2.51543	0.26034	-2.31686	0.82511
-2.27133	0.16734	-2.08128	0.75648
-2.02632	0.08355	-1.84660	0.69213
-1.78065	0.00833	-1.61258	0.63195
-1.53453	-0.05889	-1.37902	0.57580
-1.28796	-0.11786	-1.14590	0.52287
-1.04094	-0.16633	-0.91323	0.47240
-0.79365	-0.21078	-0.68083	0.42448
-0.54628	-0.24579	-0.44852	0.37939
-0.29894	-0.27378	-0.21617	0.33741
-0.05184	-0.29518	0.01642	0.29879
0.19482	-0.31062	0.24945	0.26389
0.44100	-0.32059	0.48296	0.23289
0.68673	-0.32477	0.71691	0.20524
0.93213	-0.32276	0.95120	0.18045
1.17721	-0.31479	1.18580	0.15901
1.42173	-0.30120	1.42098	0.14150
1.66547	-0.28239	1.65692	0.12812
1.90844	-0.25863	1.89364	0.11880
2.15059	-0.22976	2.13118	0.11295
2.39198	-0.19569	2.36947	0.11011
2.63272	-0.15716	2.60842	0.11097
2.87313	-0.11508	2.84770	0.11677
3.11356	-0.07029	3.08696	0.13000
3.31347	-0.03164	3.28679	0.14794
3.43200	-0.00838	3.40618	0.16054
3.48205	0.02185	3.46416	0.14584
3.50000	0.08854	3.50000	0.08854

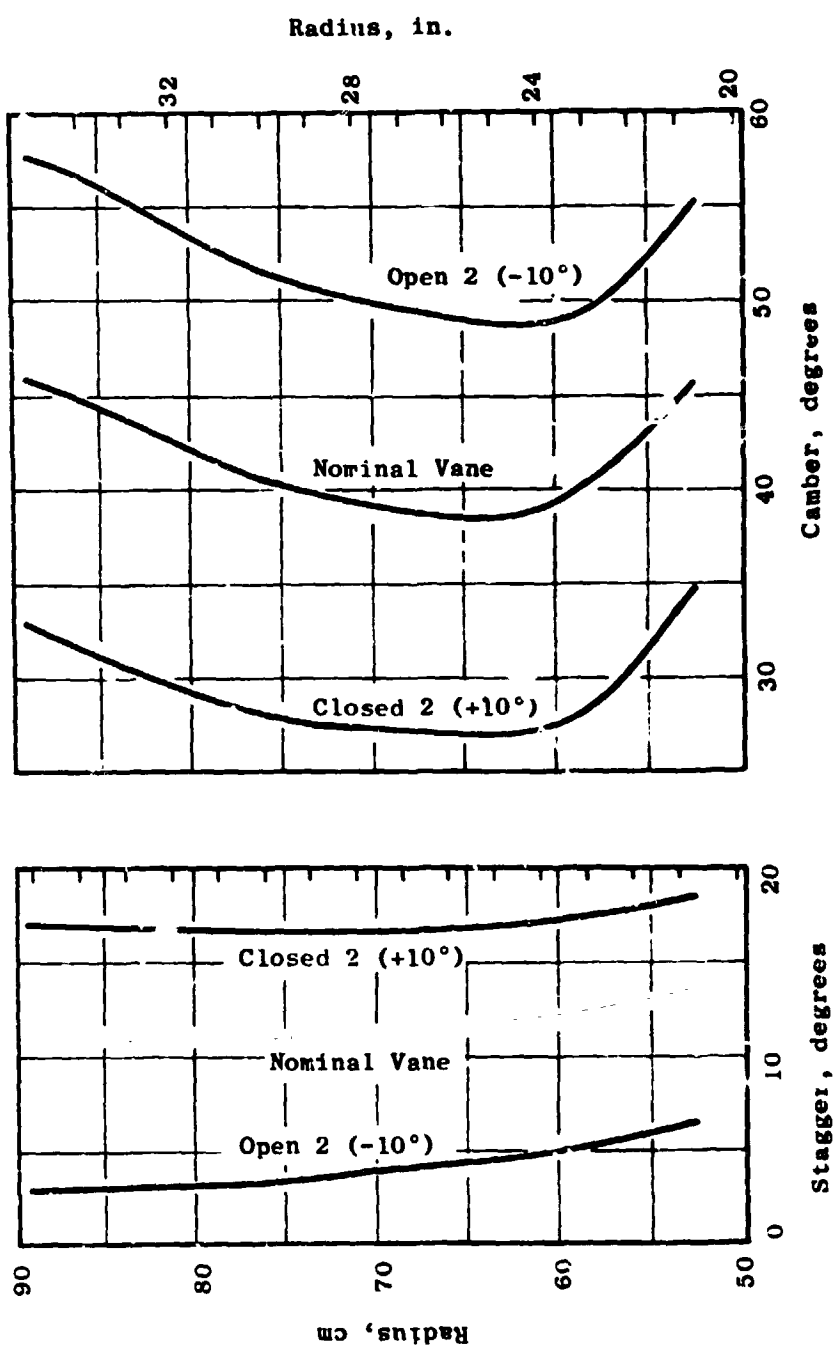


Figure 25. Vane-Frame (Fan Bypass OGV) Stagger and Camber Distributions.

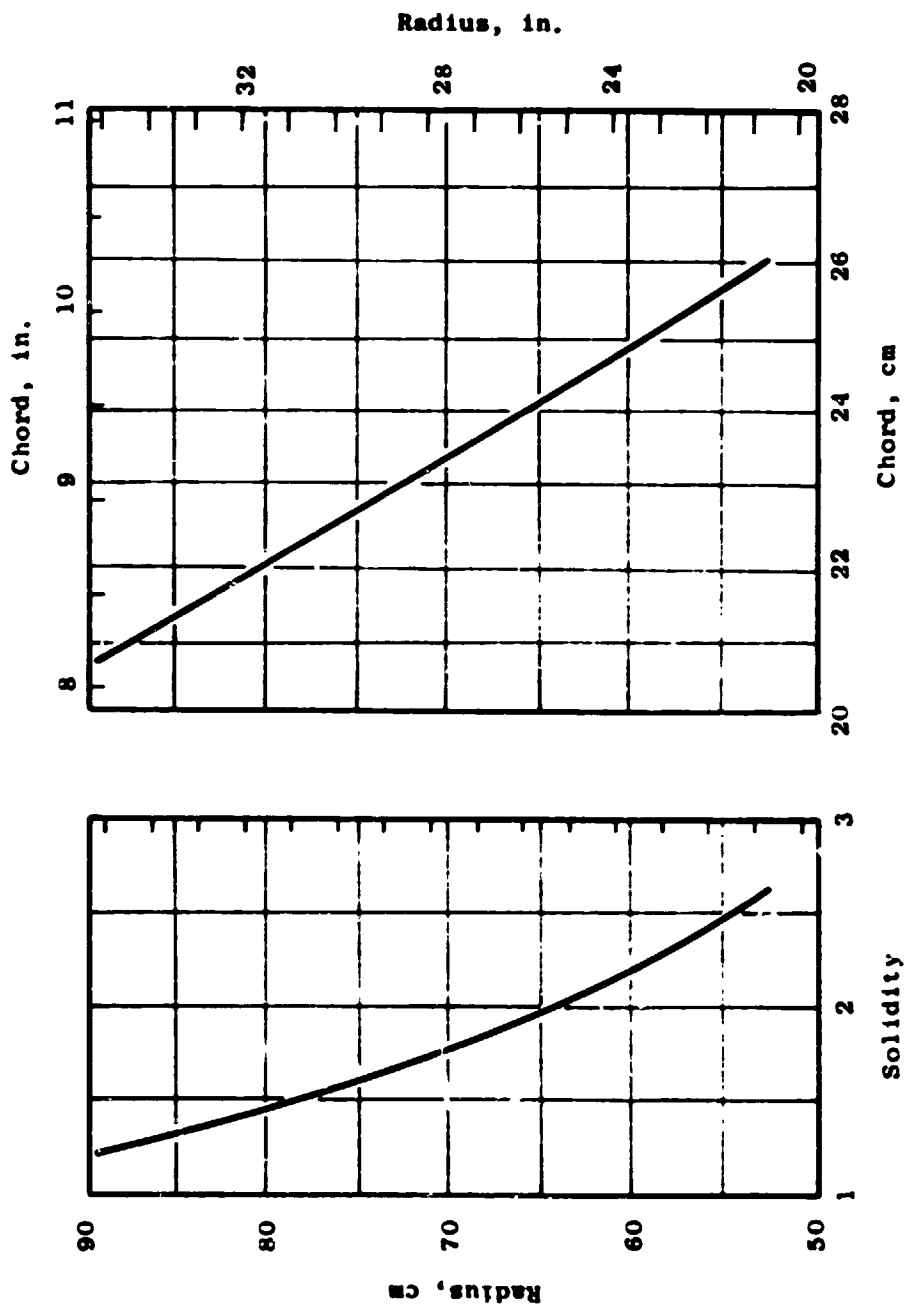


Figure 26. Vane-Frame (Fan Bypass OGV) Solidity and Chord Distributions.

Sufficient data were obtained to define the fan bypass and core flow performance maps at each stagger angle. The three bypass stream maps were curve fit using a technique that allowed the stagger angle to be used as a parameter along with the usual parameters of speed and throttle area. This permitted convenient prediction of fan performance at any given stagger angle by interpolation within the group of maps based upon test data. A universal characteristic approach was tried as a means of unifying the data obtained at different rotor angle settings in forward thrust, but was not as successful as the curve-fit interpolation method. The curve-fit method was in excellent agreement with the test data with respect to pressure ratio versus flow and speed and generally fit the efficiency data within one point.

The fan bypass performance map for the design stagger angle is shown in Figure 27, scaled to UTW engine size but based very closely on 50.8-cm (20-inch) scale model test data at this setting angle. The design point is indicated on this figure, and comparison with the 100% corrected speed line shows that the fan demonstrated the design flow at design speed but was low in pressure ratio. This is believed to be due to the rotor deviation angles being larger than assumed during the design process. Along a fixed-area operating line through the aero design point, the fan achieved a pressure ratio of 1.30 and a scaled flow of 386 kg/sec (851 lbm/sec) at design speed and nominal stagger angle. These values are, respectively, 3.0% and 5.5% less than the objectives.

The fan design point, however, was selected simply as an intermediate point between the two critical engine operating conditions of take-off and maximum cruise power settings; it is fan flow and pressure ratio at these conditions that must be met in order for the engine to meet its thrust goals. The variable-pitch rotor and variable-area bypass stream exhaust nozzle features of the UTW fan allow these objectives to be met even though the design point was not achieved. In particular, the variable-pitch feature results in better overall engine system operating characteristics than would have been possible if changing only fan speed and nozzle area were used to reach these fan operating conditions. Figure 28 shows the estimated fan performance map at the maximum cruise condition. In this case, the flow of 405.5 kg/sec (894 lbm/sec) and pressure ratio of 1.38 required to achieve the thrust goal are achieved at a corrected speed of 109% and a stagger angle adjustment of -1.4° (open). The estimated efficiency at this condition is 0.811, about the same as would be obtained at nominal stagger by running the fan at 112% speed. The lower-speed, open-stagger setting was selected in order to stay below a physical speed limitation on the fan drive turbine.

Similarly, the estimated take-off condition fan performance map (Figure 29) shows that for a fan stagger angle adjustment of -3° (open), the required fan flow of 405.5 kg/sec (894 lbm/sec) and pressure ratio of 1.27 are achieved at 95% corrected speed and an efficiency of 0.833. This efficiency is lower than the value of 0.86 achieved at 100% speed and nominal stagger angle, but the lower fan speed is needed to reduce engine take-off noise to objective levels.

ORIGINAL PAGE IS
OF POOR QUALITY

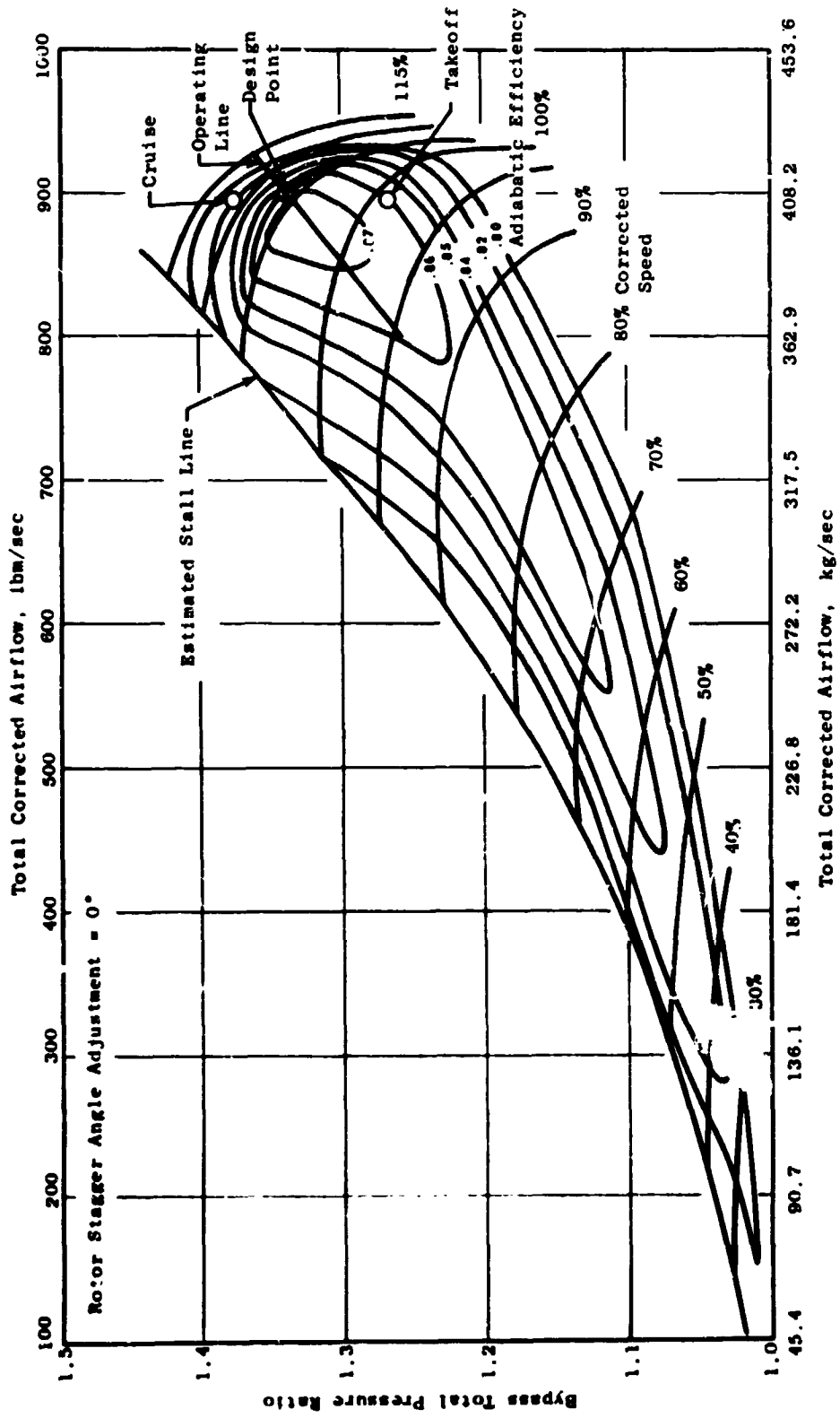


Figure 27. UTW Fan Bypass Stream Performance Map at Design Rotor Stagger Setting.

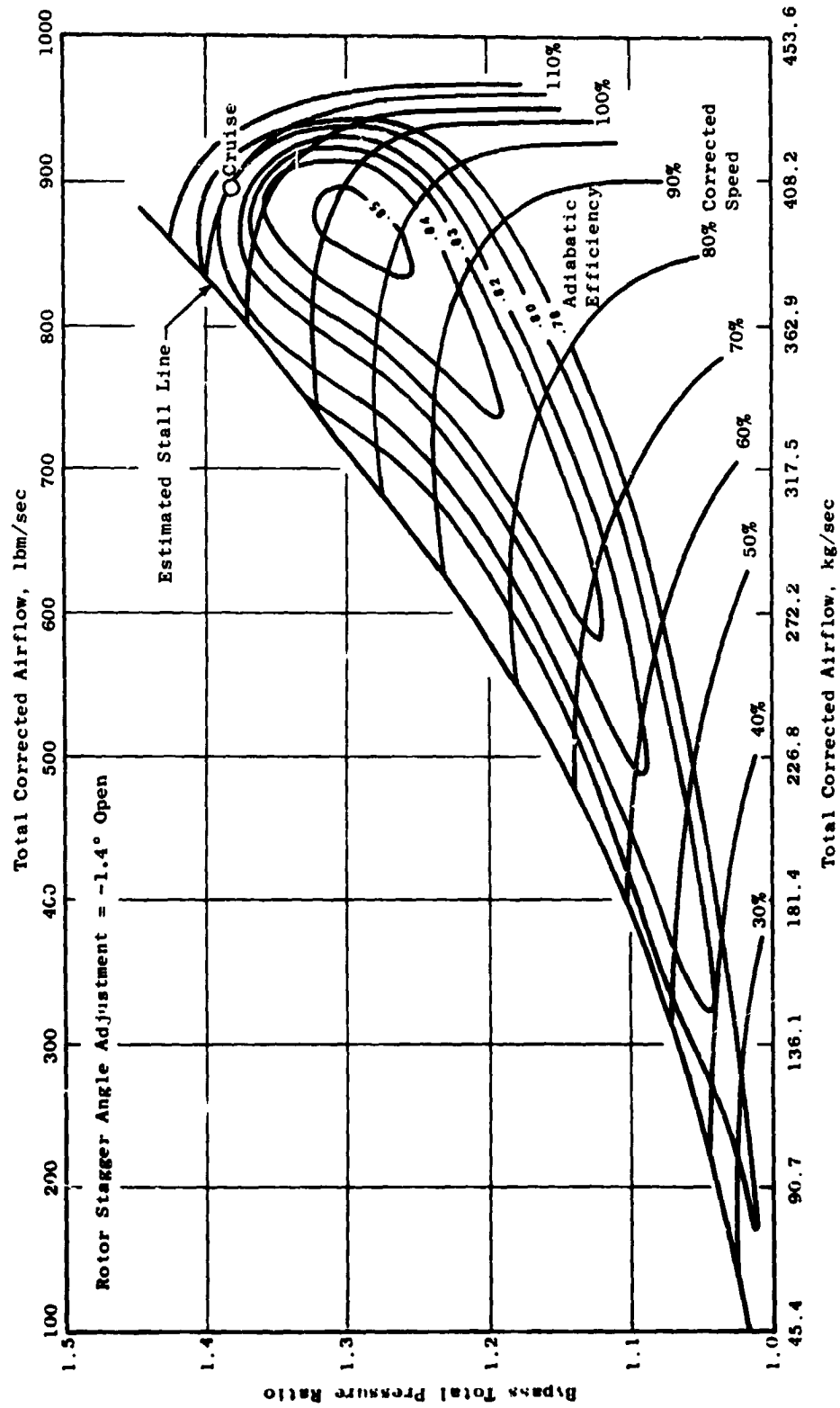


Figure 28. UTW Fan Bypass Stream Performance Map at Cruise Rotor Stagger Setting.

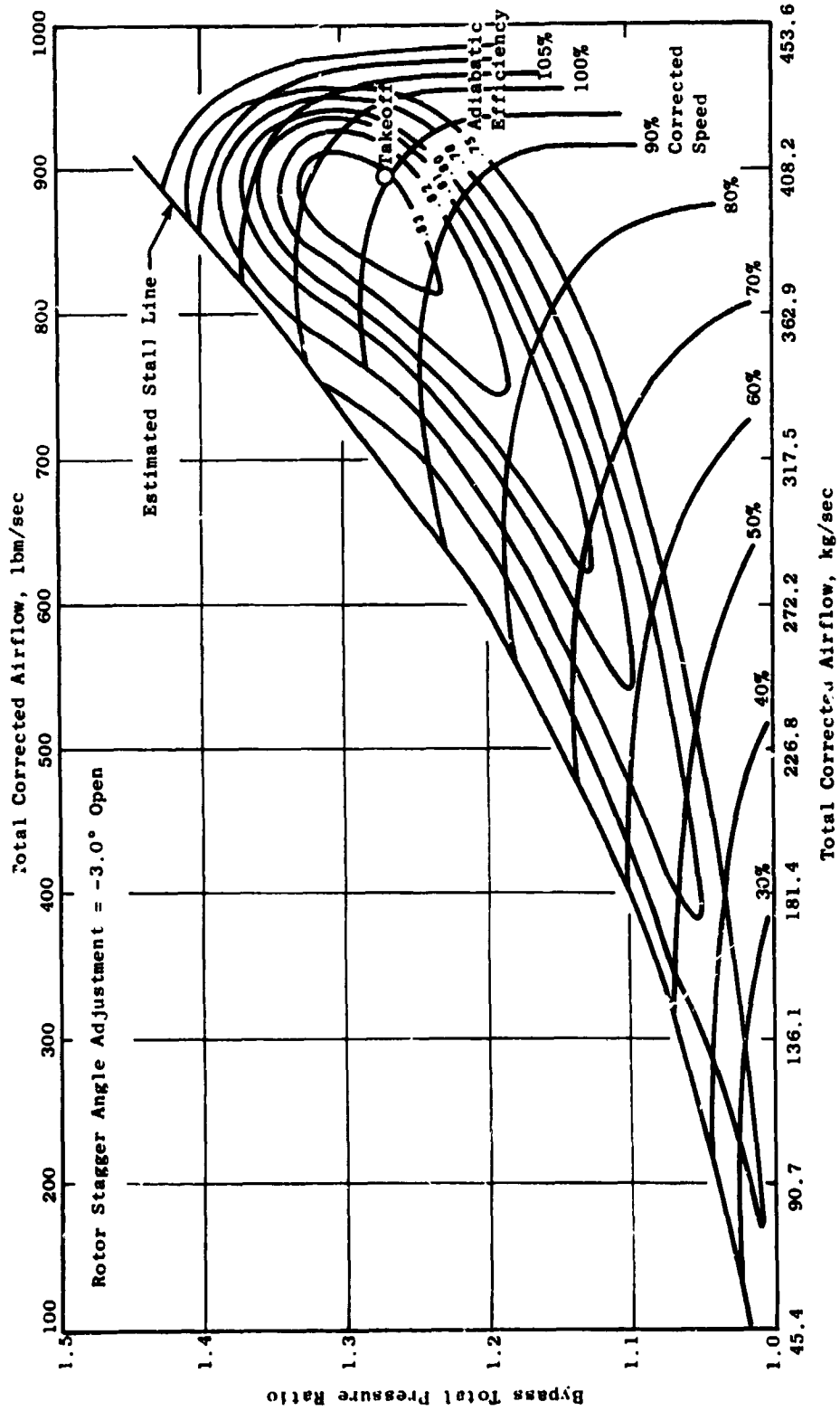


Figure 19. UTW Fan Bypass Stream Performance Map at Take-off Rotor Stagger Setting.

For purposes of describing estimated full-scale engine performance, the fan hub performance data from the simulator fan tests were expressed in the form of modifying factors applied to the bypass stream performance maps. The fan hub pressure ratio is found as a function of bypass stream pressure ratio as shown in Figure 30. This curve is an average of numerous data points at various throttle settings, rotor stagger angles, and speeds. In general, the fan hub pressure ratio at a given bypass pressure ratio slightly exceeds the objectives, assuring that the core engine will be adequately supercharged by the fan. Fan hub efficiency is related to bypass stream efficiency according to the relationship shown in Figure 31. Along a reference constant-throttle-area operating line passing somewhat below the design point, having a throttle area parameter of 1.34, the hub efficiency is a function of corrected speed. At a given corrected speed, the hub efficiency varies from its value at the reference operating line according to the variation in throttle area. These curves also are composites of a large number of data points. As mentioned by Giffin, et al., the fan hub efficiency exceeded the objective value at design speed with the nominal rotor pitch setting.

Performance in the reverse thrust mode of operation was determined for several rotor angle settings during the 50.3-cm (20-inch) scale model fan tests, and is discussed in detail by Giffin, et al. Pressure ratio and efficiency data are shown in Figure 32, plotted versus flow in the 50.8-cm (20-inch) scale model size. In UTW engine size, the resulting trends of gross corrected fan reverse thrust versus fan corrected speed are shown in Figure 33. The general conclusion from these data is that reverse thrust objectives can be met with the rotor blades reversed through stall pitch, but probably not when reversed through flat pitch. Engine system cycle analysis, however, is required to evaluate effects of bypass duct/core engine inlet duct recoveries on available core engine power and achievable fan speed before determining the best pitch angle setting for reverse thrust.

The test data recorded in reverse thrust mode were expressed in terms of a universal stage characteristic. A work coefficient, defined in Figure 34, was calculated involving a correction for rotor stagger angle variations such that this coefficient represents the work input that would have been produced if the rotor had always been set at a nominal stagger angle rather than at the angle for the particular data point. Similarly, a flow coefficient, defined in Figure 34, was calculated to represent the flow that would have been passed at the nominal rotor angle setting, for the same incidence as the actual test data point. Two such characteristics were actually obtained, one for reverse through stall pitch and one for reverse through flat pitch. The stagger angle settings used as normalizing values were -100° and $+73^\circ$ for reverse through stall pitch and flat pitch, respectively. The resulting characteristic curves are shown in Figure 34, while the trends of efficiency versus speed and stagger angle used to represent the reverse mode data are shown in Figure 35.

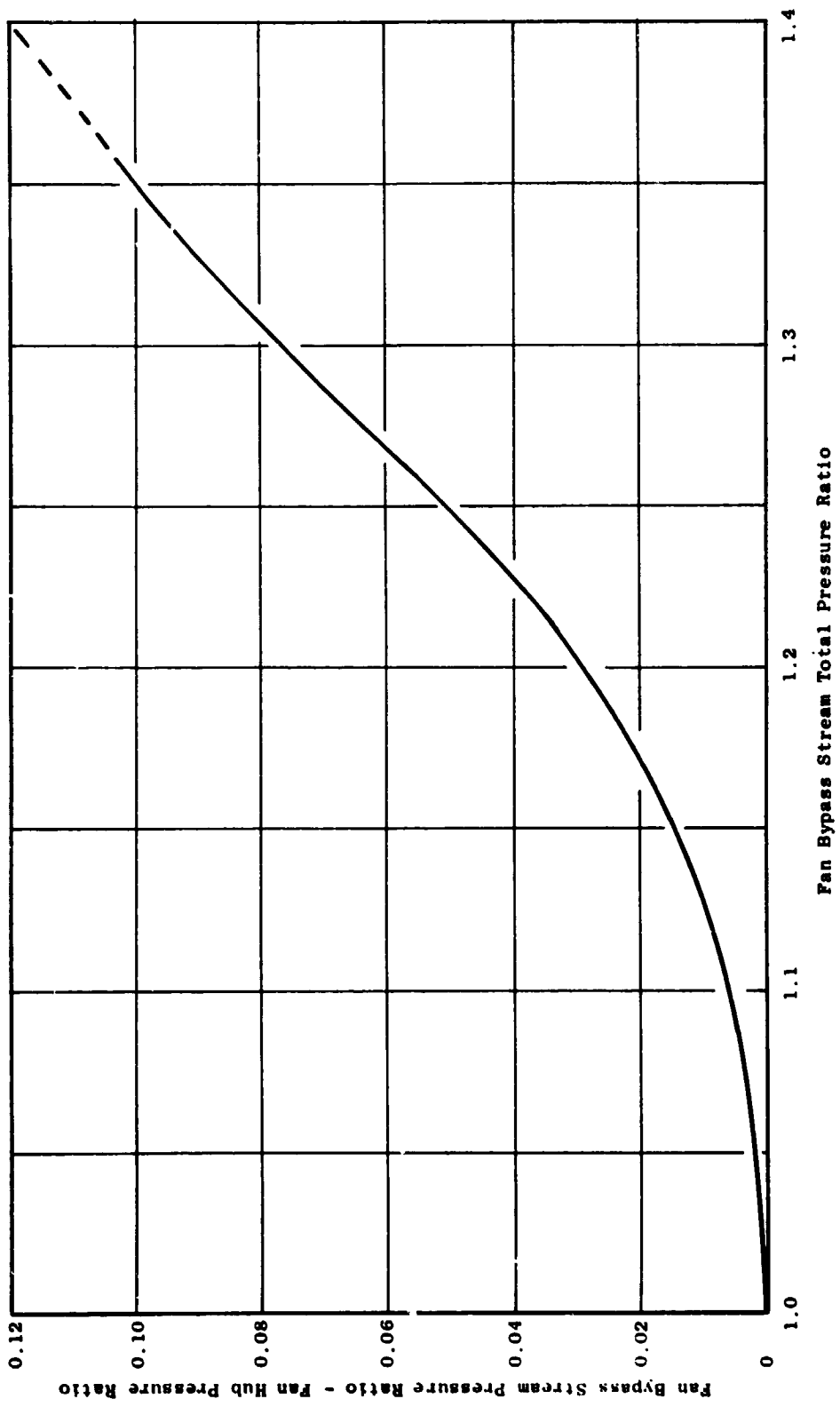
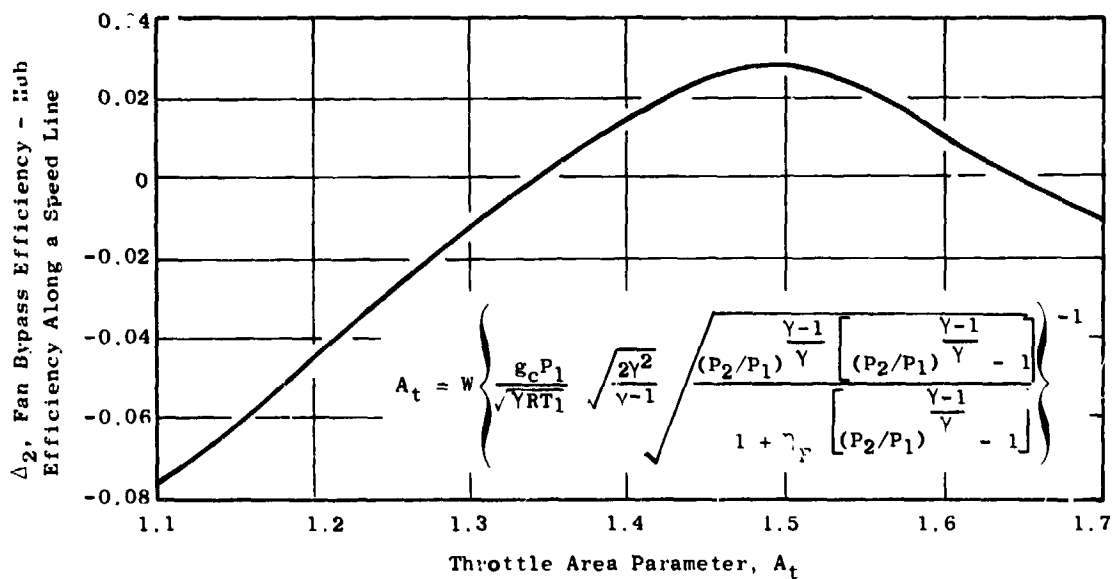
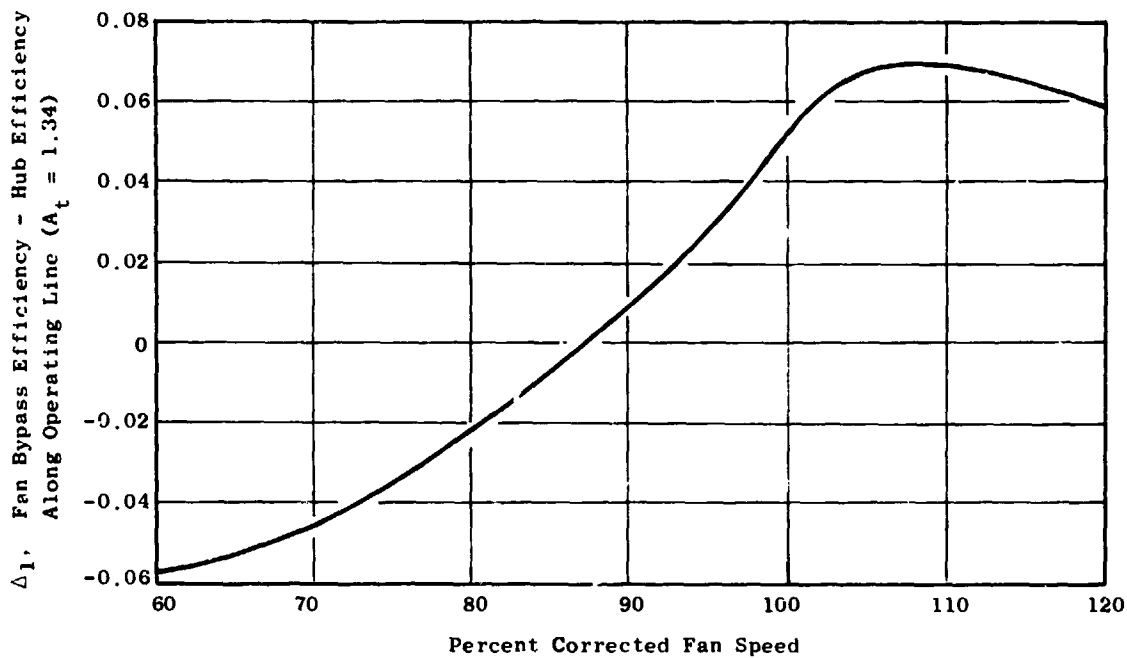


Figure 30. Fan Hub Pressure Ratio Correlation (Forward Mode).



- W = Total Fan Corrected Airflow
- P₁, T₁ = Fan Inlet Total Pressure and Temperature
- P₂/P₁ = Fan Bypass Pressure Ratio
- η_F = Fan Bypass Adiabatic Efficiency
- Fan Hub Efficiency = η_H = η_F - Δ₁ - Δ₂

Figure 31. Fan Hub Efficiency Correlation (Forward Mode).

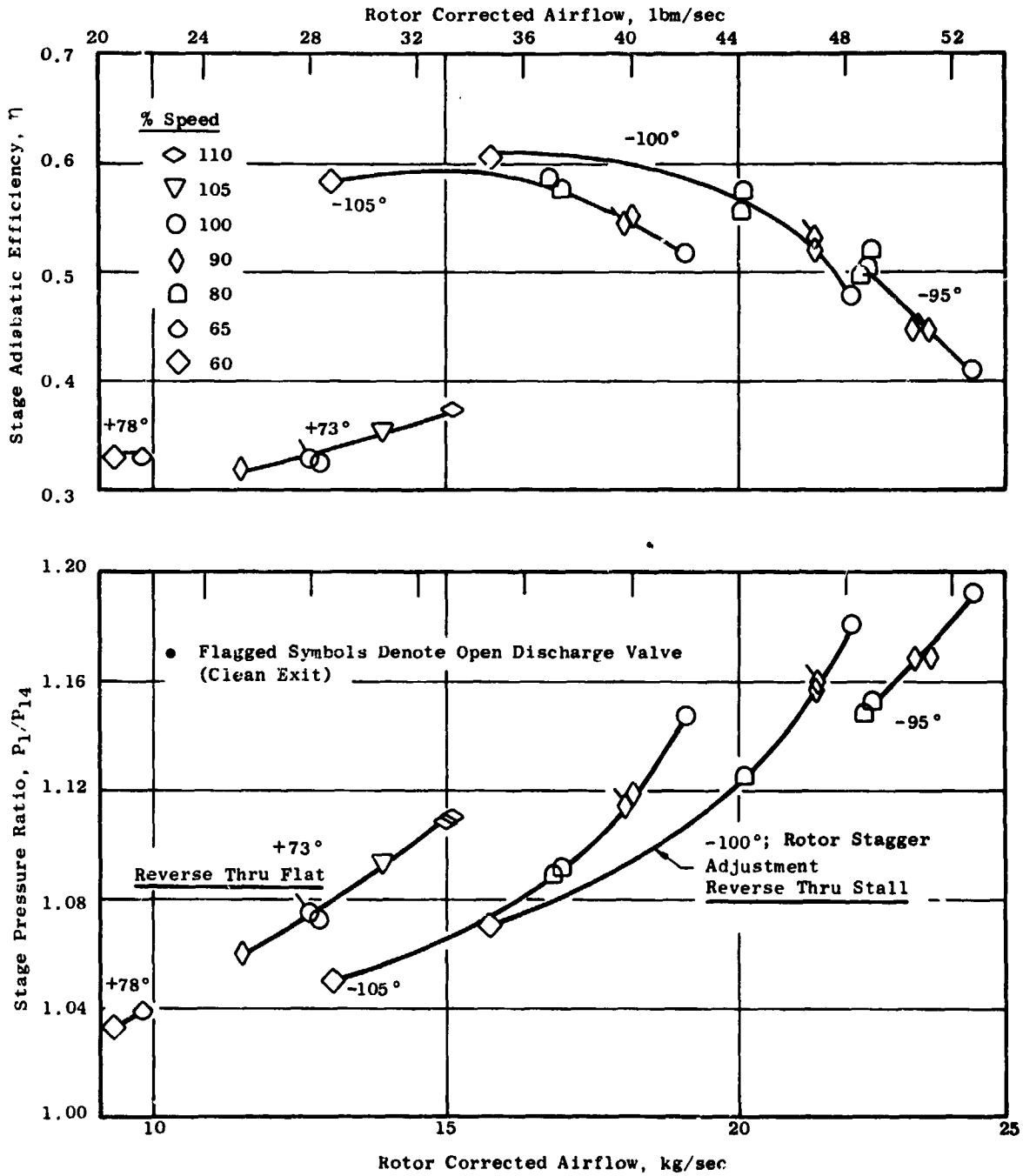


Figure 32. Reverse Mode Fan Performance.

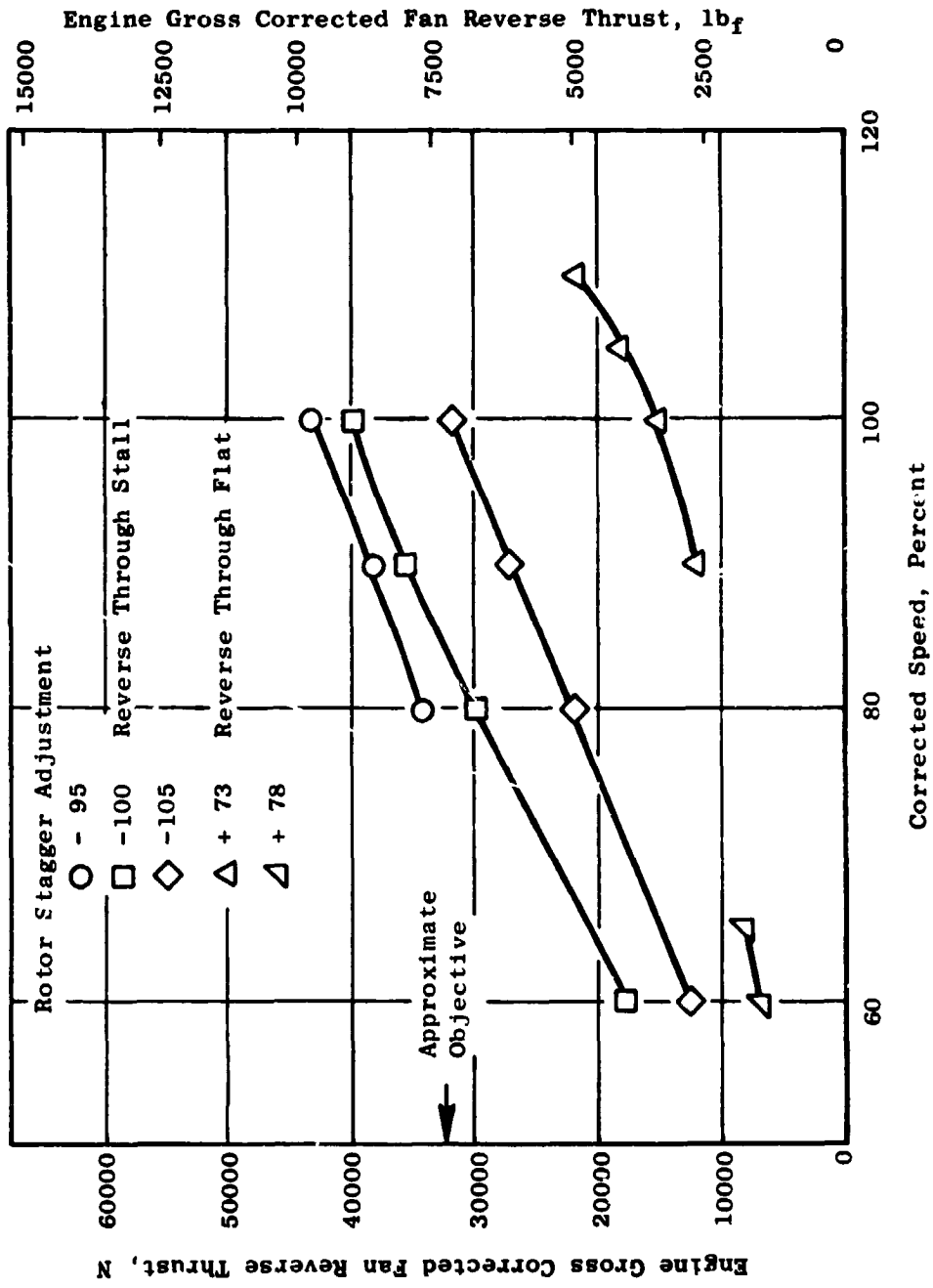
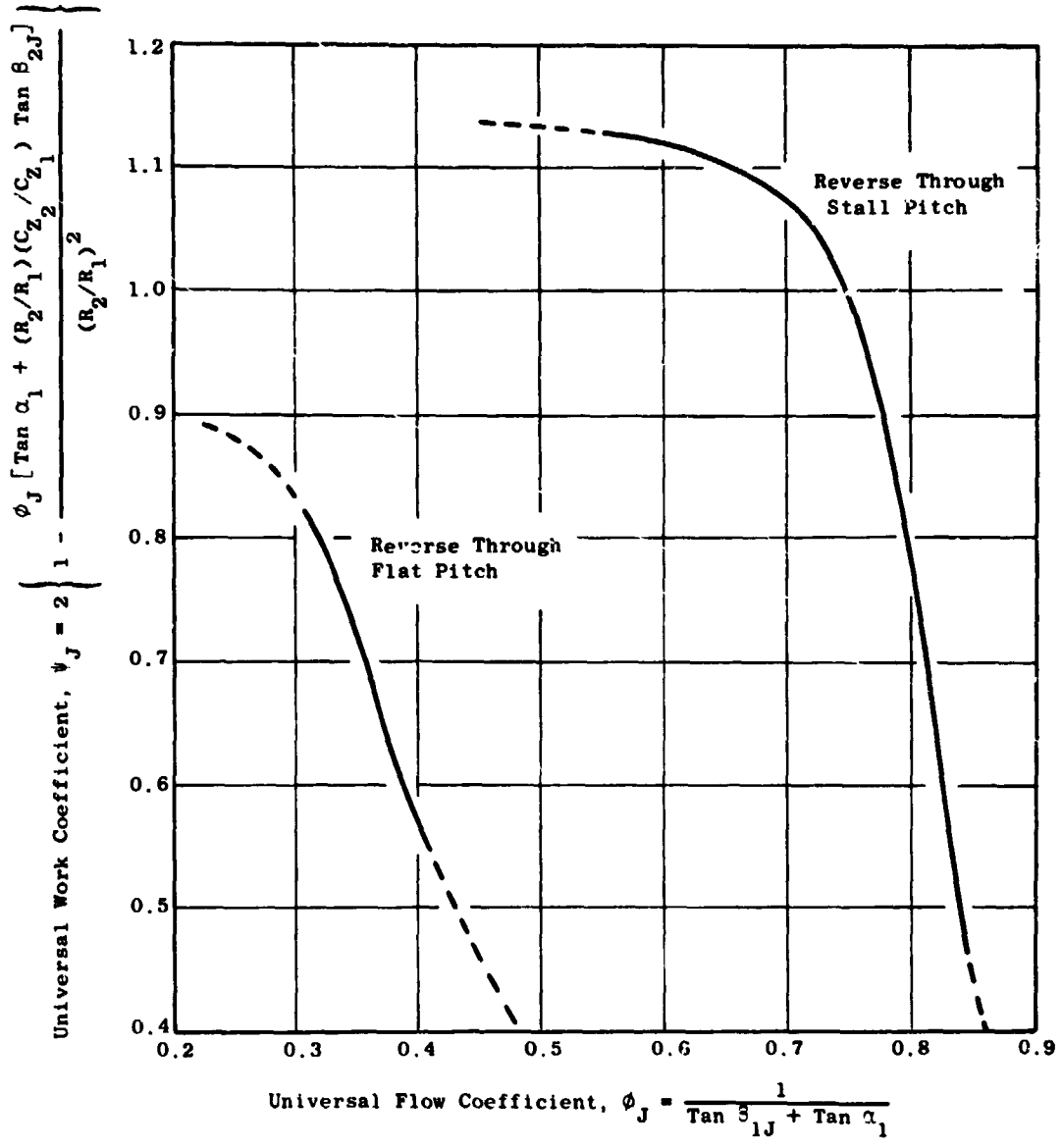


Figure 33. UTW Fan Scale Model Gross Reverse Thrust, Scaled to Engine Size.



- P_{Norm} = Normalizing Value of Rotor Stagger Angle Setting
- P = Rotor Stagger Angle
- β_1 = Rotor Inlet Relative Air Angle
- α_1 = Rotor Inlet Absolute Air Angle
- β_{1J} = $\beta_1 + P - P_{Norm}$; $\alpha_{1J} = \alpha_1 + P - P_{Norm}$
- C_{Z_2}/C_{Z_1} = Axial Velocity Ratio Across the Rotor
- R_2/R_1 = Radius Ratio Across the Rotor

Figure 34. UTW Fan Reverse Mode Universal Characteristics.

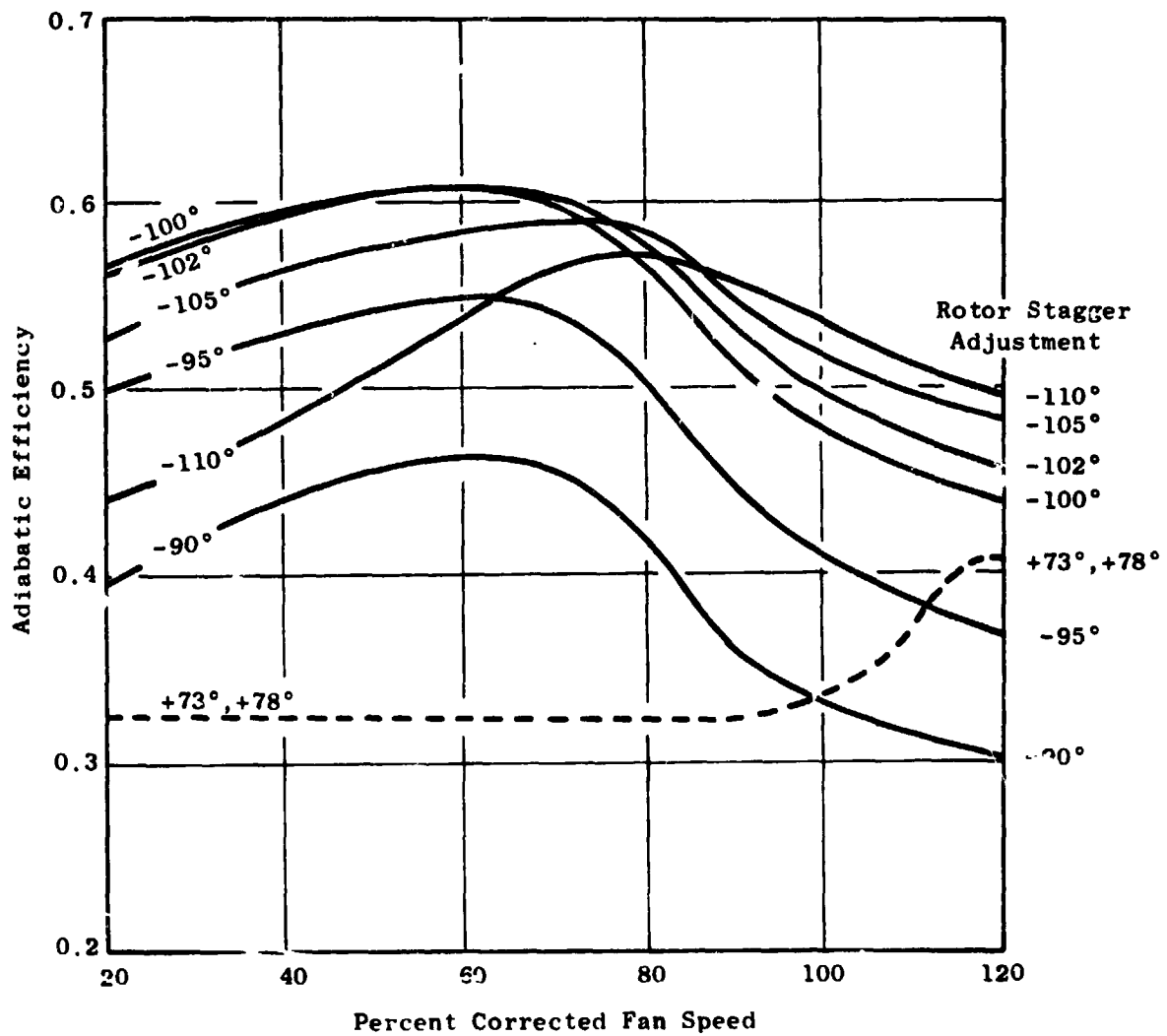


Figure 35. UTW Fan Reverse Mode Adiabatic Efficiency.

SECTION 3.0

UTW FAN ROTOR MECHANICAL DESIGN

3.1 FAN ROTOR SUMMARY

The UTW fan rotor illustrated in Figure 36 is a variable-pitch design that offers full reverse thrust capability. The design includes 18 composite fan blades fabricated from a hybrid combination of Kevlar-49, Type AS graphite, boron, and S-Glass fibers in a PR288 epoxy resin matrix. The blades incorporate a metal leading edge to provide FOD and erosion protection. Solidity of the blade airfoil is 0.95 at the OD and 0.98 at the ID which permits rotation of the blades into the reverse thrust mode of operation through both the flat pitch and the stall pitch directions. A spherical casing radius and a spherical blade tip provide good blade tip clearances throughout the range of blade pitch angle settings.

Each blade is attached to a rotor trunnion at the blade's root. The trunnions are retained by the disk. Retainer straps, attached to the trunnion, lock the blade in axial position and resist trunnion opening deflections under blade centrifugal loading.

Centrifugal force of each blade and trunnion is carried by a single-row ball thrust bearing. This bearing has a full complement of balls to reduce the per-ball loading. The race has a much higher conformance than is standard for thrust bearings because of its highly loaded, intermittently actuated environment. The bearing is grease lubricated, with a cup shield completely covering the upper race and most of the lower race, preventing the grease from leaking out under high radial "g" loads. This concept was successfully demonstrated on General Electric's reverse pitch fan. Fail-safe lubrication is accomplished by a tungsten disulfide coating applied to the balls and races. Under the planned loading, this coated bearing is capable of operating 9000 engine hours after loss of lubricant with only a slight increase in coefficient of friction and negligible wear. Secondary and vibratory loads from the trunnion are resisted by dry thrust and journal bearings located at the OD of the fan disk.

In a concept similar to that used on the CF6-50 fan, balance weights are accessible in the fan spinner, and field balance of the fan is possible without removing the spinner. Ease of maintenance has also been considered in the design of the other rotor components. After removal of the rotor spinner and the forward retaining straps, the blades can be individually removed and replaced without disassembly of the blade trunnion. Access holes in the flange of the aft rotating flowpath permit bolt removal to allow removal of the fan rotor, blade actuator, and the reduction gear as a complete subassembly.

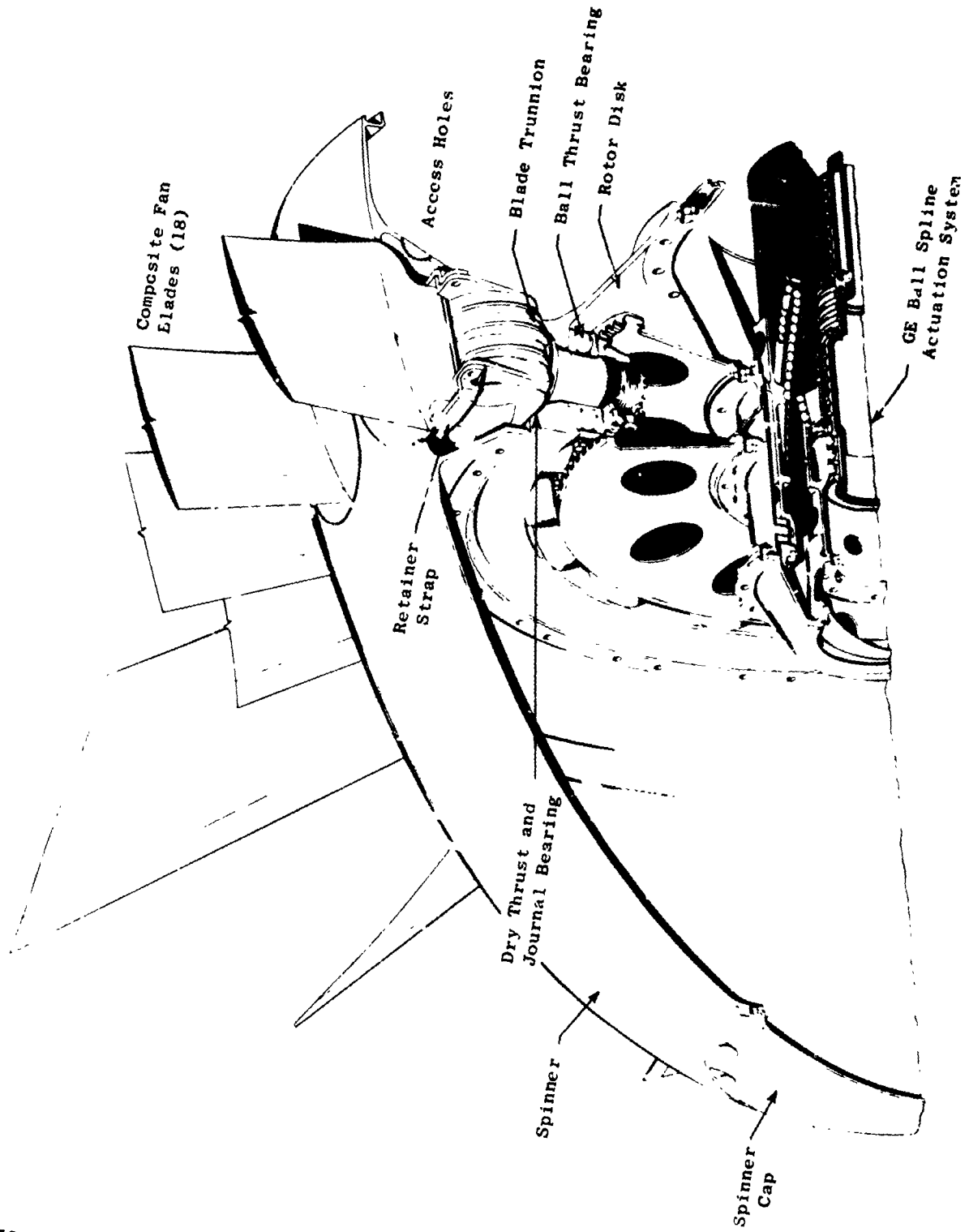


Figure 36. UTW Fan Rotor Configuration.

ORIGINAL PAGE IS
OF POOR QUALITY

All UTW fan rotor components are of flight-weight design. Rotor material selections were made to satisfy life requirements with minimum weight. Normal flight engine design practices, including consideration of LCF life and FAA flight requirements such as burst speed margin and bird strike capability, have been adhered to in the rotor design.

3.2 COMPOSITE FAN BLADES

3.2.1 Design Requirements

Design requirements for the JTW composite fan blade were established to provide realistic long-life operation of a flight engine. The major design requirements are listed as follows:

- Design Mechanical Speeds
 - 100% mechanical design - 3244 rpm
 - 100% SLS hot-day takeoff - 3143 rpm
 - Maximum steady-state duty cycle speed - 3326 rpm
 - Maximum design overspeed - 3614 rpm
 - Maximum burst speed - 4700 rpm
- Design Life and Cycles
 - 36,000 hours
 - 48,000 cycles (based on a 45-minute mission)
 - 1,000 ground check-out cycles, full power
- Mechanical Design Requirements
 - Blade is capable of operation from flat pitch through stall pitch.
 - Blades are individually replaceable without major teardown.
 - Blade untwist has been factored into airfoil configuration.
 - Stresses are within allowable stress range diagram, with sufficient vibratory margin.
 - First flexural frequency crosses 2/rev above flight idle and below take-off and climb engine speeds.

- First flexural frequency has greater than 15% margin over 1/rev. at 115% speed.
- Blade nickel leading edge protection has been kept within aero airfoil limits.

Of these mechanical design requirements, the first is of prime importance. Successful operation of the experimental engine hinges to a great degree on having a rugged blade which can withstand reverse pitch operation and other inlet disturbances including crosswind testing. Initially the design requirements included provisions for satisfying FAA specifications for FOD resistance. During the testing of preliminary blades, however, it was found that the blade FOD capability was less than desired and FOD requirements were dropped pending further developments on other NASA and related programs.

3.2.2 Basic Design Features

The UTW composite blade is illustrated in Figure 37. Design features of the blade are described in the following paragraphs.

Aerodynamic Blade Parameters

A summary of the aero blade parameters is presented in Table 6. Detailed blade aerodynamic design characteristics, including blade chord, maximum thickness, stagger angle, and camber are presented in Section 2.0, Fan Aerodynamic Design. The blade length, thickness, and twist geometries are similar to composite blade. They have undergone extensive development and proof testing on other programs.

Blade Configuration

Finished configuration of the fan blade is shown in Figure 38 and consists of a molded composite blade and a molded composite platform. The molded blade is shown in Figure 39. The platform is described in a subsequent section.

The blade molded configuration consists of a solid composite airfoil and a straight bell-shaped composite dovetail. The molded blade leading edge is slightly reduced in thickness along the entire span to allow for a nickel plate over wire mesh protection. The dovetail is undercut at the leading edge and trailing edge to reduce local stresses and to permit better transitioning of the cambered airfoil section into the straight dovetail.

Airfoil definition is described by 15 radially spaced airfoil cross sections which are stacked on a common axis. These are shown along with some details of the blade cross sections in Figure 40. Each section location corresponds to the like designated elevation defined on the blade, Figure 38. The dotted portion of the leading edge defines the aero profile and the solid inner portion describes the molded composite cross section. Only a portion of these sections lie below the platform, and therefore do not need to corres-

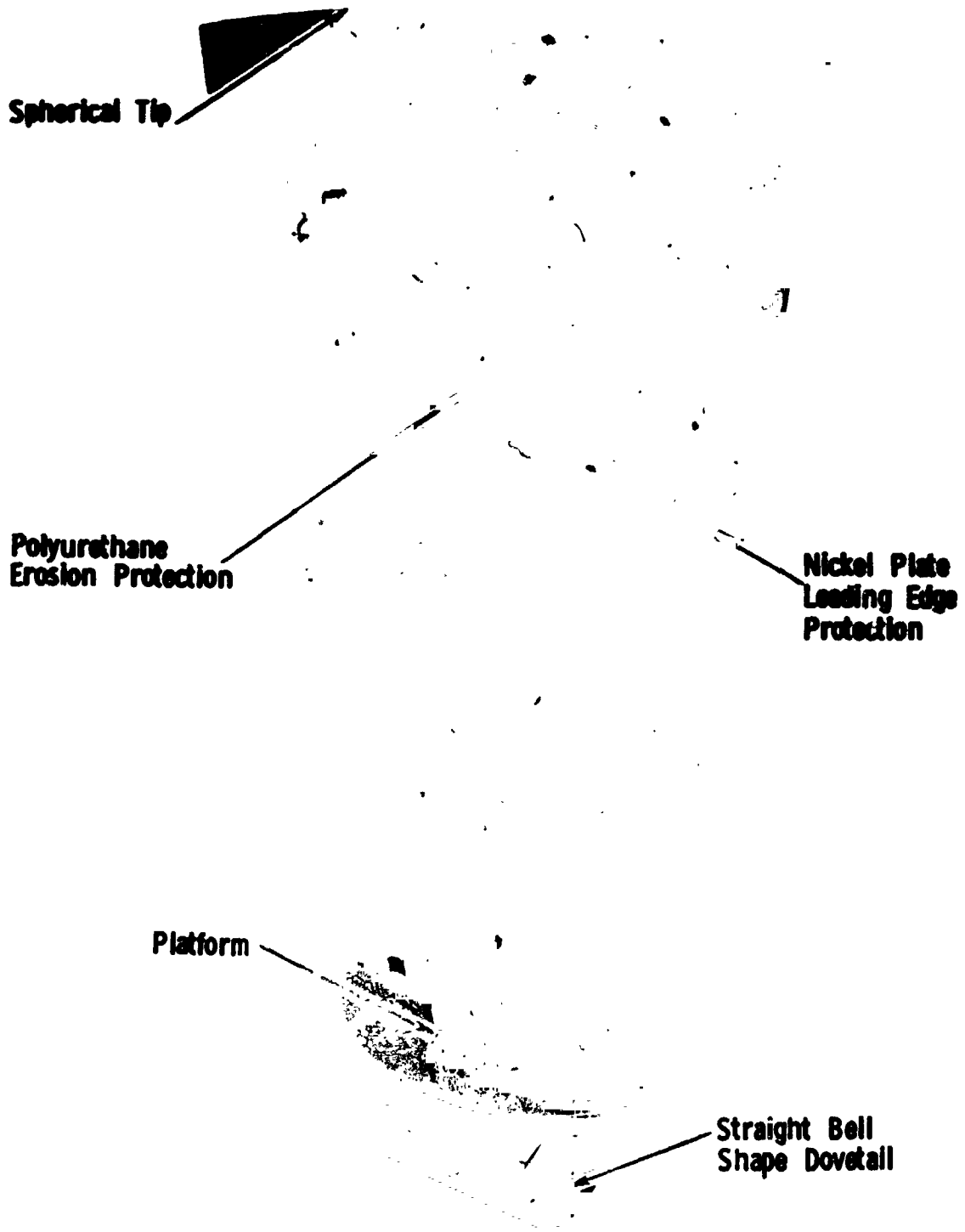


Figure 37. QCSEE UTW Composite Fan Blade and Platform.

Table 6. QCSEE UTW Composite Fan Blade Design Summary.

Aero Definition

Tip Speed	306 m/sec (1005 ft/sec)
Tip Diameter	180 cm (71 in.)
Radius Ratio	0.44
Number of Blades	18
Bypass Pressure Ratio	1.27 Takeoff
Aspect Ratio	2.11
Tip Chord	30.3 cm (11.91 in.)
Root Chord	14.8 cm (5.82 in.)
T_H Root	1.92 cm (0.76 in.)
T_H Tip	0.91 cm (0.36 in.)
Root Camber	66.2°
Total Twist	44°
Solidity	
Tip	0.95
Root	0.98
Angle Change from Forward to Reverse	
Through Flat Pitch	85°
Through Stall	95°

ORIGINAL FACE IS
OF POOR QUALITY

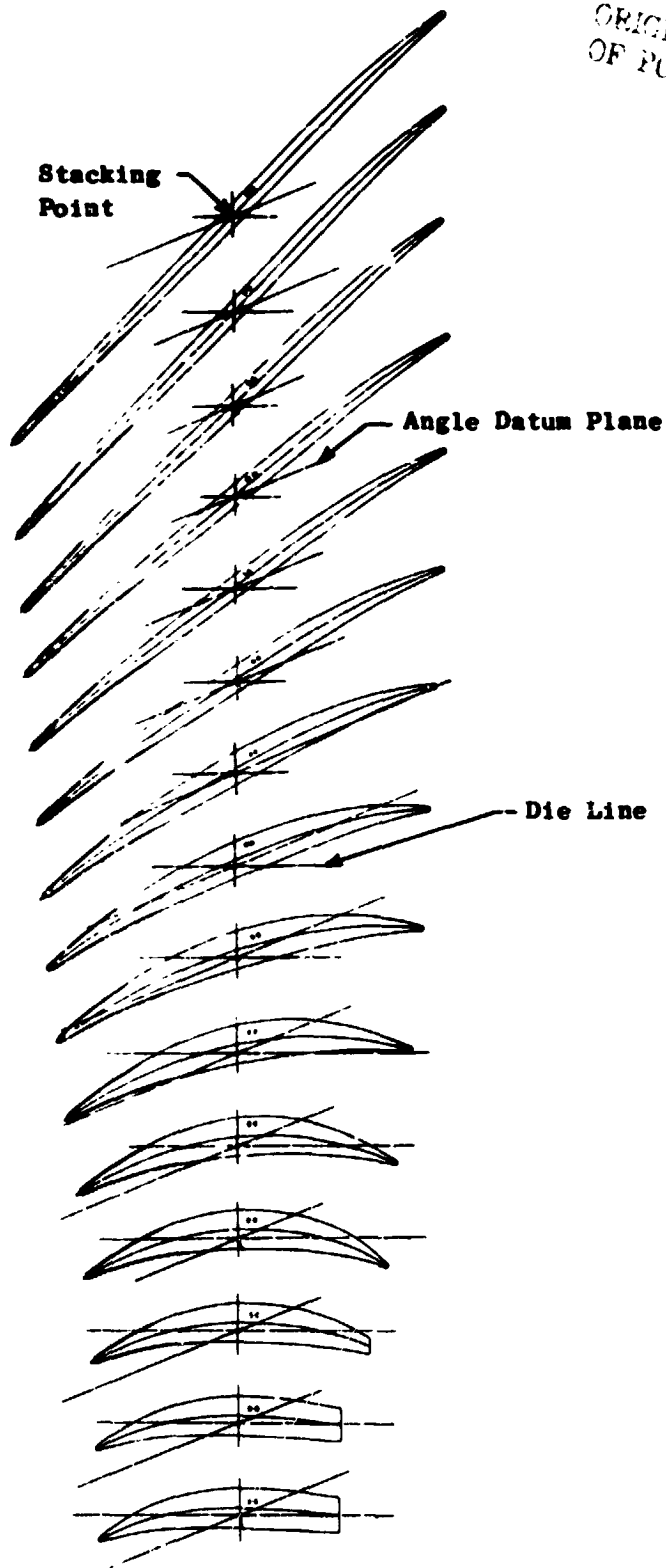


Figure 40. Blade Airfoil Sections.

pond with aero defined profiles. Erosion and small FOD protection of the basic organic composite material blade consists of nickel plating on stainless steel wire mesh which is bonded onto the molded blade and is applied to the leading edge portion of the blade. The details of the blade leading edge protection are shown on the finished blade drawing (Figure 38).

Radial sections through the molded blade are shown in Figure 41. Sections correspond to the like designated locations on the molded blade. The dovetail axial centerline is offset from the stacking axis by 0.254 cm (0.1 in.) to provide a smooth airfoil-to-dovetail transition.

Material Selection/Blade Lay-up Configuration

Material selection and ply arrangement for the UTW hybrid composite blade is based on previous development efforts conducted by General Electric and sponsored by NASA under contract NAS3-16777 and development effort conducted during the preliminary design phase of the QCSEE program. These efforts led to the selection of a combination of fibers in a single blade to provide the proper frequency responses to satisfy STOL engine conditions. Figure 42 shows the general ply shapes, lay-up arrangement, fiber orientations, and material in each ply of the blade. Figure 43 shows a trimetric view of the general arrangement of the plies in the blade. The flex root surface plies in the lower region of the blade contain S-glass fibers. These plies being near the surface and having relatively low bending stiffness and high tensile strength provide higher strain-to-failure characteristics, thereby allowing the blade to absorb large bird impact loading without the classic root failure that usually accompanies brittle composite materials. Torsional stiffening plies in the airfoil region of the blade are oriented at $\pm 45^\circ$ to provide the shear modulus required for a high first torsional frequency. These plies contain boron toward the outer surfaces of the blade and graphite in the inner regions. Plies of Kevlar-49 are interspersed throughout the blade with the majority of them being oriented with their fibers in the longitudinal direction of the blade. Several of the Kevlar plies in the tip region of the blade are oriented at 90° to the longitudinal axis to provide chordwise strength and stiffness to the blade.

The resin system being used in this program is a product of the 3M Company and is designated as PR288. This is a resin system that has proven characteristics in the prepreg form which are:

- Has consistent processing characteristics
- Can be prepregged with many different fibers including hybrids
- Uniform prepreg thickness and resin content control

Typical properties of the PR288/AS prepreg are shown in Table 7. Material properties for several fiber composite prepreps are shown in Table 8.

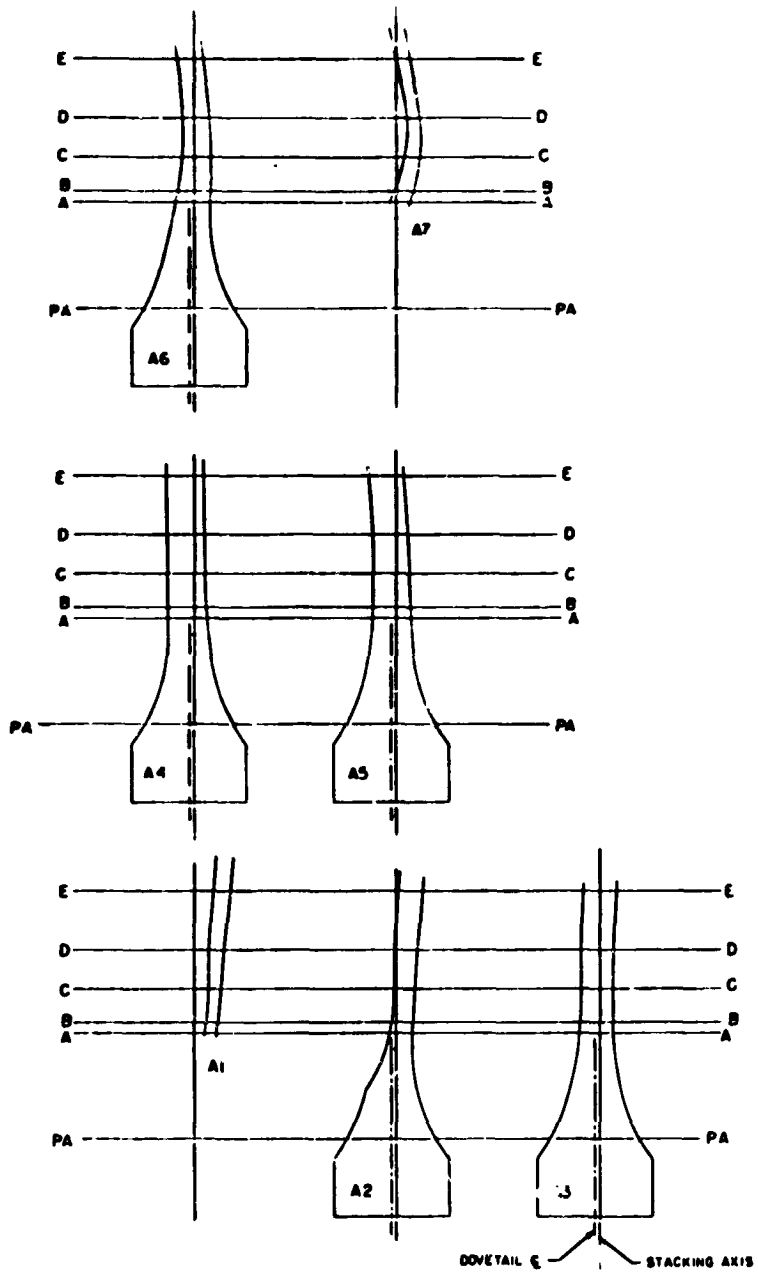


Figure 41. Radial Sections through the Molded Blade.

ORIGINAL PAGE IS
OF POOR QUALITY

FOLDOUT FRAME

ORIGINAL PAGE IS OF POOR QUALITY

PLY NO	PLY ORIENT ANGLE	MATERIAL
1	0°	CR
2	0°	CR
3	0°	CR
4	0°	CR
5	0°	CR
6	0°	CR
7	0°	CR
8	0°	CR
9	0°	CR
10	0°	CR
11	0°	CR
12	0°	CR
13	0°	CR
14	0°	CR
15	0°	CR
16	0°	CR
17	0°	CR
18	0°	CR
19	0°	CR
20	0°	CR
21	0°	CR
22	0°	CR
23	0°	CR
24	0°	CR
25	0°	CR
26	0°	CR
27	0°	CR
28	0°	CR
29	0°	CR
30	0°	CR
31	0°	CR
32	0°	CR
33	0°	CR
34	0°	CR
35	0°	CR
36	0°	CR
37	0°	CR
38	0°	CR
39	0°	CR
40	0°	CR
41	0°	CR
42	0°	CR
43	0°	CR
44	0°	CR
45	0°	CR
46	0°	CR
47	0°	CR
48	0°	CR
49	0°	CR
50	0°	CR
51	0°	CR
52	0°	CR
53	0°	CR
54	0°	CR
55	0°	CR
56	0°	CR
57	0°	CR
58	0°	CR
59	0°	CR
60	0°	CR
61	0°	CR
62	0°	CR
63	0°	CR
64	0°	CR
65	0°	CR
66	0°	CR
67	0°	CR
68	0°	CR
69	0°	CR
70	0°	CR
71	0°	CR
72	0°	CR
73	0°	CR
74	0°	CR
75	0°	CR
76	0°	CR
77	0°	CR
78	0°	CR
79	0°	CR
80	0°	CR
81	0°	CR
82	0°	CR
83	0°	CR
84	0°	CR
85	0°	CR
86	0°	CR
87	0°	CR
88	0°	CR
89	0°	CR
90	0°	CR
91	0°	CR
92	0°	CR
93	0°	CR
94	0°	CR
95	0°	CR
96	0°	CR
97	0°	CR
98	0°	CR
99	0°	CR
100	0°	CR

* CONTAINS 90° PLYS IN TIP REGION

PLY NO	PLY ORIENT ANGLE	MATERIAL
101	0°	CR
102	0°	CR
103	0°	CR
104	0°	CR
105	0°	CR
106	0°	CR
107	0°	CR
108	0°	CR
109	0°	CR
110	0°	CR
111	0°	CR
112	0°	CR
113	0°	CR
114	0°	CR
115	0°	CR
116	0°	CR
117	0°	CR
118	0°	CR
119	0°	CR
120	0°	CR
121	0°	CR
122	0°	CR
123	0°	CR
124	0°	CR
125	0°	CR
126	0°	CR
127	0°	CR
128	0°	CR
129	0°	CR
130	0°	CR
131	0°	CR
132	0°	CR
133	0°	CR
134	0°	CR
135	0°	CR
136	0°	CR
137	0°	CR
138	0°	CR
139	0°	CR
140	0°	CR
141	0°	CR
142	0°	CR
143	0°	CR
144	0°	CR
145	0°	CR
146	0°	CR
147	0°	CR
148	0°	CR
149	0°	CR
150	0°	CR
151	0°	CR
152	0°	CR
153	0°	CR
154	0°	CR
155	0°	CR
156	0°	CR
157	0°	CR
158	0°	CR
159	0°	CR
160	0°	CR
161	0°	CR
162	0°	CR
163	0°	CR
164	0°	CR
165	0°	CR
166	0°	CR
167	0°	CR
168	0°	CR
169	0°	CR
170	0°	CR
171	0°	CR
172	0°	CR
173	0°	CR
174	0°	CR
175	0°	CR
176	0°	CR
177	0°	CR
178	0°	CR
179	0°	CR
180	0°	CR
181	0°	CR
182	0°	CR
183	0°	CR
184	0°	CR
185	0°	CR
186	0°	CR
187	0°	CR
188	0°	CR
189	0°	CR
190	0°	CR
191	0°	CR
192	0°	CR
193	0°	CR
194	0°	CR
195	0°	CR
196	0°	CR
197	0°	CR
198	0°	CR
199	0°	CR
200	0°	CR

PLY NO	PLY ORIENT ANGLE	MATERIAL
201	0°	CR
202	0°	CR
203	0°	CR
204	0°	CR
205	0°	CR
206	0°	CR
207	0°	CR
208	0°	CR
209	0°	CR
210	0°	CR
211	0°	CR
212	0°	CR
213	0°	CR
214	0°	CR
215	0°	CR
216	0°	CR
217	0°	CR
218	0°	CR
219	0°	CR
220	0°	CR
221	0°	CR
222	0°	CR
223	0°	CR
224	0°	CR
225	0°	CR
226	0°	CR
227	0°	CR
228	0°	CR
229	0°	CR
230	0°	CR
231	0°	CR
232	0°	CR
233	0°	CR
234	0°	CR
235	0°	CR
236	0°	CR
237	0°	CR
238	0°	CR
239	0°	CR
240	0°	CR
241	0°	CR
242	0°	CR
243	0°	CR
244	0°	CR
245	0°	CR
246	0°	CR
247	0°	CR
248	0°	CR
249	0°	CR
250	0°	CR
251	0°	CR
252	0°	CR
253	0°	CR
254	0°	CR
255	0°	CR
256	0°	CR
257	0°	CR
258	0°	CR
259	0°	CR
260	0°	CR
261	0°	CR
262	0°	CR
263	0°	CR
264	0°	CR
265	0°	CR
266	0°	CR
267	0°	CR
268	0°	CR
269	0°	CR
270	0°	CR
271	0°	CR
272	0°	CR
273	0°	CR
274	0°	CR
275	0°	CR
276	0°	CR
277	0°	CR
278	0°	CR
279	0°	CR
280	0°	CR
281	0°	CR
282	0°	CR
283	0°	CR
284	0°	CR
285	0°	CR
286	0°	CR
287	0°	CR
288	0°	CR
289	0°	CR
290	0°	CR
291	0°	CR
292	0°	CR
293	0°	CR
294	0°	CR
295	0°	CR
296	0°	CR
297	0°	CR
298	0°	CR
299	0°	CR
300	0°	CR

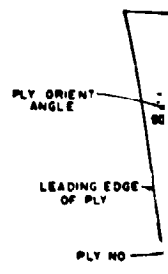
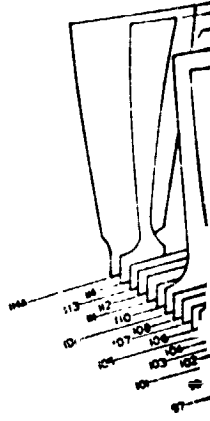
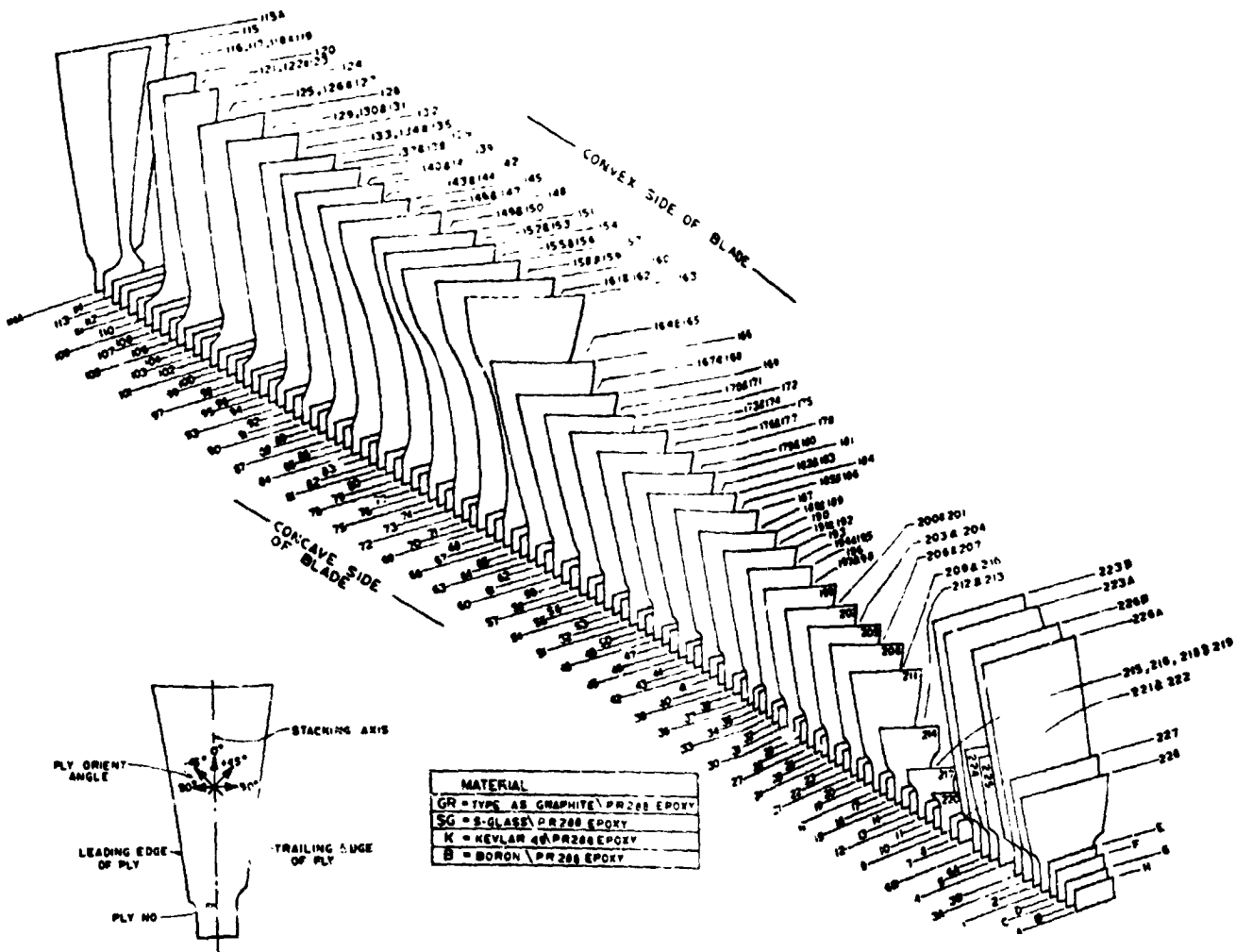


Figure 42. Ply Lay-up and Material A

PRECEDING PAGE BLANK NOT

ORIGINAL PAGE IS
POOR QUALITY

EOLDOUT FRAME



...up and Material Arrangement.

PAGE BLANK NOT FILMED

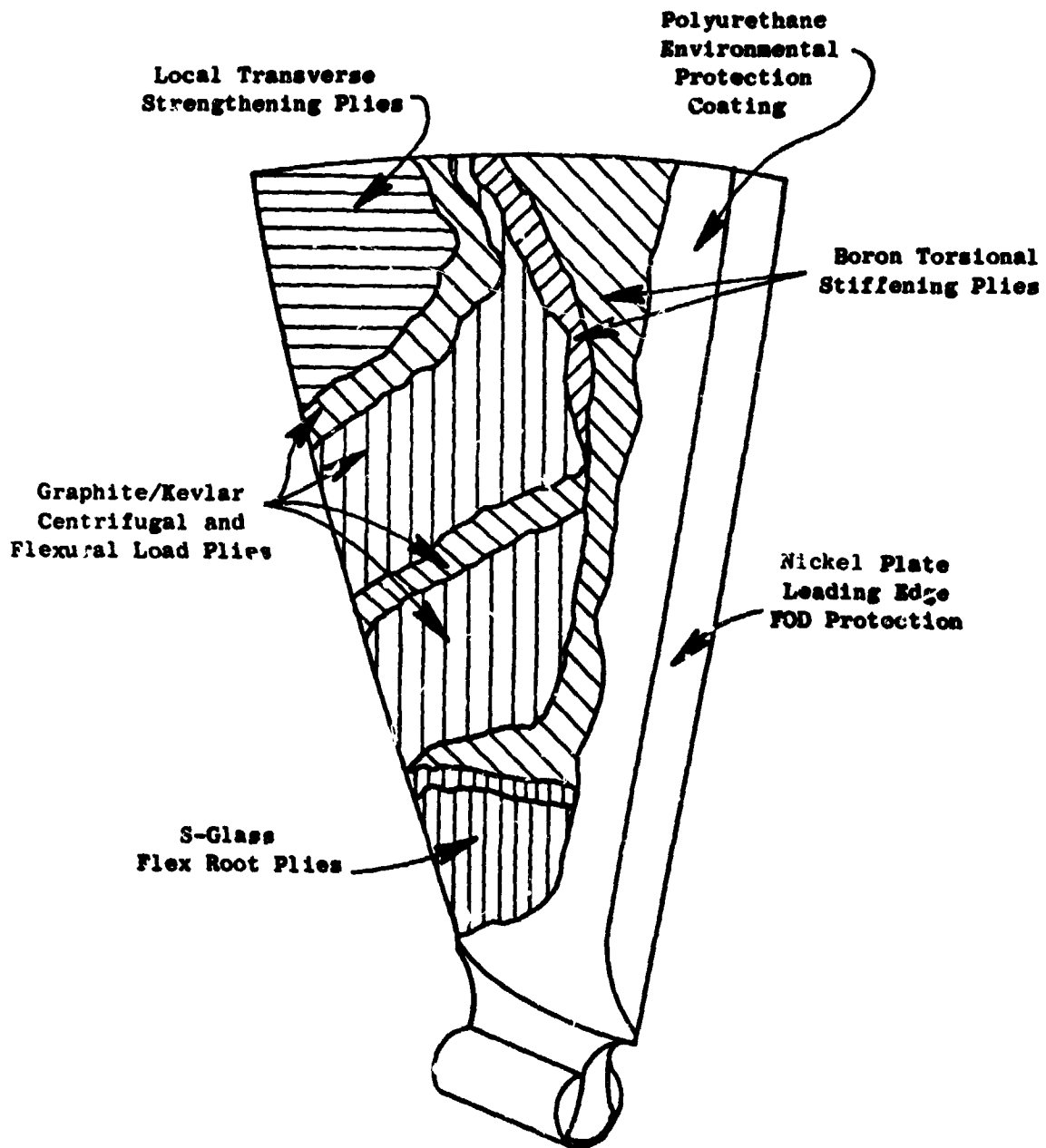


Figure 43. QCSEE UTW Composite Blade.

ORIGINAL PAGE IS
OF POOR QUALITY

Table 7. PR288/AS Prepreg Properties.

<u>Property</u>	<u>PR288/AS</u>
Supplier	3M
Process	Film - Cont. Tape
Cure Schedule	2.5 hrs at 129° C (265° F)
Postcure Schedule	4 hrs at 135° C (275° F)
Flexural Strength	
Room Temperature	193 kN/cm ² (280 ksi)
121° C (250° F)	138 kN/cm ² (200 ksi)
Elastic Mod.	
Room Temperature	11.9 kN/cm ² (17.2 ksi)
121° C (250° F)	11.6 kN/cm ² (16.8 ksi)
Short Beam Shear	
Room Temperature	9.0 kN/cm ² (13.0 ksi)
121° C (250° F)	5.2 kN/cm ² (7.5 ksi)
Charpy Impact	8.0 m-N (6.0 ft-lb)
Fiber Volume, %	59.8
Sp. Gr., g/cc	1.58
Void Content %	0.0

C-2

Table 8. Composite Material Properties.

	PR288 AS-Graphite	PR288 Boron	PR288 S-Glass	PR288 Kevlar 49
Fiber volume, Percent	60	55	60	60
Elastic Modulus, 10^6 N/cm^2 (10^6 psi) (0° Orientation)	11.5 (17.2)	20.0 (29.0)	5.9 (8.5)	7.6 (11.0)
Elastic Modulus, 10^6 N/cm^2 (10^6 psi) (90° Orientation)	1.1 (1.6)	1.2 (1.8)	0.8 (1.1)	0.6 (0.8)
Elastic Modulus, 10^6 N/cm^2 (10^6 psi) ($0/22/0/-22$ Orientation)	9.5 (13.8)	11.7 (17.0)	4.7 (6.8)	5.9 (8.6)
Shear Modulus, 10^6 N/cm^2 (10^6 psi) ($0/22/0/-22$)	1.1 (1.6)	1.9 (2.7)	0.6 (0.9)	0.6 (0.93)
Poisson's Ratio ($0/22/0/-22$)	0.65	0.97	0.39	0.90
Density, G/cm^3 (lb/in^3)	1.5 (0.056)	1.9 (0.070)	2.0 (0.072)	1.4 (0.050)
Tensile Strength, kN/cm^2 (ksi) (0°)	138 (200)	138 (200)	138+ (200+)	138 (200)
Tensile Strength, kN/cm^2 (ksi) ($0/22/0/-22$)	95 (138)	95 (138)	95+ (138)	95 (138)
Flex Strength, kN/cm^2 (ksi) (0°)	193 (280)	---	---	62 (90)
Flex Strength, kN/cm^2 (ksi) ($0/22/0/-22$)	168 (244)	---	172 (250)	59 (85)
Shear Strength, kN/cm^2 (ksi) (0°)	9.0 (13.0)	7.6 (11.0)	8.1 (11.8)	3.4-7 (5-10)
Charpy Impact, m-N (ft-lb) ($\pm 10^\circ$)	8 (6)	10 (7.5)	47 (35)	23 (17)

Dovetail Design

The dovetail design for the composite fan blade consists of a straight bell-shaped dovetail with a 8.89-cm (3-1/2-in.) radius. The bell-shaped dovetail design reflects many years of development efforts to achieve an efficient dovetail configuration having both high static pull strength and good fatigue strength. All airfoil plies extend continuously down into the dovetail and are interspersed with insert plies which act to fill out the enlarged cross section. This is seen in Figure 44 which shows a radial section of the blade root and dovetail prior to dovetail machining. The final dovetail is shown in Figure 41.

Platform Design

The QCSEE UTW engine incorporates a variable-pitch fan. The blade variable-pitch operation requires a circular opening through the spinner and hub to permit airfoil clearance in the different blade position rotations - either actuated in the flat pitch or stall direction. To maintain reasonable actuation forces and blade dovetail stresses, the centrifugal loading on each blade platform and dovetail must be kept to a minimum. This requires a lightweight design. Therefore, composite platforms in addition to composite blades are necessary. The following paragraphs summarize the design requirements and description of the platform.

The platform design selected for the QCSEE UTW blade satisfies several requirements including (1) lightweight - less than 0.16 kg (0.35 lb), (2) a structural stress margin of safety of 2 at 3326 rpm to provide for positive margin at the design burst condition of 4700 rpm, (3) a fail-safe design in the event the platform-to-blade bond becomes ineffective, and (4) a low radial deflection - less than 0.05 cm (0.020 in.) at tip of platform overhang. In addition, the circular opening required for blade rotation is filled by the platform. The platform is attached to the blade and contoured to match closely the spinner and hub which make up the fan inner aerodynamic contours and provide a smooth inner flowpath. The platform is also designed to avoid interference with adjacent blades and adjacent platforms during variable-pitch blade turning.

Structurally the platform is a varying width tapered beam cantilevered from the blade root. It consists of honeycomb core stabilized by upper and lower graphite/epoxy face sheets which are simultaneously molded and bonded onto the blade using a co-curing process. The result is a one piece platform design. With structural plies extending around the blade root leading and trailing edge undercuts, the single-piece design has the inherent capability of being retained even with a complete loss of the blade-to-platform adhesive bond. This satisfies the fail-safe requirements.

Figure 38 shows the final platform on the blade, while Figure 45 is a schematic showing the platform details.

ORIGINAL PAGE IS
OF POOR QUALITY

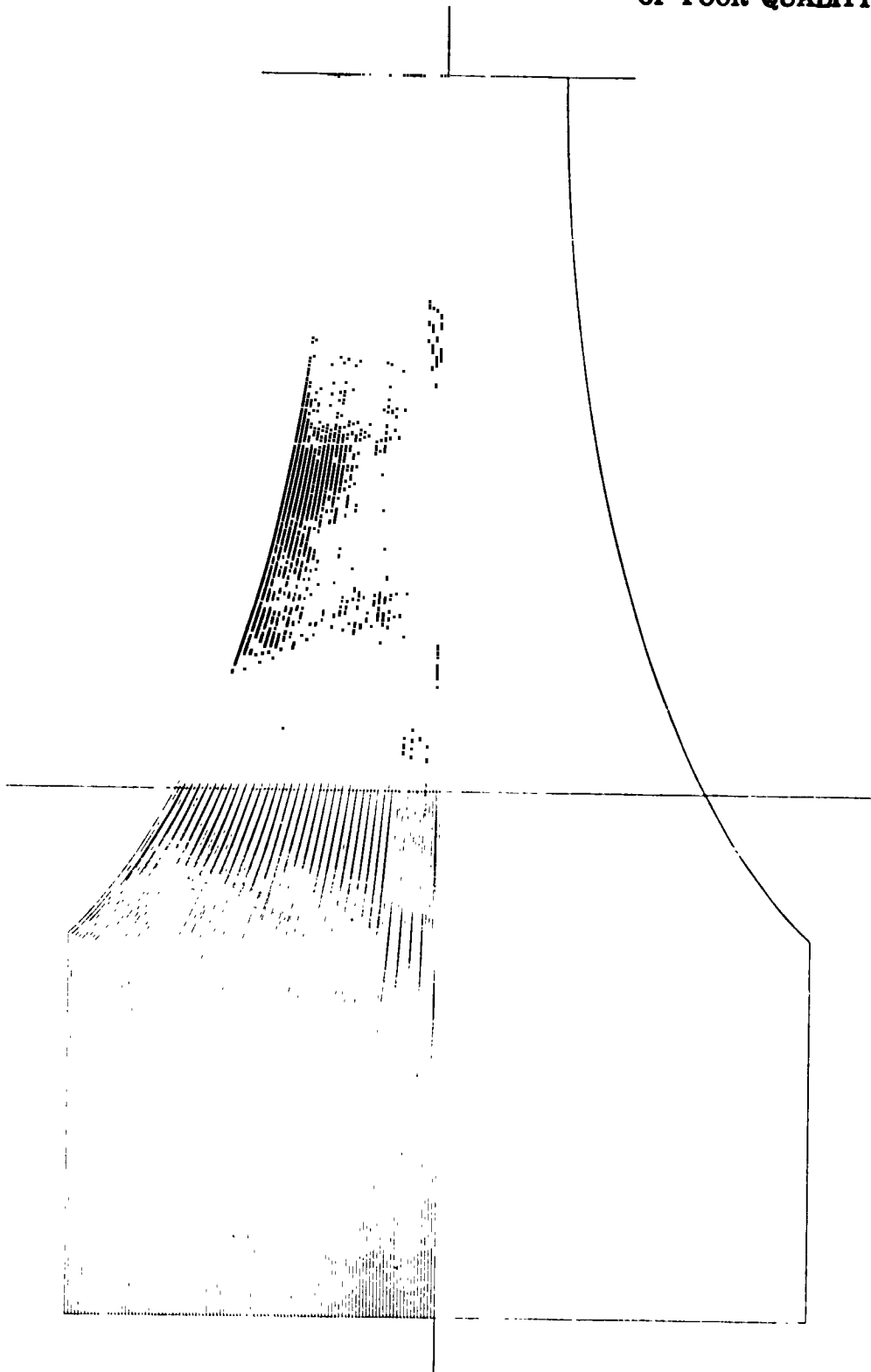


Figure 44. Dovetail Molded Section.

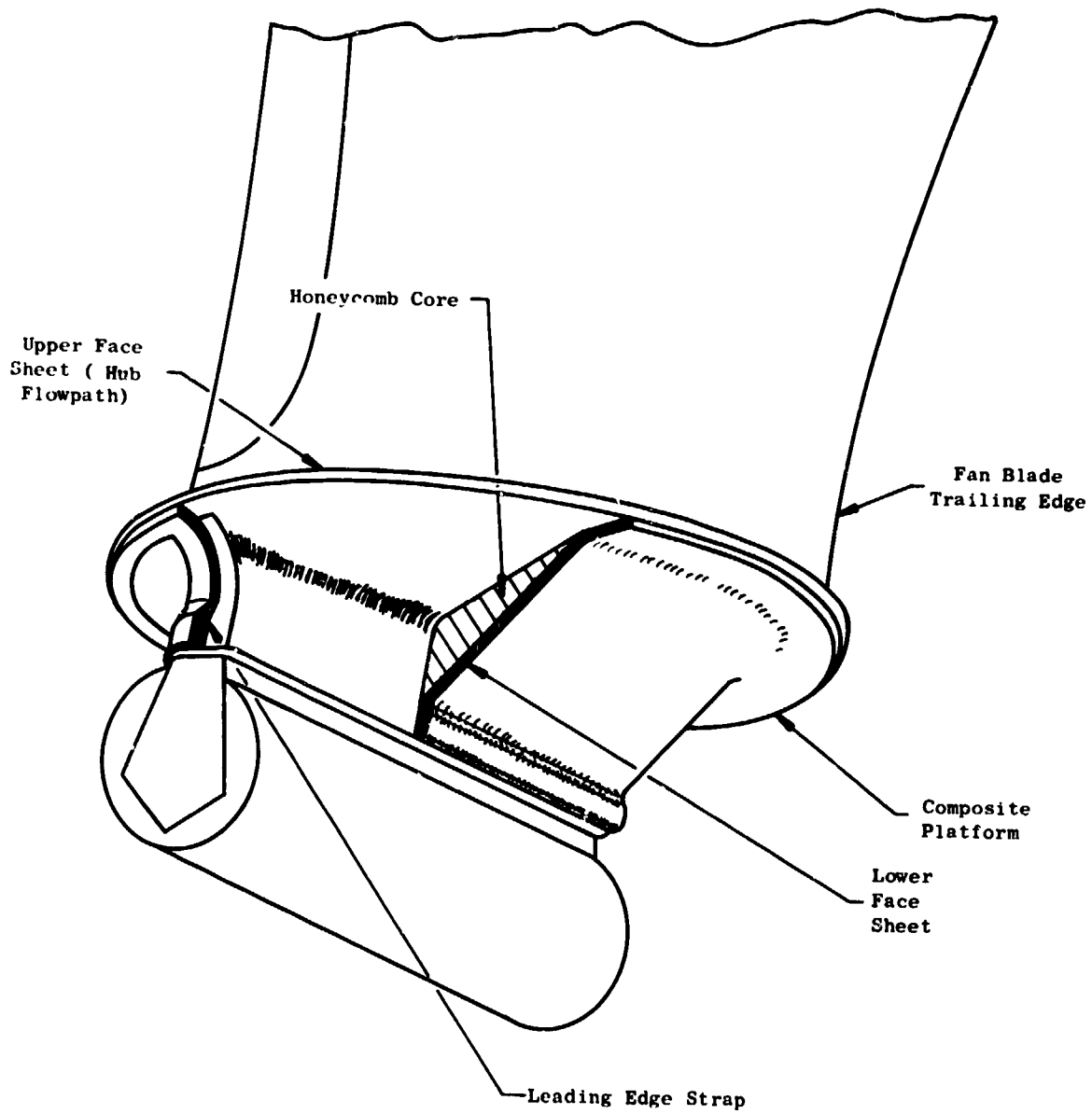


Figure 45. Platform Design.

3.2.3 Design Analysis

Blade Stress and Deflection Analysis

The blade stress analysis was performed using the 3-D finite element computer program "PARA-TAMP-EIG". This program is a parametric, 3-D finite element eigenvalue and thermal stress computer program. The program accounts for the inertia forces of rotation and vibration. Account is taken of the stiffening effect of rotation. The program gives directly the lowest eight modes, stresses, and frequencies for a specified speed of rotation. In addition, it gives deflections and stresses at any given operating rpm. The material properties are 3-D anisotropic. Thermal stresses are also computed.

The finite element model used for the blade analysis was generated to geometrically represent the blade design, without platform, as shown in Figure 41.

A number of computer runs were made to provide steady-state stresses under centrifugal and pressure loading conditions and vibratory (eigenvalue/eigenvector) relative stresses at zero and speed conditions assuming the blade dovetail to be fixed at the radial cross section corresponding to the PA plane as defined in Figure 41. The steady-state results at 3326 rpm (the blade duty cycle steady-state speed) show that the highest tensile stresses exist in the airfoil-to-dovetail transition region slightly above the leading edge undercut. The highest calculated tensile stress is $15,490 \text{ N/cm}^2$ (22,460 psi). The highest compressive stress is 3790 N/cm^2 (5,500 psi) at the corresponding trailing edge location. The highest calculated shear stress is 3400 N/cm^2 (4,930 psi) in the region of the leading edge overhang. The material minimum tensile, compressive, and shear strengths are $58,600 \text{ N/cm}^2$ (85,000 psi), $17,240 \text{ N/cm}^2$ (25,000 psi), and $4,480 \text{ N/cm}^2$ (6,500 psi), providing margins of safety of 2.7, 3.5, and 0.3, respectively. The margin of safety in shear at the leading edge undercut region is expected to be improved by the addition of the platform which will share in carrying the shear loads to the dovetail. Figure 46 shows a plot of stresses as a function of blade span length, while Figures 47, 48, and 49 show stress maps for the concave and convex blade faces for radial stress, chordwise stress, and interlaminar shear stress, respectively. Figure 50 gives a plot of blade deflection and twist as a function of span length. Figures 51, 52, and 53 show relative radial stresses over the blade for the first three vibratory modes. These maps of relative radial stresses under vibratory conditions show the changes in stress locations for the different vibratory modes.

Blade vibratory strengths as determined from specimens and preliminary QCSEE blade testing are shown on the stress range diagram in Figure 54. The anticipated maximum vibratory stress is 11 ksi single amplitude on the basis of testing on other engine programs. For the steady-state conditions shown, that of a hot-day takeoff and maximum standard-day cruise, the combination of steady-state mean stress and expected maximum vibratory stress results in an acceptable blade life.

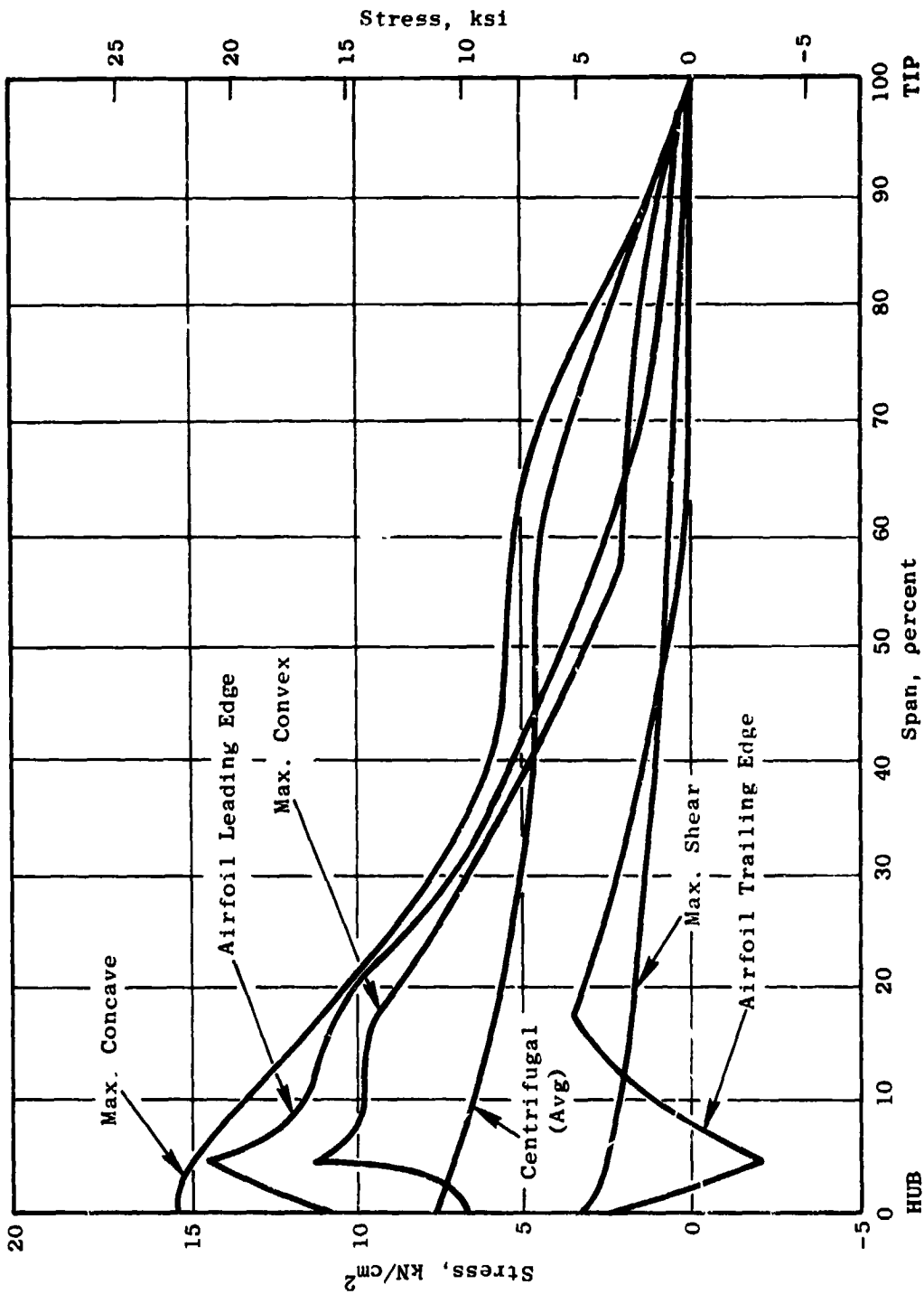


Figure 46. UTW Blade Resultant Radial Stress - 3326 rpm.

ORIGINAL PAGE IS
OF POOR QUALITY

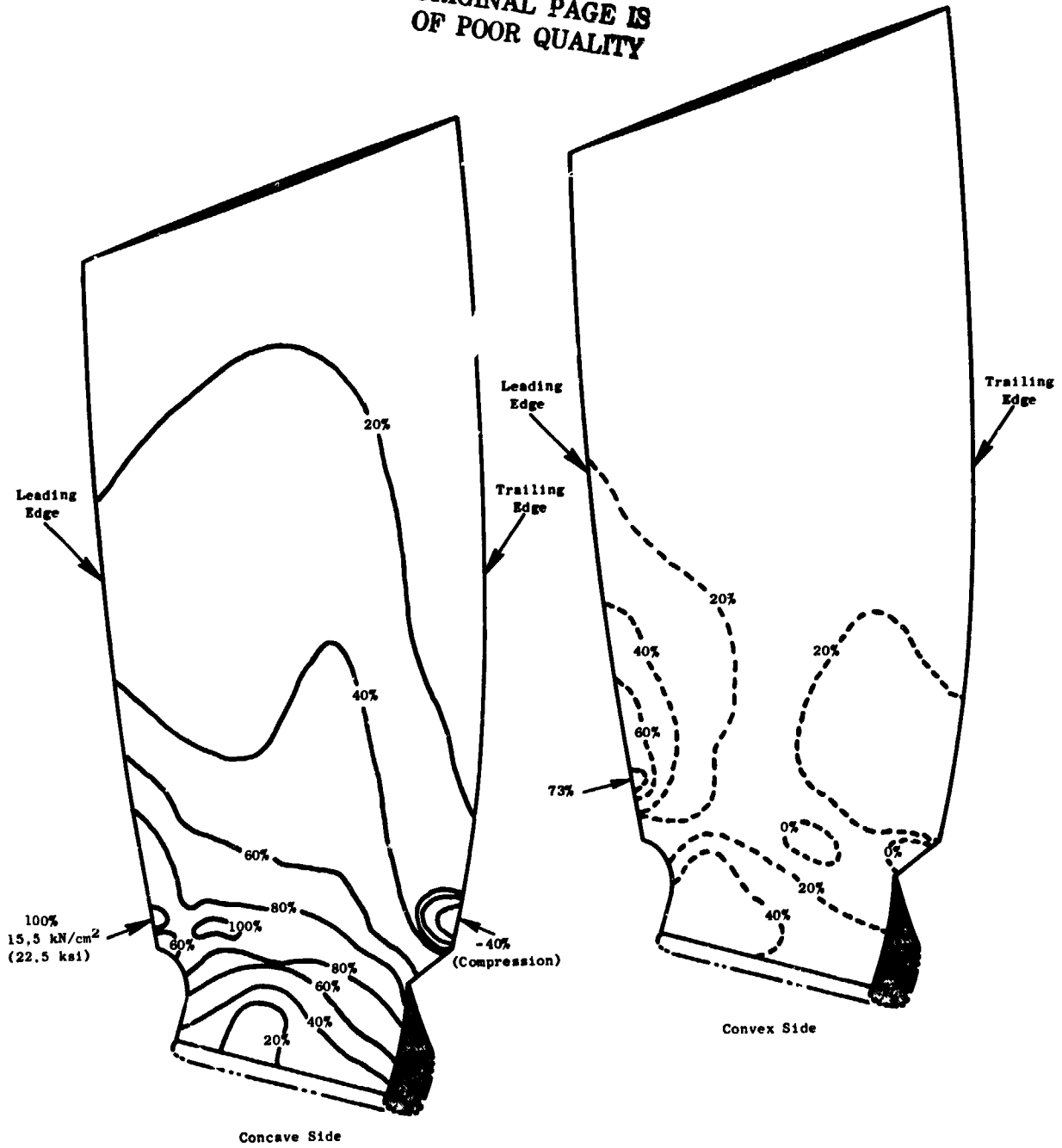


Figure 47. Calculated Blade Radial Stress.

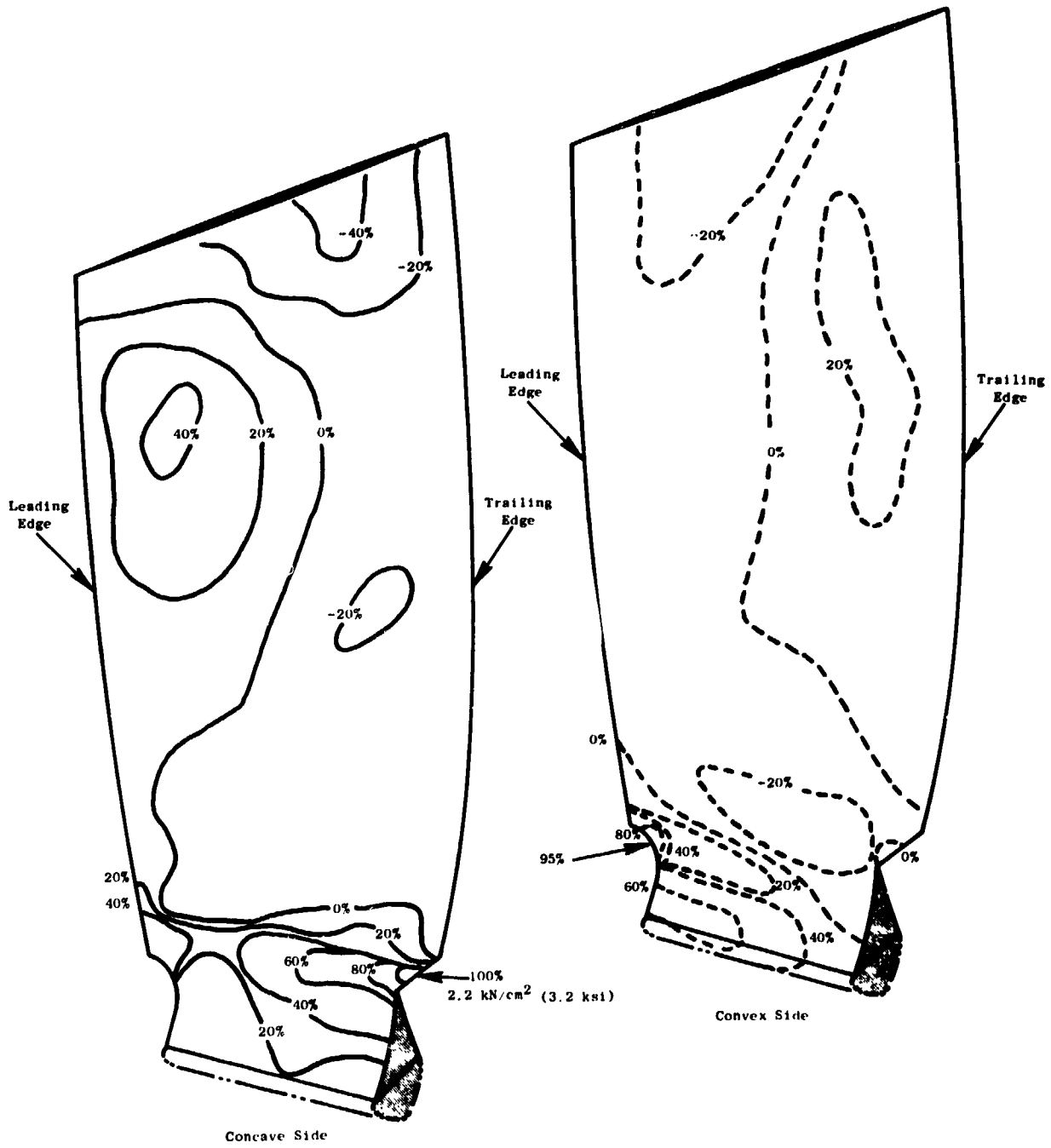


Figure 48. Calculated Blade Chordal Stress.

ORIGINAL PAGE IS
OF POOR QUALITY

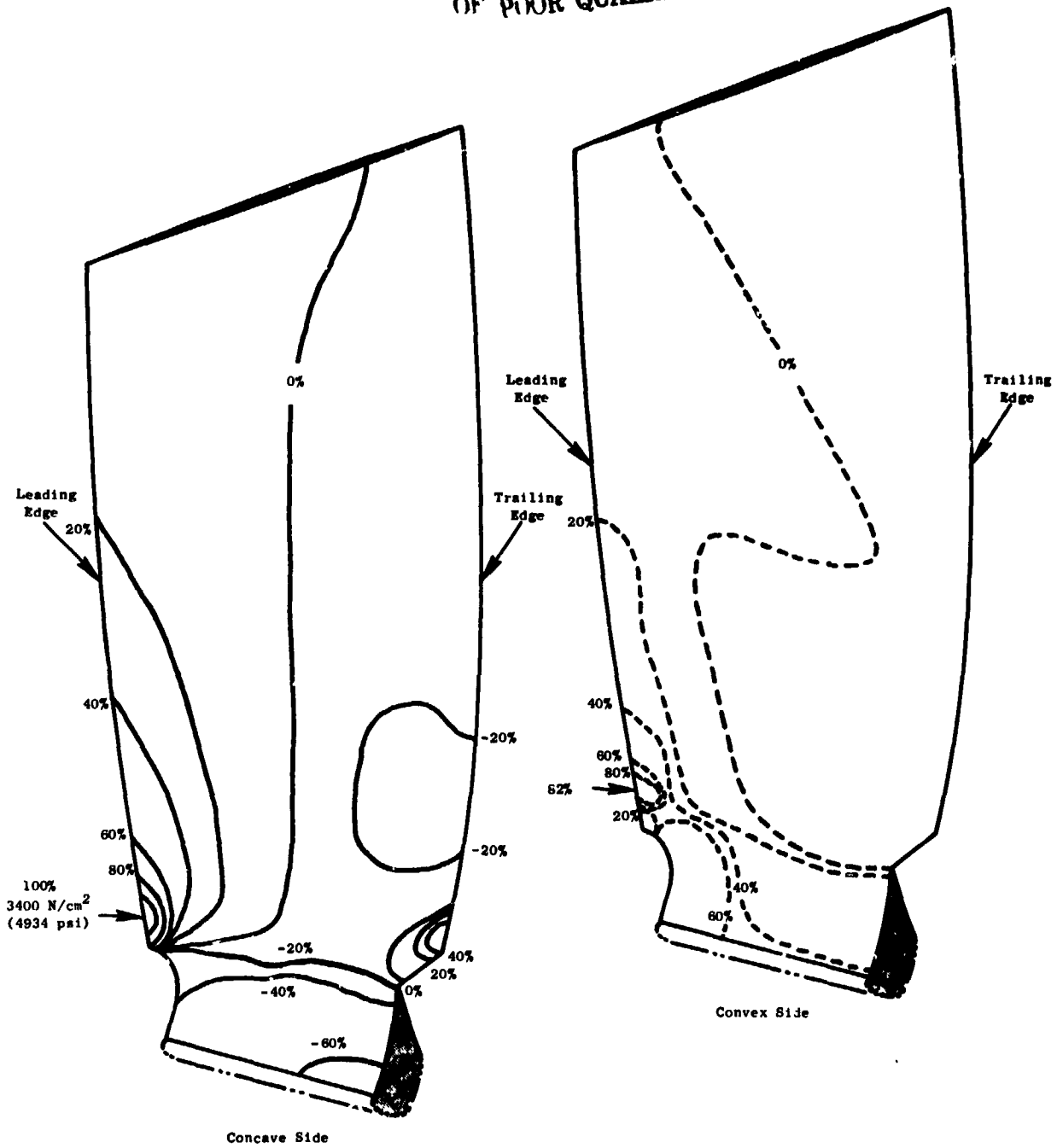


Figure 49. Calculated Blade Interlaminar Shear Stress.

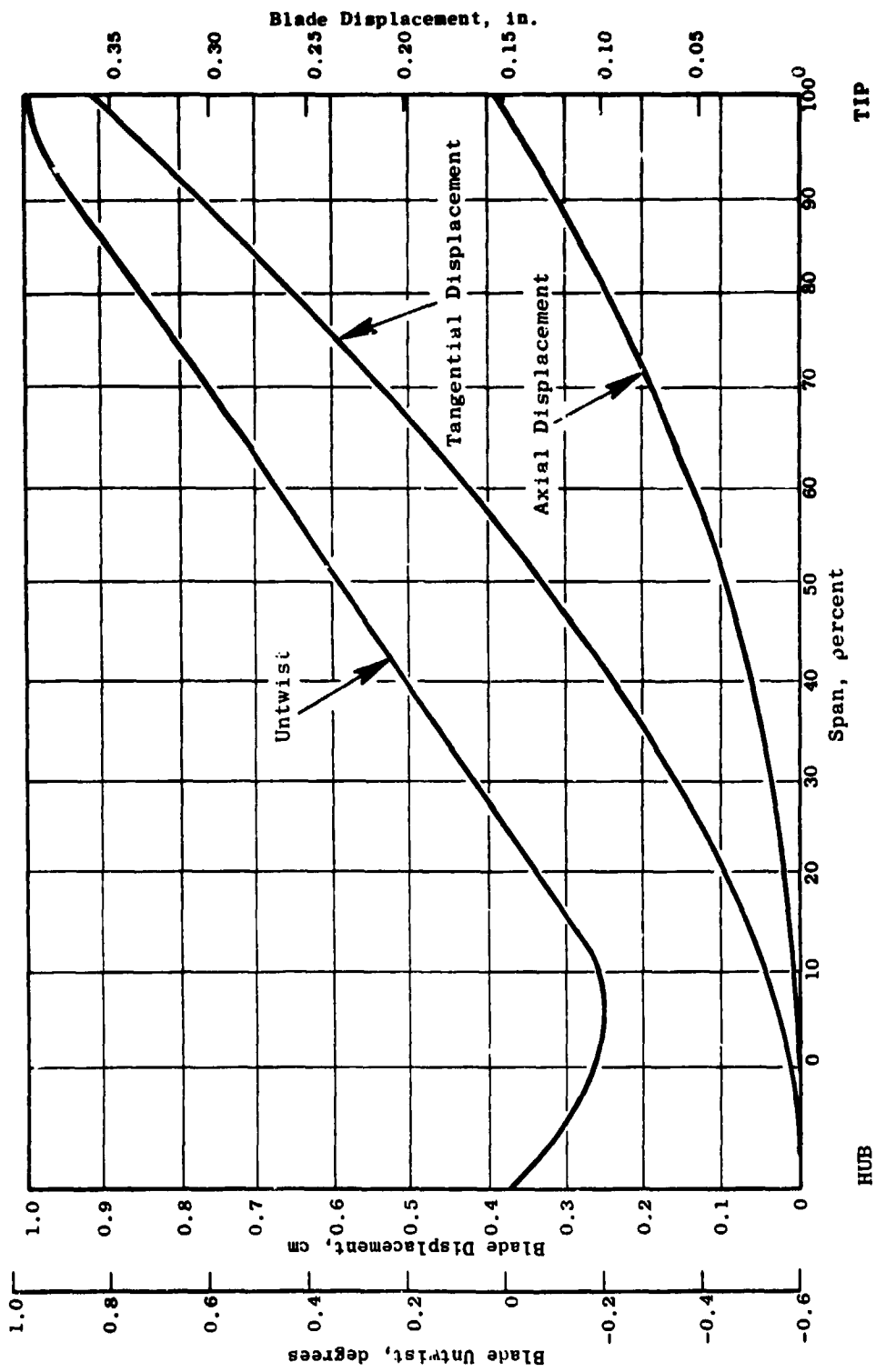


Figure 50. UTW Blade Displacements and Twist.

ORIGINAL PAGE IS
OF POOR QUALITY

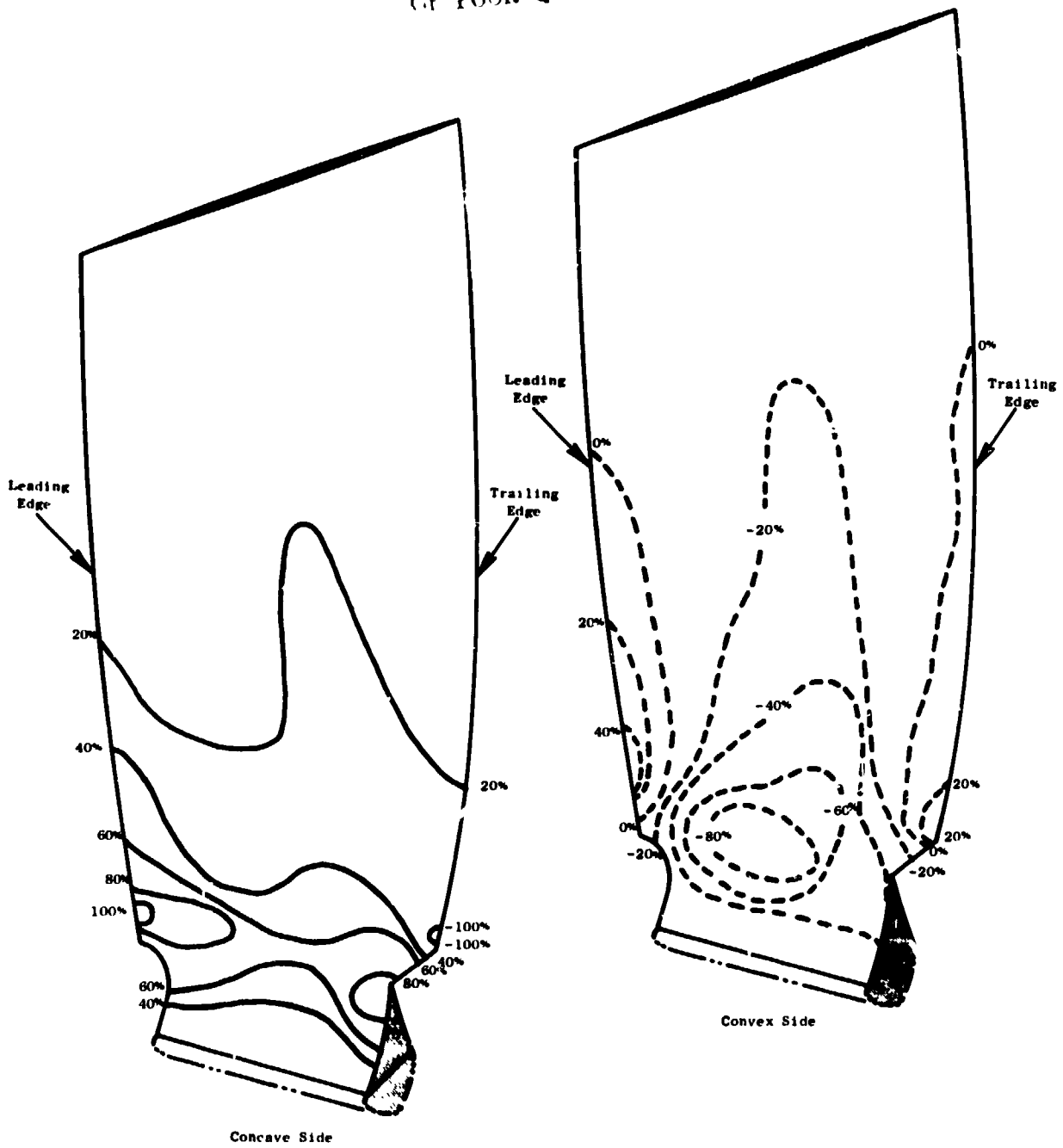


Figure 51. Calculated Blade Relative Radial Stresses for First Flexural Mode.

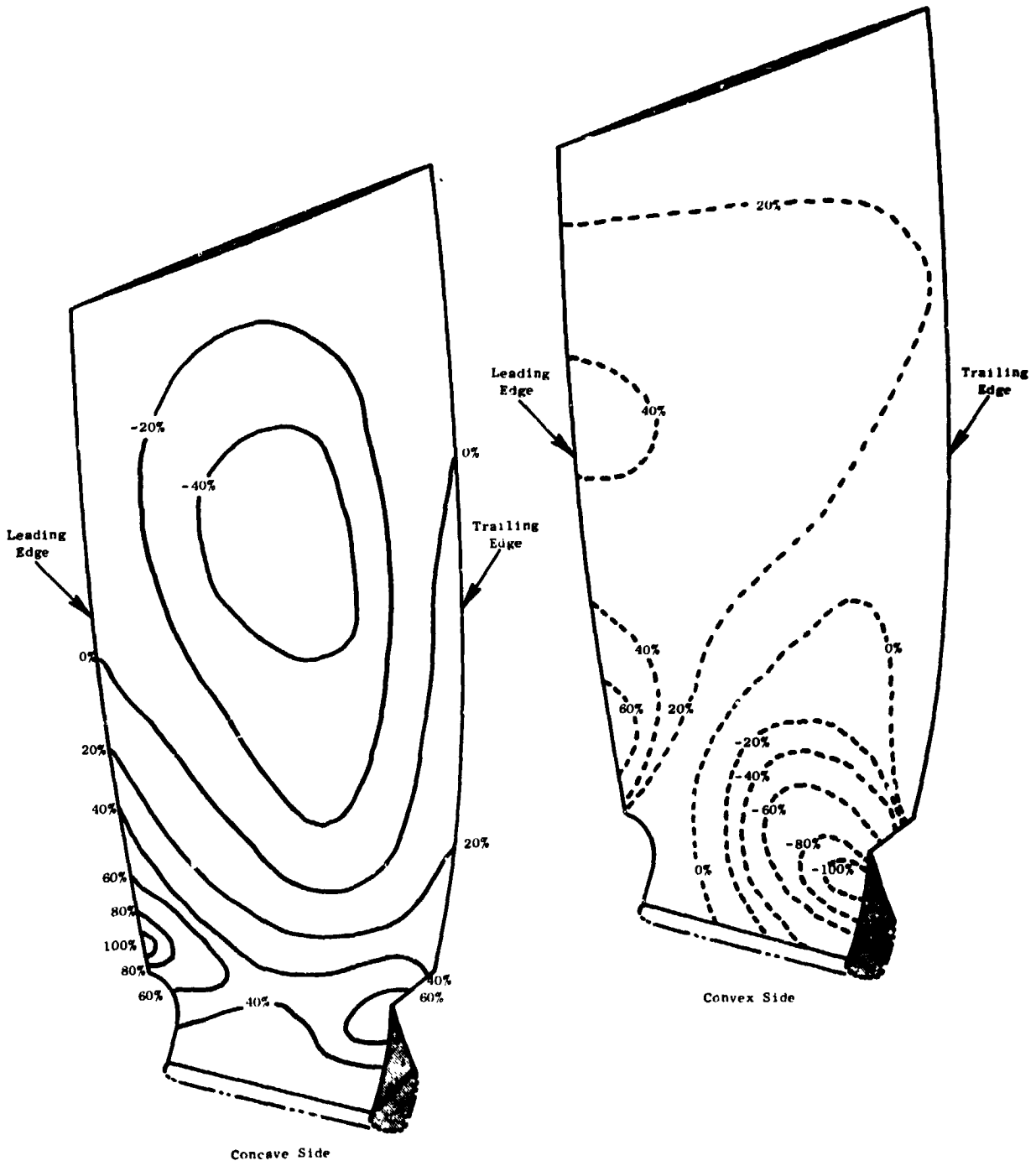


Figure 52. Calculated Blade Relative Radial Stresses for Second Flexural Mode.

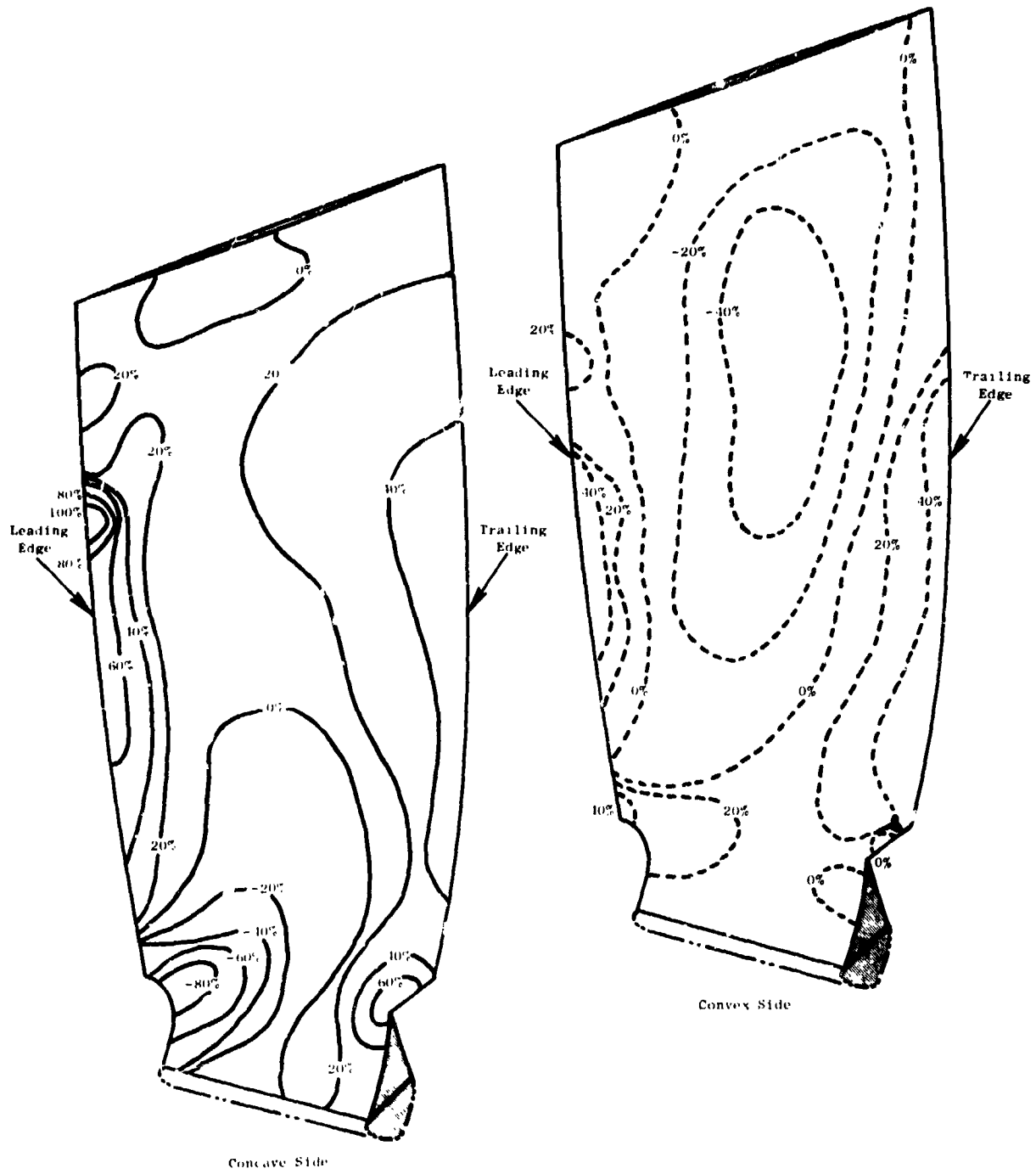


Figure 53. Calculated Blade Relative Radial Stresses for First Torsional Mode.

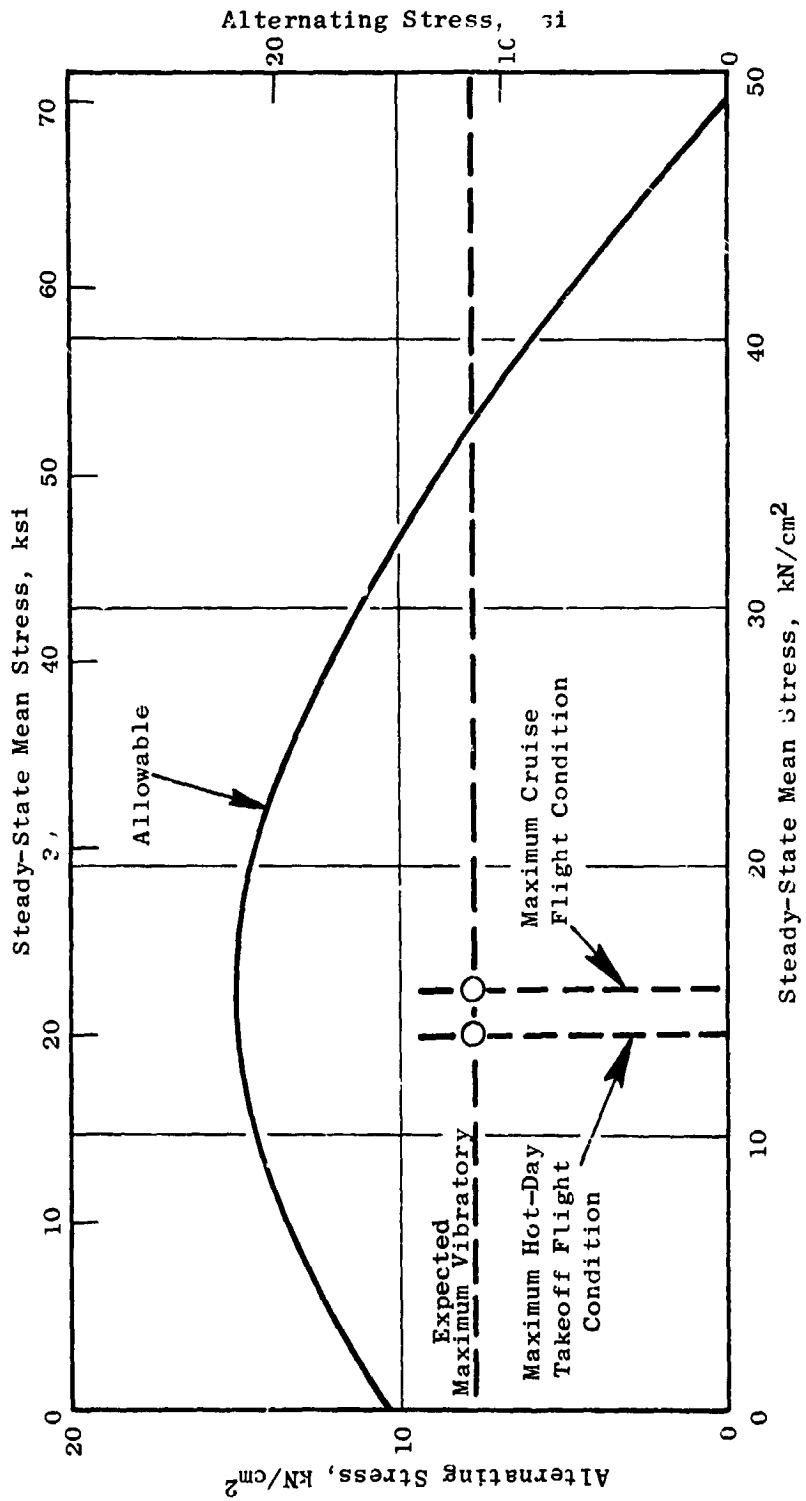


Figure 54. Allowable Stress Range Diagram - Blade Radial Stress.

The blade composite dovetail stresses were determined using the radial load distribution from the above blade analysis and experimental data from previous 2-D dovetail specimens and blade testing. Maximum dovetail crushing stress is calculated to be 15,290 N/cm² (22,180 psi), and maximum dovetail calculated shear stress is 4,760 N/cm² (6,900 psi) at a blade speed of 3326 rpm. The allowable dovetail crushing and shear strengths are 55,160 N/cm² (80,000 psi) and 16,550 N/cm² (24,000 psi), respectively, showing adequate static strength margins of safety in each case. These strengths were further verified by two blade-dovetail pull tests which demonstrated corresponding minimum crushing and shear strengths of 56,750 N/cm² (82,300 psi) and 17,650 N/cm² (25,600 psi) respectively. It is expected that these strengths would actually be higher in that the test load reached the capability of the loading fixture without dovetail failure.

The dovetail vibratory strengths were projected from previous composite experimental data and the QCSEE dovetail static strength data. Figure 55 shows the allowable stress range diagram for dovetail crushing, and Figure 56 shows the allowable stress range diagram for dovetail shear. The anticipated maximum single-amplitude vibratory stresses are 5,580 N/cm² (8,100 psi) in crushing and 2,340 N/cm² (3,400 psi) in shear and are based on the anticipated maximum blade radial vibratory stresses. For the steady-state conditions shown, that of hot-day takeoff and maximum cruise, the combination of steady-state mean stress and expected maximum vibratory stress results in an acceptable dovetail life.

Platform Stress and Vibration Analysis

The analytical approach used in evaluating the platform was to calculate the stresses and mechanical frequencies using simple conservative models of unit width cross sections representing the platform design. The stresses were calculated for the platform operating in the 5259 "G" centrifugal force field resulting from 100% speed operation at 3326 rpm. Positive margin at a 41% overspeed condition of 4700 rpm is met by maintaining a margin of safety, MS = 2 at 3326 rpm. As a further precaution to guard against a possible material property loss from the planned manufacturing co-curing process, only 70% of the published material allowable is used.

Figure 57 shows a cross section of the platform. Since the outer face sheet (location 5 flowpath surface, Figure 57) is an eccentric compressively loaded sheet operating in a centrifugal force field producing lateral loading and is stabilized by the honeycomb bond, it has been investigated for its beam-column capability. It is designed to be adequate even with a partial loss of honeycomb bond. For correlation with the analysis and to investigate various alternate design features, typical platform sections have been manufactured and tested. The testing has supported the analytical findings and at location 3, has identified the load carrying capability to be greater than 490 N/cm (280 lb/in.) normal to the blade centerline. This has allowed a MS = 2 at location 3 to be identified by test where an otherwise difficult analysis would be required to identify the maximum stress.

A stress and margin-of-safety summary is presented in Table 9 for six points of interest.

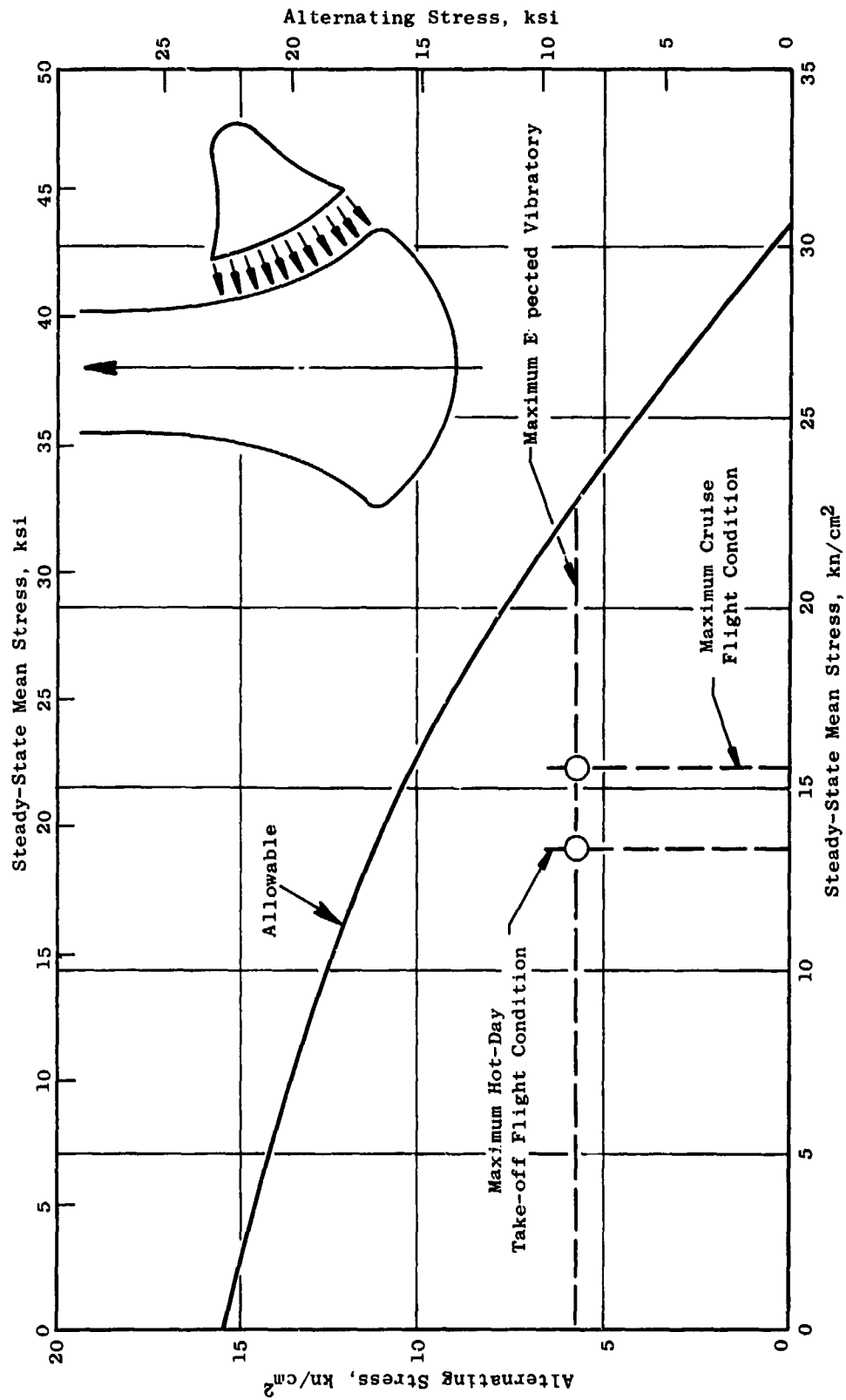


Figure 55. Allowable Stress Range Diagram - Blade Radial Stress.

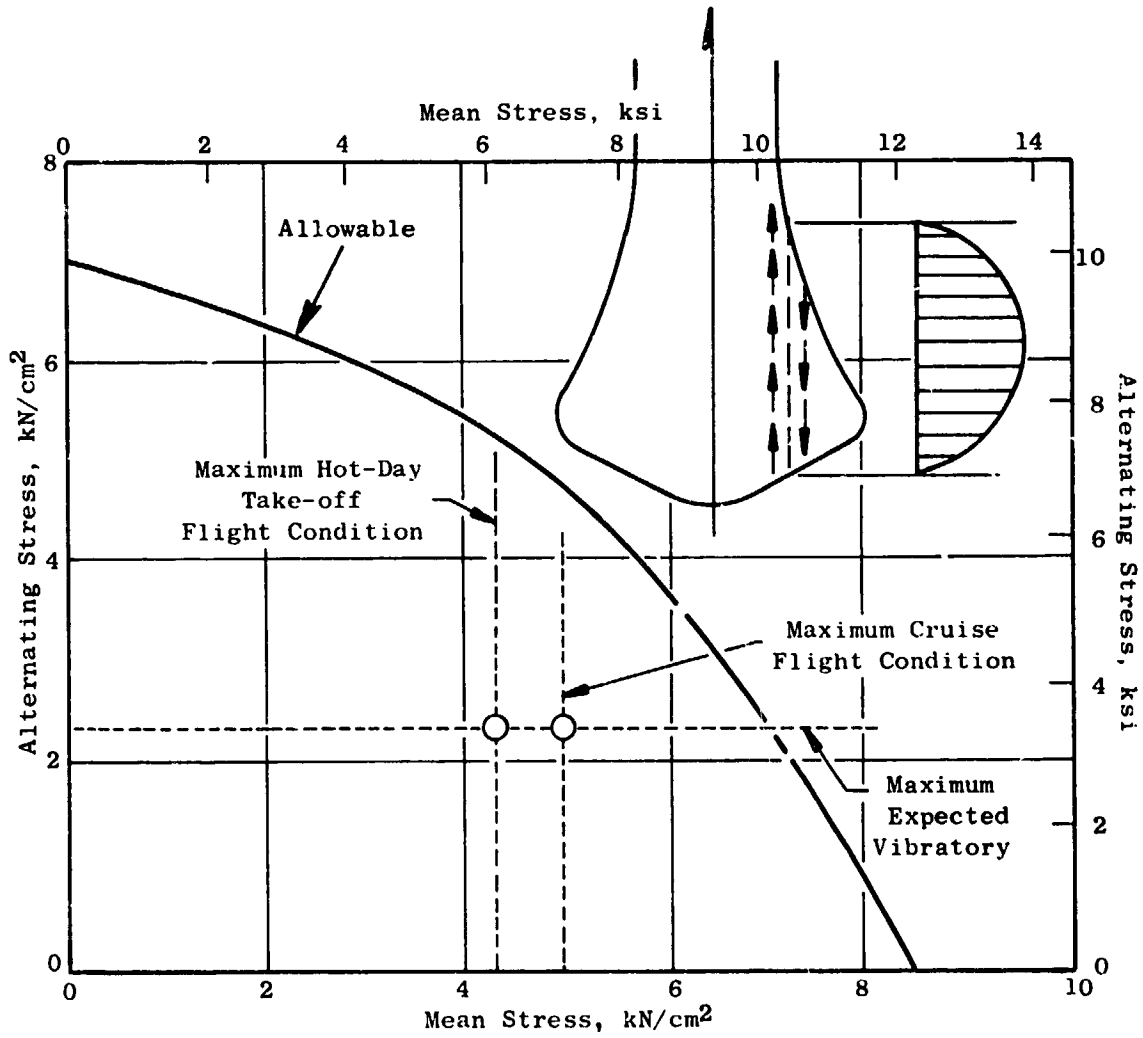


Figure 56. Allowable Stress Range Diagram - Dovetail Shear Stress.

ORIGINAL PAGE IS
OF POOR QUALITY

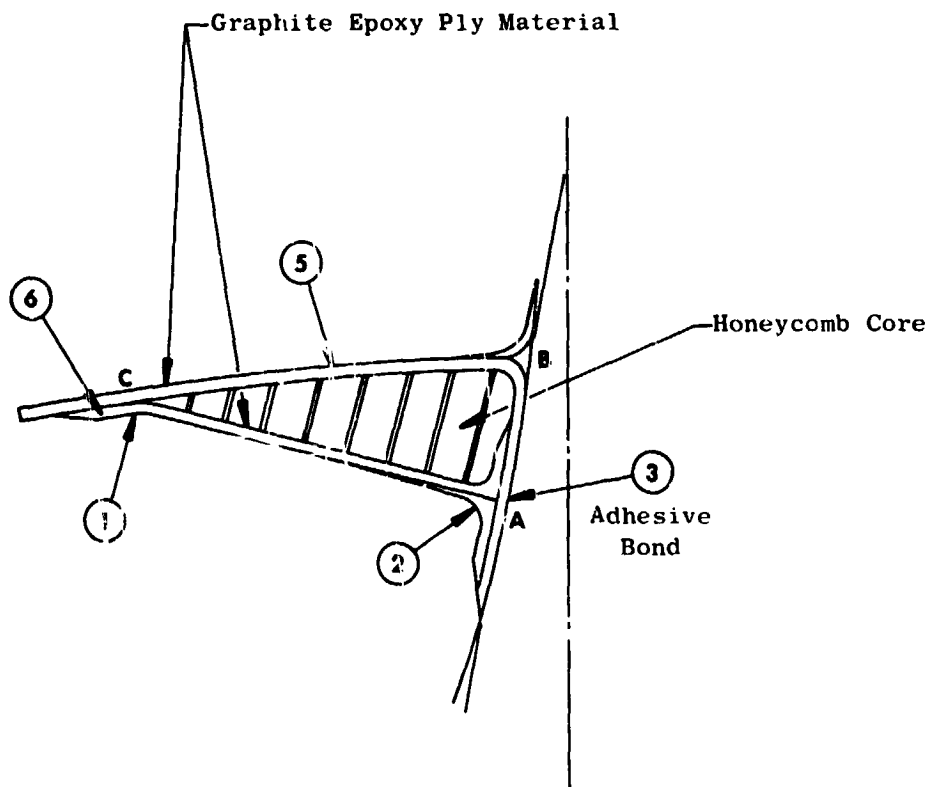


Figure 57. Platform Cross Section.

Table 9. Platform Stresses and Margins of Safety.

Location of Interest	Description and Type of Stress	Stress, kN/cm ² (ksi)	Margin of Safety
1	Flexural Stress in Overhang up to 2.5 cm (1 inch) with Additional Single Thickness Overhang up to 1 cm (.400 inch)	$\sigma \leq 16.5$ (24)	> 2.0
2	Tensile Stress in Lower Face Sheet	$\sigma < 13.8$ (20)	> 2.2
3	Tensile Stress Capability at this Location is Correlated with Test Results	-	> 2.0
4 Not Shown	Tensile Stress in Leading Edge Strap	$\sigma \leq 13.8$ (20)	> 2.0
5	Combined Compression and Flexural Stress in Upper Face Sheet	$\sigma \leq 24$ (35)	> 2.0
6	Shear Stress Between Upper and Lower Face Sheets	$\tau < .05$ (.07)	> 2.1

The platform is modeled and the vibratory characteristics are investigated from three points of view. First, the platform is considered cantilevered from the blade. Second, as a member running from fore to aft, it is considered free from the blade to flex in a free-free (floating) condition and, in the tangential direction (still free from the blade), it is considered to be cantilevered from the leading and trailing edge straps. Third, the upper face sheet with a partial loss of the honeycomb bond is considered. The first natural frequencies for these various models are tabulated in Table 10.

The platform is stiffer than any of the models used to calculate the first natural frequency. Therefore, the platform's first natural frequency is higher than those calculated and will be above the excitation frequencies of the blade.

The platform weight at less than 0.16 kg (0.35 lb) is composed of 20% honeycomb, 10% adhesive, and 70% graphite/epoxy composite.

The platform is fabricated in one piece which is simultaneously molded and bonded onto the composite blade using a co-curing process. The upper face sheet or flowpath contour is controlled by a hard die fitted around the blade. The graphite/epoxy upper face sheet is layed-up on the contour formed by the die and blade root surface. A contoured aluminum honeycomb core is next put in place followed by the lower face sheet layed-up on the honeycomb core. The layed-up assembly is then put into a vacuum bag and the entire assembly is co-cured onto the blade. The result is a one-piece platform design. The outer contour of the platform overhang is then trimmed to final dimensions.

Blade Vibration Analysis

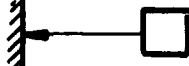
Blade "instability" or "limit cycle vibration" can be a problem on fans. It is characterized by a high amplitude vibration in a single mode (normally the first flexural or torsional mode) at a nonintegral per-rev frequency. Because of the nonlinearity in the aerodynamics involved, it has resisted practical solutions by solely theoretical means. Accordingly, General Electric has adopted a semiempirical "reduced velocity parameter" approach for limit cycle avoidance. Reduced velocity parameter, V_R , gives a measure of a blade's stability against self-excited vibration. This parameter is defined as:

$$V_R = \frac{W}{bf_t}$$

where:

- b = 1/2 chord at 5/6 span, m
- W = average air velocity relative to the blade over the outer third of the span, m/sec
- f_t = first torsional frequency at design rpm, rad/sec

Table 10. Platform Natural Frequencies.

Models Considered	First Natural Frequency
 <p data-bbox="628 659 782 717">Cantilever (Platform)</p>	<p data-bbox="947 687 1132 717">$f_1 > 5000$ Hz</p>
 <p data-bbox="572 892 858 950">Cantilever (Platform Overhang)</p>	<p data-bbox="947 924 1132 955">$f_1 > 2000$ Hz</p>
 <p data-bbox="648 1129 799 1187">Free-Free (Platform)</p>	<p data-bbox="947 1162 1132 1192">$f_1 > 8000$ Hz</p>
 <p data-bbox="572 1334 833 1457">Cantilevered Mass (End Straps Supporting a Free Platform)</p>	<p data-bbox="947 1381 1132 1412">$f_1 > 1500$ Hz</p>
 <p data-bbox="561 1619 858 1711">Clamped Beam (Face Sheet Partial Loss of H/C Bond)</p>	<p data-bbox="947 1651 1132 1681">$f_1 > 1500$ Hz</p>

The basic criterion used for setting the design of the UTW composite blade was the requirement of having a reduced-velocity parameter in the range of 1.3 to 1.4. This allowable range is based on previous testing of a variety of fan configurations in combination with the specific aerodynamic design of the UTW blade. The 18-blade design using a hybrid of boron, graphite, and Kevlar material was selected to provide the desired aeromechanical requirements. The operating and stall characteristics of this blade are presented in Figure 58 in terms of reduced velocity versus incidence angle. This shows the capability of reaching full-rotation stall prior to encountering blade instability.

The Campbell diagram for the UTW blade assembled in the trunnion and disk is shown in Figure 59. The coupled frequency of the blade-trunnion assembly, as plotted here, is somewhat lower than the individual blade frequencies due to the flexibility of the supporting trunnion and disk. The expected first flexural frequency at 2/rev crossover is shown to be at 67% speed. This is above the engine flight idle speed and below the normal operating speed for takeoff, climb, and maximum cruise flight conditions; it is therefore considered a transient point in the flight mission and not subject to continuous steady-state conditions. Blade excitation stresses at 2/rev crossover will be monitored during engine testing. Blade pitch and speed changes will be employed should the stress levels become excessive.

The margin for first flexural frequency over 1/rev at 115% speed is approximately 50%, and the margin for first flexural frequency below 2/rev at 100% speed is approximately 13%.

The second flexural mode crosses several per/rev lines in the operating speed range. Each of these crossings represent a potential for forced resonances; however, it takes considerably more energy to drive the higher vibration frequencies such as second flex, and no problems are anticipated.

The first torsional frequency 6/rev crossover is at approximately 33% speed with the 100% speed frequency margin being approximately 6% over 5/rev. Since the excitation forces should be small at the higher order crossovers, no vibratory problems are anticipated during normal engine operating conditions.

Blade Impact Analysis

In addition to the need to satisfy flutter requirements, resistance to bird impact is also of major importance. Flight-engine (QCSEE) blades must be capable of absorbing the impact of 16 0.085-kg (3-oz) birds (starlings), eight 0.68-kg (1.5-lb) birds (pigeons), and a 1.8-kg (4-lb) bird in order to satisfy FAA specifications. The objectives are to sustain little or no damage during starling ingestion, be able to maintain 75% engine thrust following pigeon ingestion, and to be able to have a safe engine shutdown with all damage being contained within the engine casing following ingestion of a 1.8-kg (4-lb) bird.

Two different damage modes require consideration in the design. The first is a brittle-root-type fracture which can result in the blade breaking off close to the dovetail, and the second is local damage which can result in airfoil delamination and loss of material.

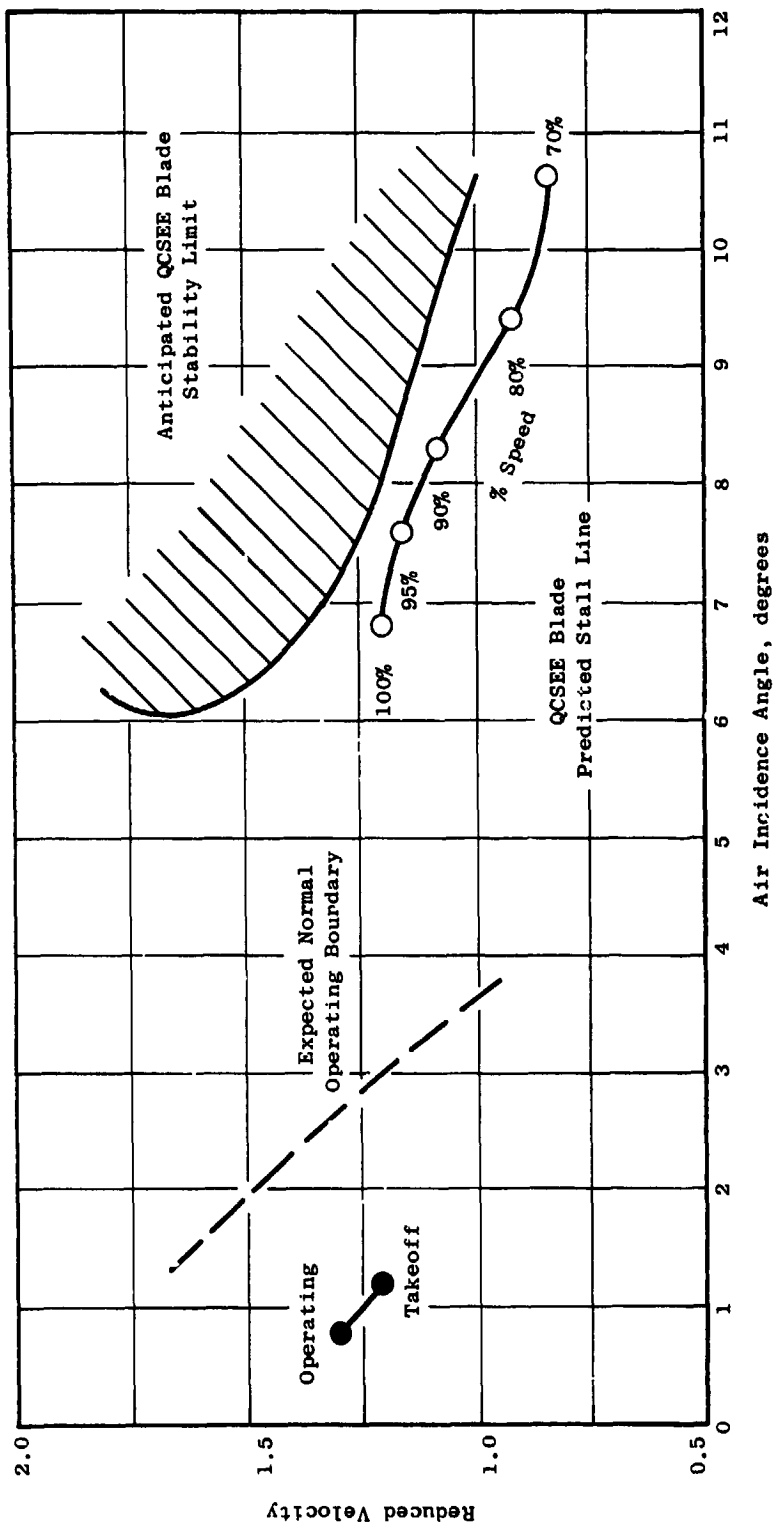


Figure 58. Limit Cycle Boundaries.

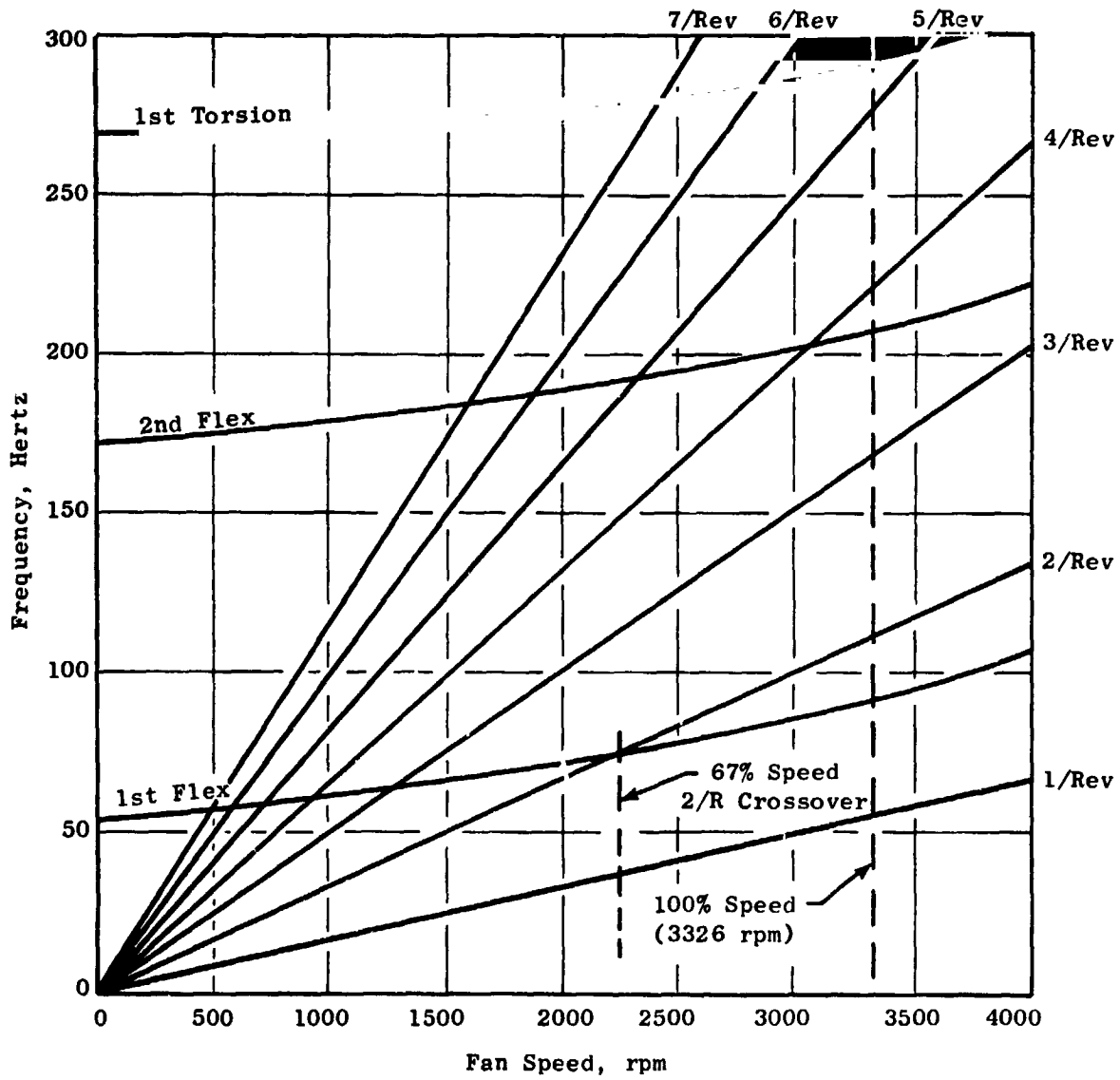


Figure 59. Campbell Diagram - UTW Composite Blade.

ORIGINAL PAGE IS
OF POOR QUALITY

The projected elimination of root failures during large-bird impact in the QCSEE blade has been achieved. The necessary flexibility and strain-to-failure capability has been built into the blade root through the use of hybrid materials. The dovetail design provides for energy dissipation through centrifugal recovery and increase in friction energy. Figure 60 illustrates the magnitude of energy that has to be absorbed by the blade at the root, tip, and pitch for the spectrum of relative bird velocities for a 1.8-kg (4-lb) bird. This shows that the most vulnerable condition and blade impact location is during climb at approximately 91.4 m/sec (300 ft/sec) and at the blade 50% span location, respectively. The predicted gross impact capability of the QCSEE blade is shown in Figure 61. This shows the advantages of the QCSEE dovetail attachment and the use of hybrid materials over the previous fixed-root solid graphite-type blade. Figure 62 shows a plot of the calculated projectile normal momentum for a 0.68-kg (1.5-lb) bird at the blade 50% and 75% span locations as a function of airplane speed.

Weight

The weight of the composite blade was computed using the final blade configuration as shown in Figure 41. The resulting weight breakdown is as follows:

	<u>kg</u>	<u>lb</u>
Composite Airfoil	1.74	3.83
Leading Edge Protection	0.20	0.45
Polyurethane Coating	0.07	0.15
Platform and Adhesive Bond	0.15	0.34
Dovetail	<u>0.47</u>	<u>1.03</u>
TOTAL WEIGHT	2.63	5.80

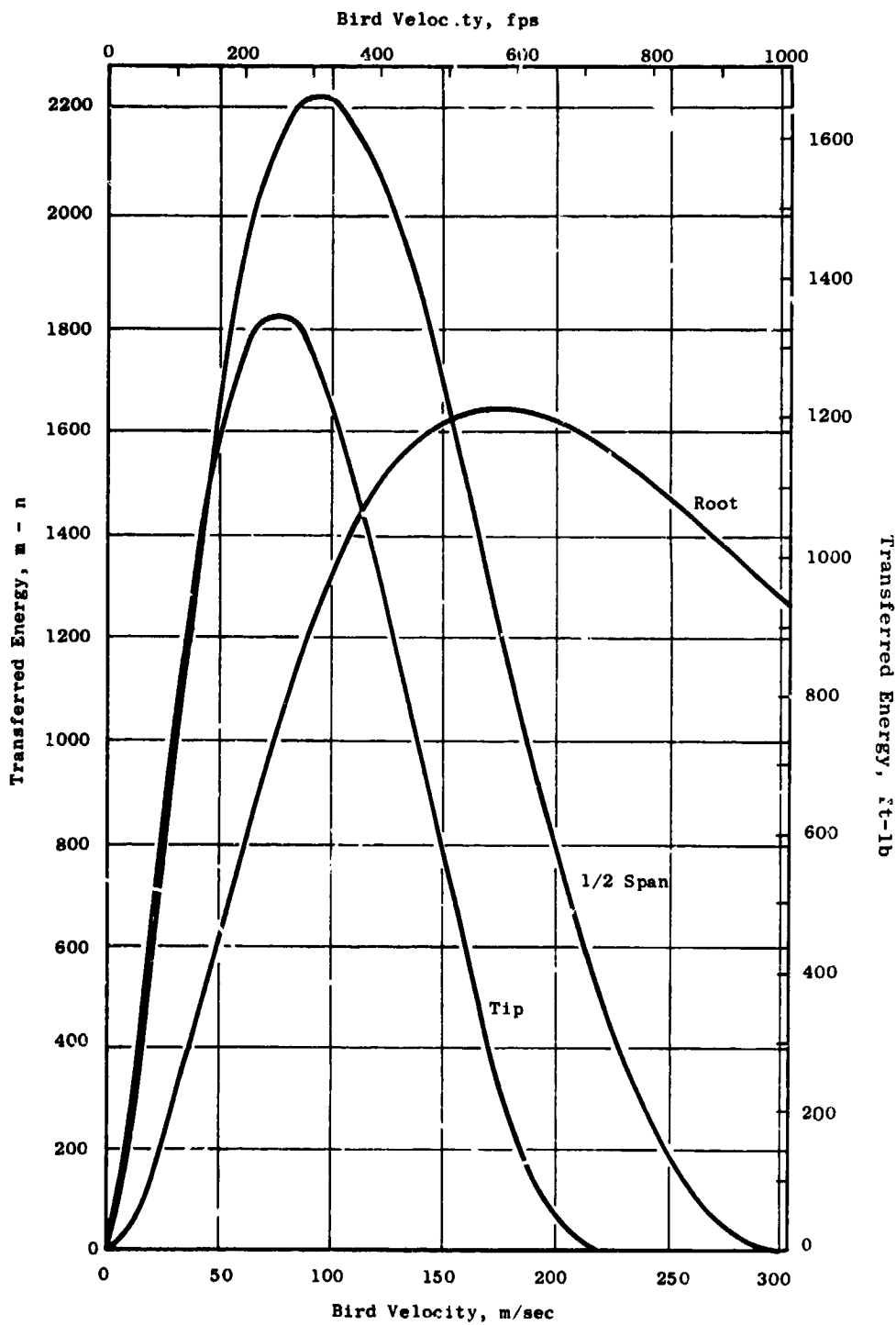


Figure 60. UTW Blade Transferred Impact Energy for a 1.81 kg (4 lb) Bird.

ORIGINAL PAGE IS
OF POOR QUALITY

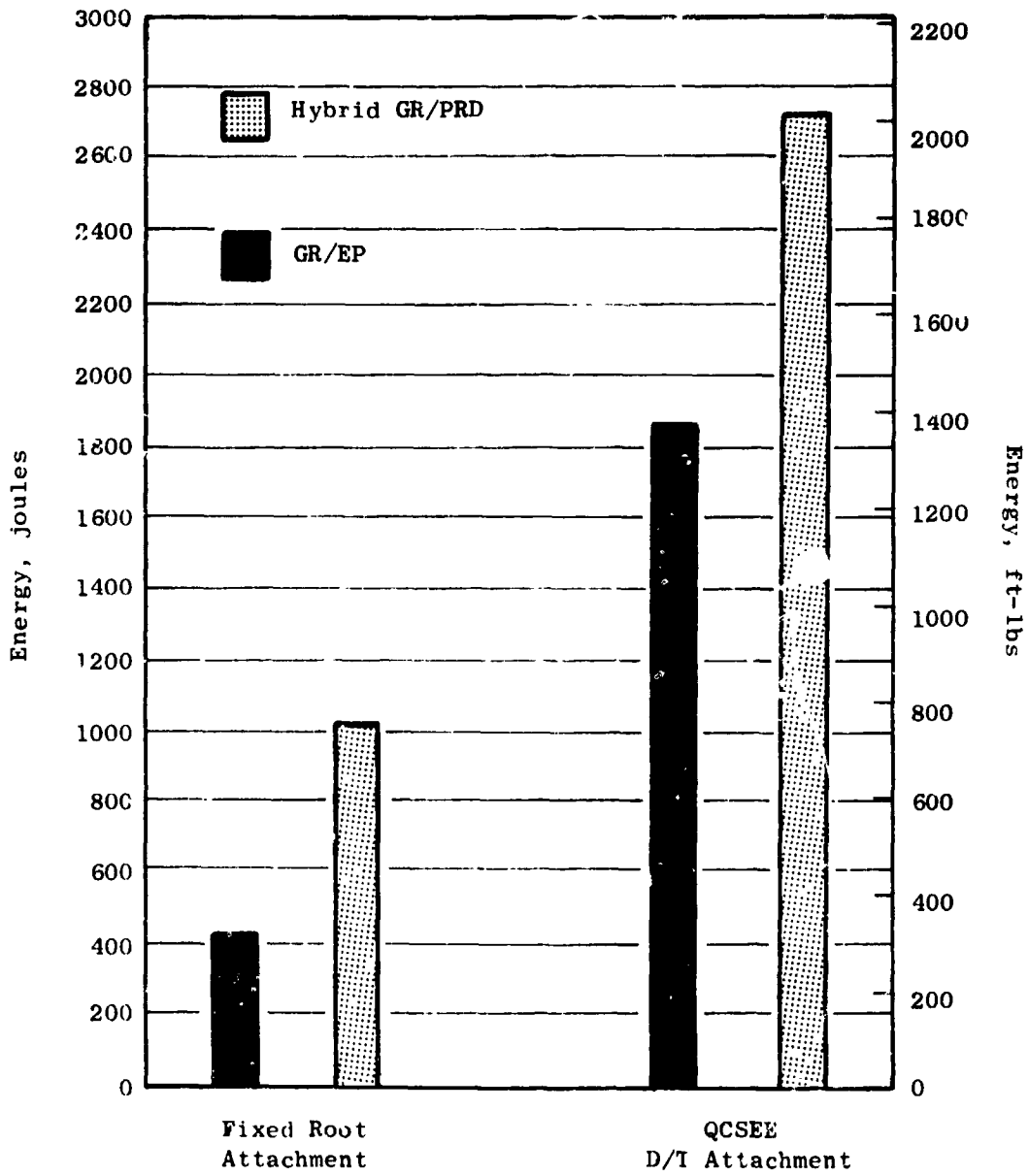


Figure 61. QCSFE Composite Blade Predicted Gross Impact Capability.

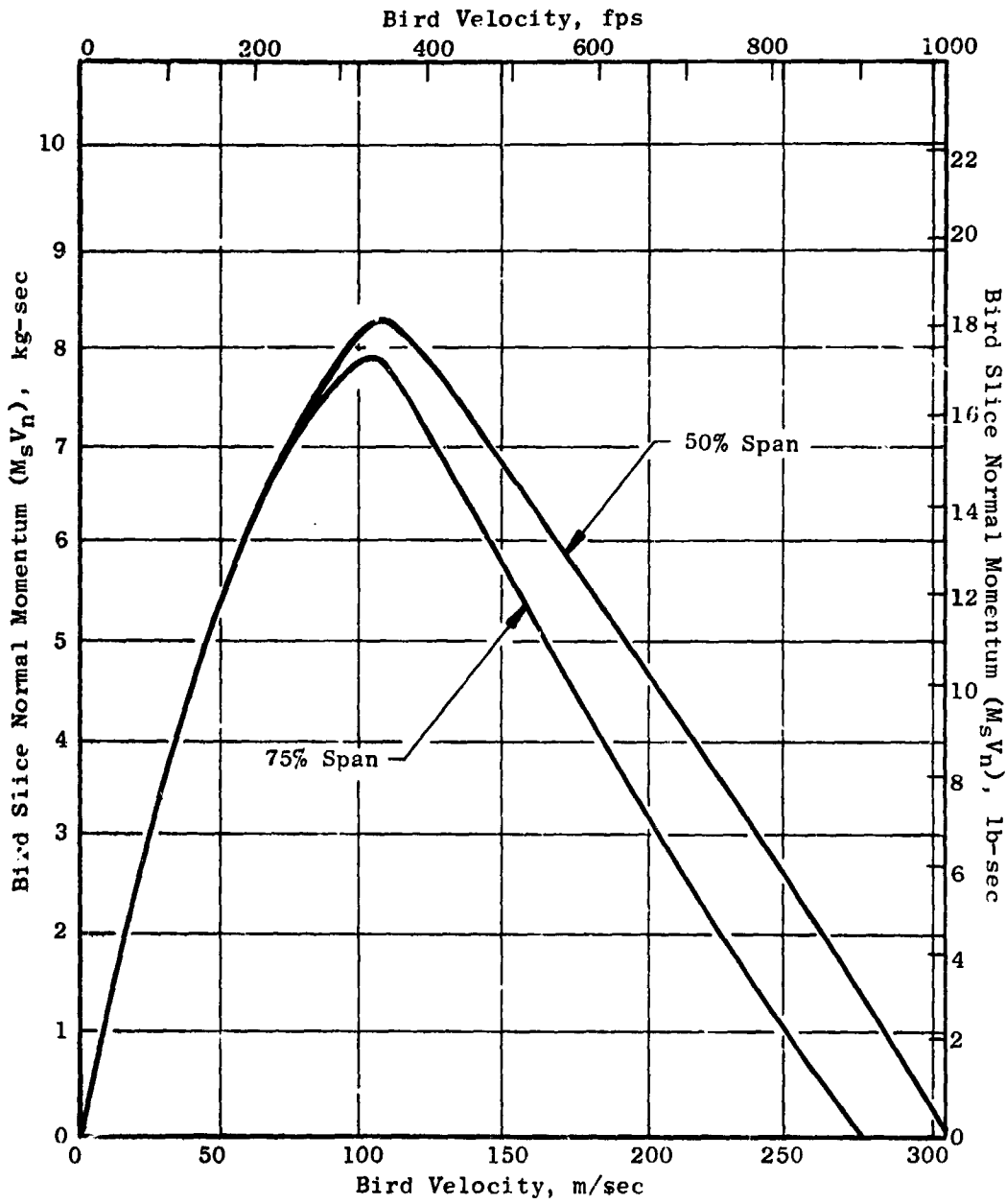


Figure 62. UTW Blade Impact Momentum for a 0.68-kg (1½-lb) Bird.

ORIGINAL PAGE IS
OF POOR QUALITY

3.3 FAN DISK

The UTW fan disk is a single-piece-machined 6Al-4V titanium ring forging designed for a commercial life in excess of 36,000 hours. This disk is shown in Figure 63. Eighteen radial holes pierce the disk ring to provide for the blade support trunnions which retain the fan blades. An integral cone on the aft side of the disk connects the disk to the fan stub shaft through a bolted flange. The disk cone is contoured to alleviate LCF problems generated by the forward and aft cycles of thrust generated during engine operation. Flanges on the outside of the disk rim provide attachment planes for the spinner and forward and aft flowpath adapter cones.

The inside of the disk rim is a turned modified spherical blade bearing seating surface for the blade retention bearing (Figure 64). This results in a low-cost, lightweight disk design with a uniformly stressed rim. Blade thrust bearings have mating spherical seats and are mounted as shown in Figure 64. The bearing seating surface is not machined perfectly spherical but is designed to become spherical under operating loads. A spherical copper shim is included between the disk and the bearing, although (at the pressure loadings expected beneath the bearing) fretting is not expected to be a problem.

The UTW fan disk design loads and stress data are shown in Table 11 for both the GE and Hamilton Standard actuators. Resulting actual and allowable stresses on the rotor configuration are shown in Figure 65 for the Hamilton Standard variable-pitch fan actuation system loads. As shown in the figure, the final design provides adequate margin of safety at all critical stress locations.

3.4 BLADE SUPPORT BEARING

The blade support bearing (Figure 63) has a full complement of balls to reduce the per-ball loading. Bearing race conformance is relatively high (51%) to achieve the required bearing fatigue life in its highly loaded environment. All surfaces on this bearing will be coated with a tungsten disulfide film. Tests on previous General Electric variable-pitch fan bearings have shown this coating provides enough lubrication to enable the bearing to safely operate for 9000 flight hours in the event of a loss-of-grease situation.

The blade support thrust bearing configuration is illustrated in Figure 66. Shields attached to the outer race create a centrifugal "cup" which prevents the grease from leaking out in the high centrifugal field when the engine is running. Grease will not leak from the clearance gaps at the bottom of the shields when the engine is not operating due to the high viscosity of the grease, provided oil separation from the grease soaping agent does not occur. General Electric has conducted centrifuge tests on various greases to determine separation tendencies and has selected one which has little tendency to separate under prolonged periods of high "g" loads.

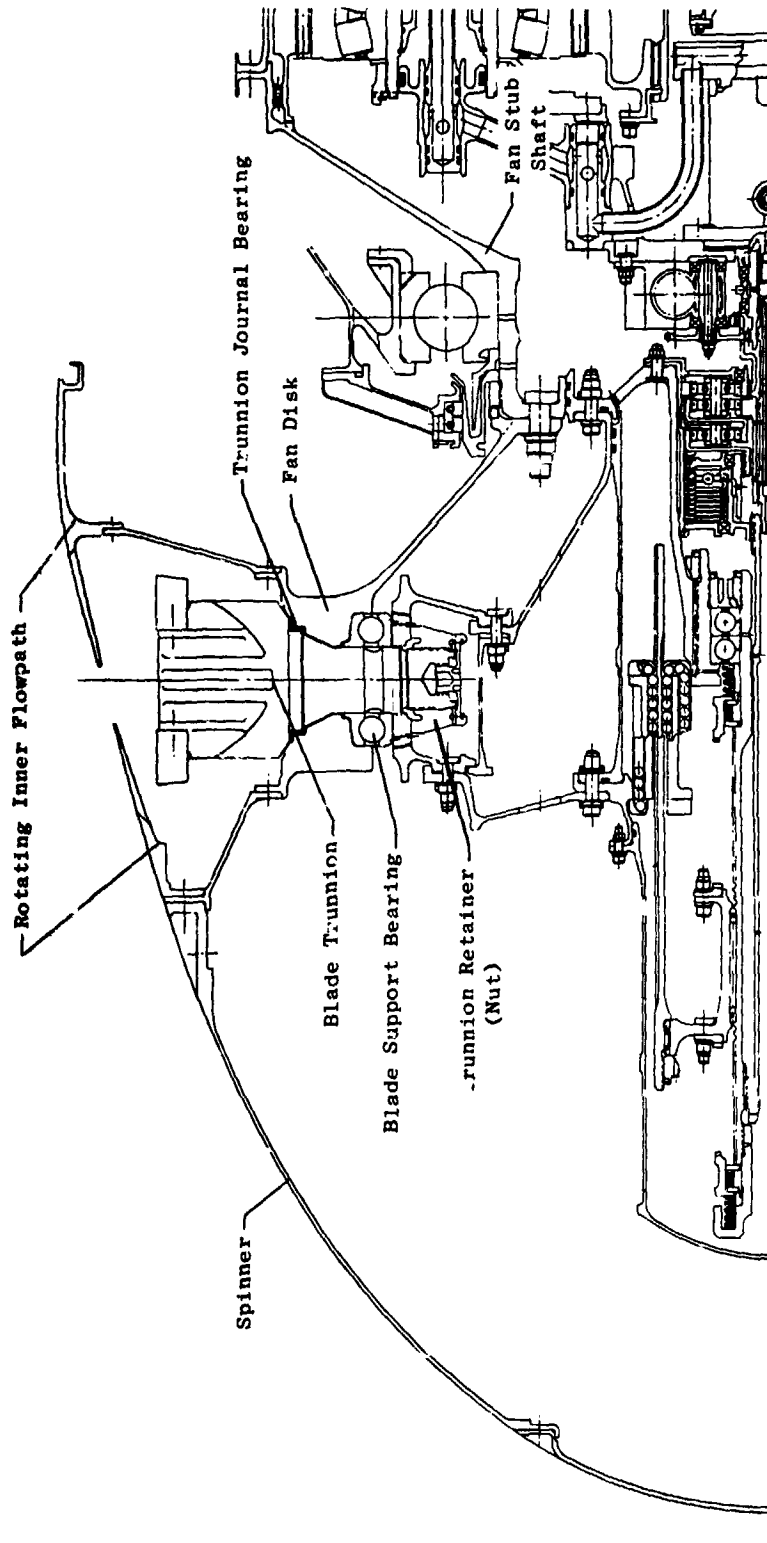


Figure 63. UTW Fan Rotor.

ORIGINAL PAGE IS
OF POOR QUALITY

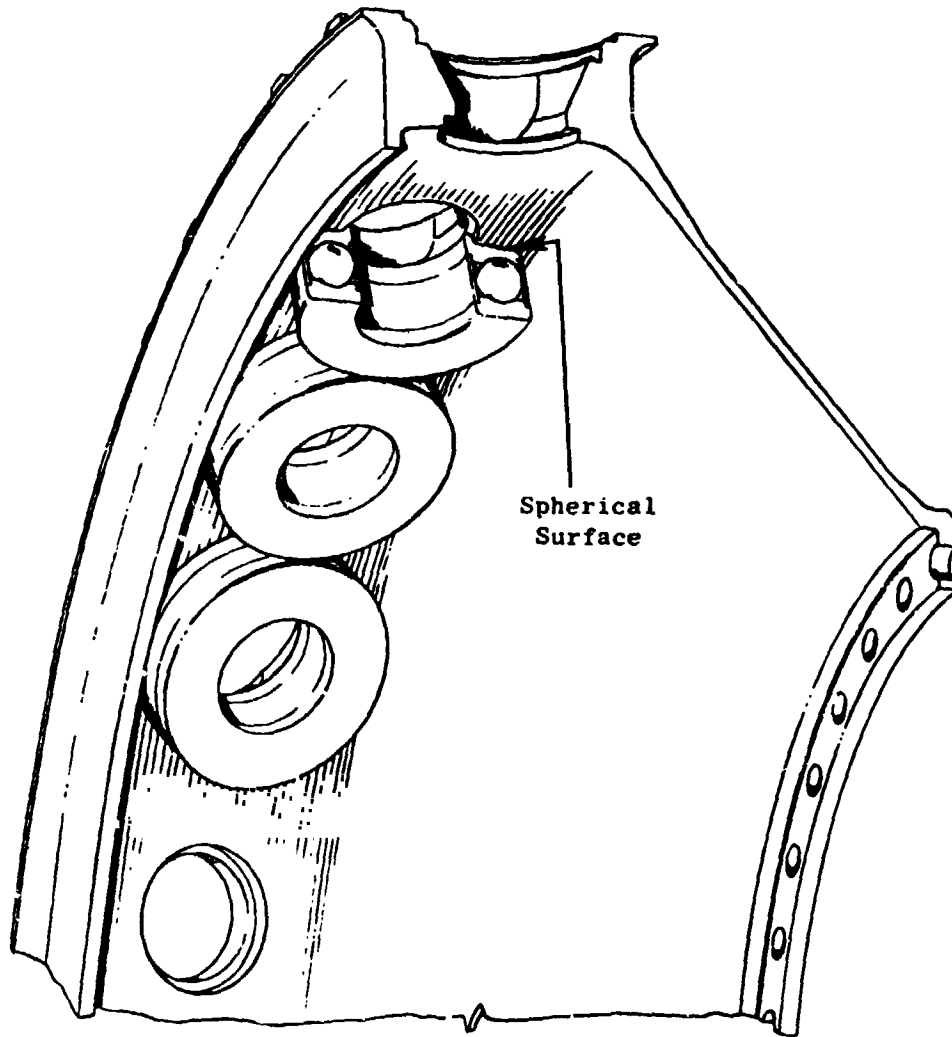


Figure 64. UFW Bearing and Disk Seat.

Table 11. UFW Fan Disk Design Data.

All Loads and Stresses Calculated at 3326 RPM

Attachment Load

With GE Pinion Gear	327,718 N/Blade	(73,674 lb/Blade)
With HS Lever Arm	328,932 N/Blade	(73,947 lb/Blade)
Average Rim Stress (GE)	$35.577 \times 10^7 \text{ N/m}^2$	(51,600 psi)
(HS)	$38.299 \times 10^7 \text{ N/m}^2$	(55,446 psi)
Burst Speed		4928 rpm
LCF Life of Disk With -3σ Material Properties		48,000 Cycles
LCF Life of Disk With 0.01×0.03 Initial Defect		16,000 Cycles

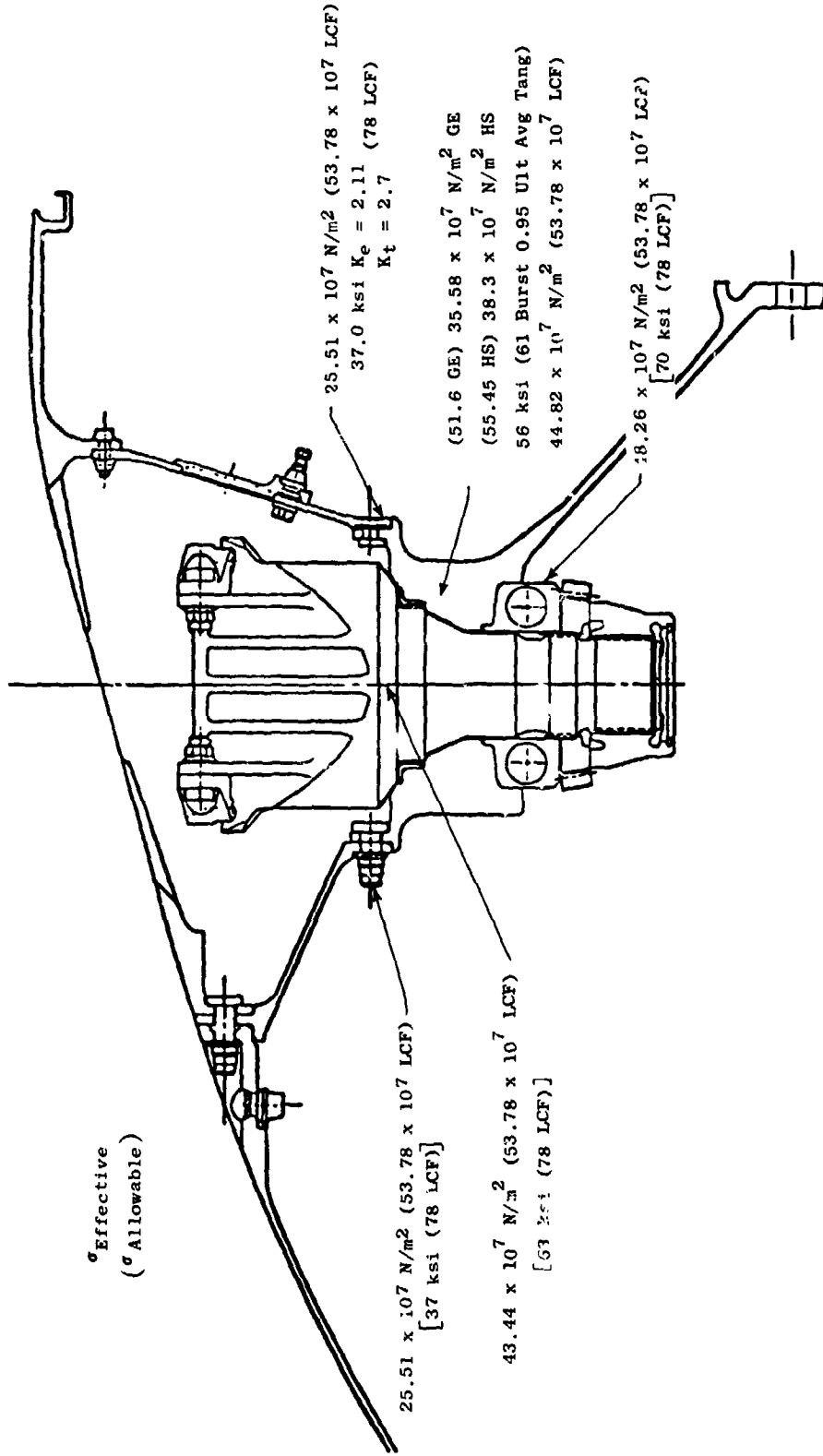
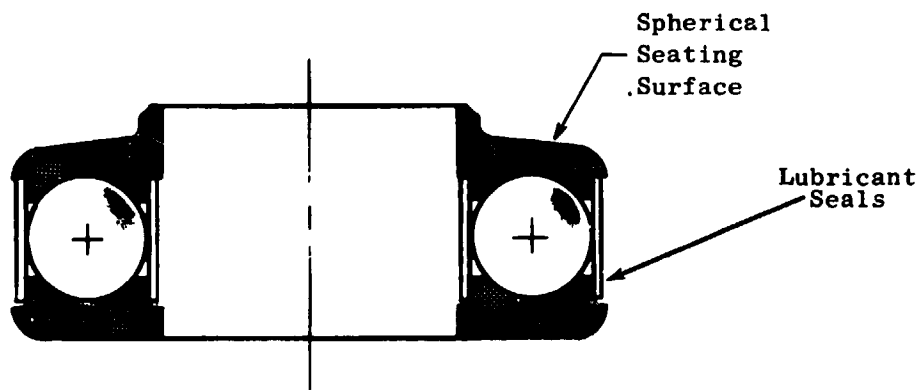
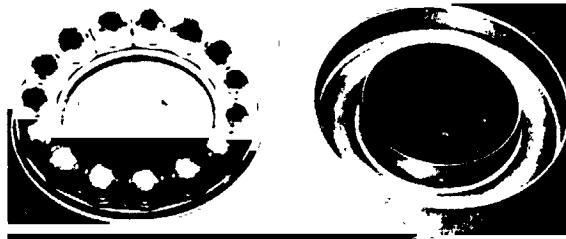


Figure 65. UTW Fan Disk Stresses with Hamilton-Standard Actuator.



- Single Row Ball Thrust Bearing
- Full Complement of Balls (12)
- High Conformance (51%)
- Separable Races
- Lubricant Seals

Figure 66. Blade Thrust Bearing.

Design criteria peculiar to variable-pitch blade support bearings were developed and applied to the design of this bearing. Unique design criteria used in designing the QCSEE UTW bearing are as follows:

1. The blade support bearing system B10 life should be 9000 flight hours. This requires an individual bearing B10 life of over 13 times the system B10 life. The need for this stringent requirement is based on the statistical problem of a multibearing (18) system in a multiengine (4) aircraft.
2. Blade support bearings will not be dependent upon the grease lubricant to obtain 9000 hours between overhauls. This restriction ensures that failure will not occur due to loss of bearing grease. In addition to normal bearing design criteria, the following requirements must also be met, or by definition, failure is said to occur:
 - a. An apparent coefficient of friction at the pitch diameter less than 0.01. This allows the blade actuator to be designed to a maximum capacity with assurance that it will not be overloaded because of worn bearings.
 - b. Bearing wear less than the bearing preload [approximately 0.00508 cm (0.002 inch) total wear]. This definition provides a simple method for condition monitoring without rotor disassembly.
3. Ball or race fracture must not occur under the maximum possible bird impact loads. The actuation system of an 18-bladed fan is sufficiently powerful to cause secondary damage upon seizure of any one of the individual bearings. Ball fracture, a potential cause of such seizure, must be eliminated as a potential problem.
4. Bearing life calculations are based on the mission/duty cycle as shown in Table 12. Blade angle and cycle amplitude data correspond to information presented in Figure 67. A total blade modulation of 180° per mission (in 2° increments) is assumed during aircraft approach for bearing life analysis.

The upper surface of the top bearing race is a spherical surface which is designed in conjunction with the disk bearing seat to minimize transmission of warping stress to the race under operating conditions. This spherical mating surface will be coated with an antifretting coating to ensure that loss of LCF life of the fan disk will not occur.

Bearing loads and life predictions are given in Table 13. As indicated in Table 12, the number of bearing cycles during 9000 hours of engine operation is approximately 12 times greater when modulation during approach is assumed than without modulation. As shown in Table 13, the bearing B10 system life in terms of engine operating hours exceeds the 9000-hour TBO requirement when modulation during approach is assumed and exceeds the total engine life requirement of 36,000 hours if blade modulation during approach is not required.

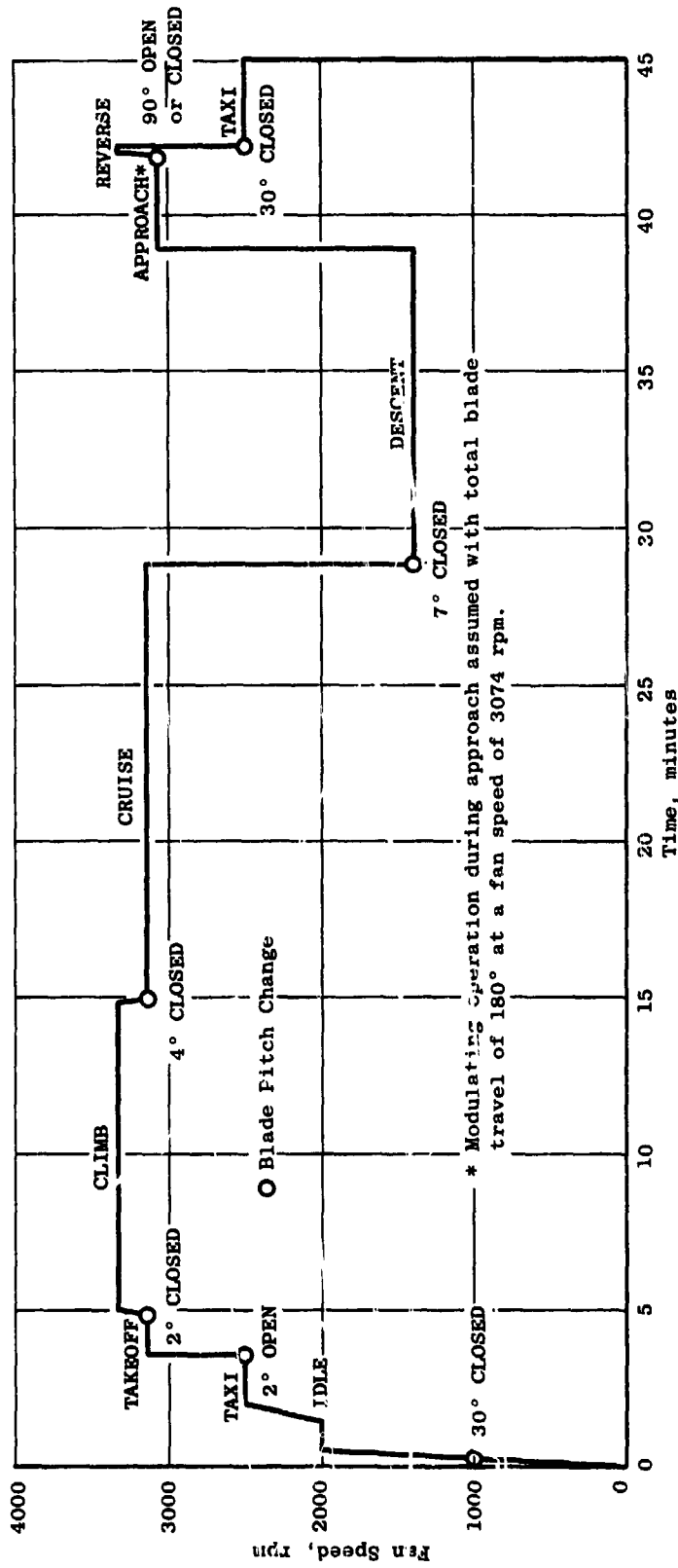


Figure 67. UTW Mission Duty Cycle.

Table 12. QCSEE UTW Blade Support Bearing.

Action	OPERATING CONDITIONS OF MISSION DUTY CYCLE				$\Delta\alpha$	Cycles/Mission
	N rpm	F		α		
		N	lb			
Ignition-Taxi	1,000	29,358	(6,600)	30° Closed	0°	1/4
Taxi-T/O	2,400	169,032	(38,000)	2° Closed	32	1/4
T/O-Climb	3,143	290,024	(65,200)	2° Closed	4	1/4
Climb-Cruise	3,143	290,024	(65,200)	4° Closed	2	1/4
Cruise-Descent	1,400	57,382	(12,900)	7° Closed	3	1/4
Approach	3,074	277,569	(69,400)	180° Mod.	±2	22-1/2
Approach-Reverse	3,074	277,569	(62,400)	90° Closed	90	1/4
Reverse-Taxi	2,400	169,032	(38,000)	30° Closed	60	1/4
Shutdown	1,000	29,358	(6,600)	30° Closed	0	1/4
				Total		<u>24-1/2 Cycles/Mission</u>

α - Blade angle setting relative to nominal (design) position

$\Delta\alpha$ - Blade angle cyclic amplitude

Total Cycles for 9,000 Engine Hours:

With 180° Modulation:

(24.5 Cycles/Mission) (60/45 Missions/Hours) (9,000 Hours) 294,000 Cycles

Without Modulation:

(2.0 Cycles/Mission) (60/45 Missions/Hours) (9,000 Hours) 24,000 Cycles

Table 13. QCSEE UTW Blade Support Bearing Design.

<u>Geometry</u>			
Number of Balls	12		
Ball Diameter	1.588 cm (0.625 in.)		
Bearing Diameter	6.147 cm (2.420 in.)		
Conformance	0.51		
Material	AISI 52100		
<u>Capacity</u>			
Dynamic Capacity	121,875 N (27,400 lb)	121,875 N (27,400 lb)	121,875 N (27,400 lb)
Static Capacity	298,016 N (67,000 lb)	298,016 N (67,000 lb)	288,016 N (67,000 lb)
Mean Effective Rotating Load	151,721 N (34,110 lb)	151,721 N (34,110 lb)	89,672 N (20,160 lb)
Material Factor	3	3	3
Bearing System Life In	43,245 hrs	17,100 hrs (GE)	17,100 hrs (GE)
Engine Operating HOURS (B ₁₀)		15,300 hrs (HS)	15,300 hrs (HS)

3.5 BLADE TRUNNION

Blade trunnions mechanically tie the composite fan blades to the fan disk through the blade support bearing. They also provide an attachment point through which torque can be applied by the blade actuator to change the pitch of the blades. The QCSEE UTW blade retention trunnion is shown in Figure 68.

The entire blade support system is designed to withstand the maximum possible loads which can be transmitted into it by the blades without blade failure. This includes not only the trunnion but all of its mating components. This ensures that, in the event of extensive foreign object damage, only small composite fan blade pieces will be broken off and secondary engine damage will be minimized.

Fan blades slide into the dovetail slots on top of the trunnion and are retained by shouldered straps. Marage 250 is used for the straps because of its very high strength. The dovetail slot will be protected by an anti-fretting coating applied to the blade dovetails. Two plasma-sprayed coatings, one plated coating, and a chemical-conversion coating are presently being considered for this wear coating.

The trunnion is machined from single forgings of 6Al-4V titanium. This material was selected based on its natural corrosion resistance, low density, and high strength. Titanium also allows relatively large-diameter threads to be rolled by more conventional capacity thread rolling equipment on the trunnion end (per Mil-S-8879) for the trunnion retainer. This rolling procedure has been used on the titanium trunnions of previous General Electric variable-pitch fans and produces above average properties in this critical region. Critical trunnion stresses are shown on the drawing in Figure 69. All stresses fall within the allowable limits with an adequate margin of safety.

Each trunnion is held in the hole of the disk by a silver-plated, threaded steel retainer. A stress summary for this trunnion retainer (nut) is presented in Table 14. This retainer can be torqued to preload the blade support bearing, and is locked by a redundant locking system. Either a pinion gear for the GE actuation system or a lever arm for the Hamilton Standard System is captured on the trunnion between the trunnion retainer and the blade support bearing [see Figures 70 (GE) and 71 (HS)]. Torque to change the blade pitch is carried through this device into mating splines just above the trunnion threads.

Outer sliding bearings support the top of the trunnion. The outer sleeve sliding bearing and axial thrust seating surfaces will be a very high capacity bearing of Nomex and Teflon fibers. This bearing seats inside the disk and can easily tolerate the circumferential strain of the disk. The high capacity of this bearing, compared to conventional ball bearings, enables it to easily withstand anticipated vibratory and bird impact loads. The outer bearing has resistance to all oils, fuels, and solvents which might normally come in contact with engine parts.

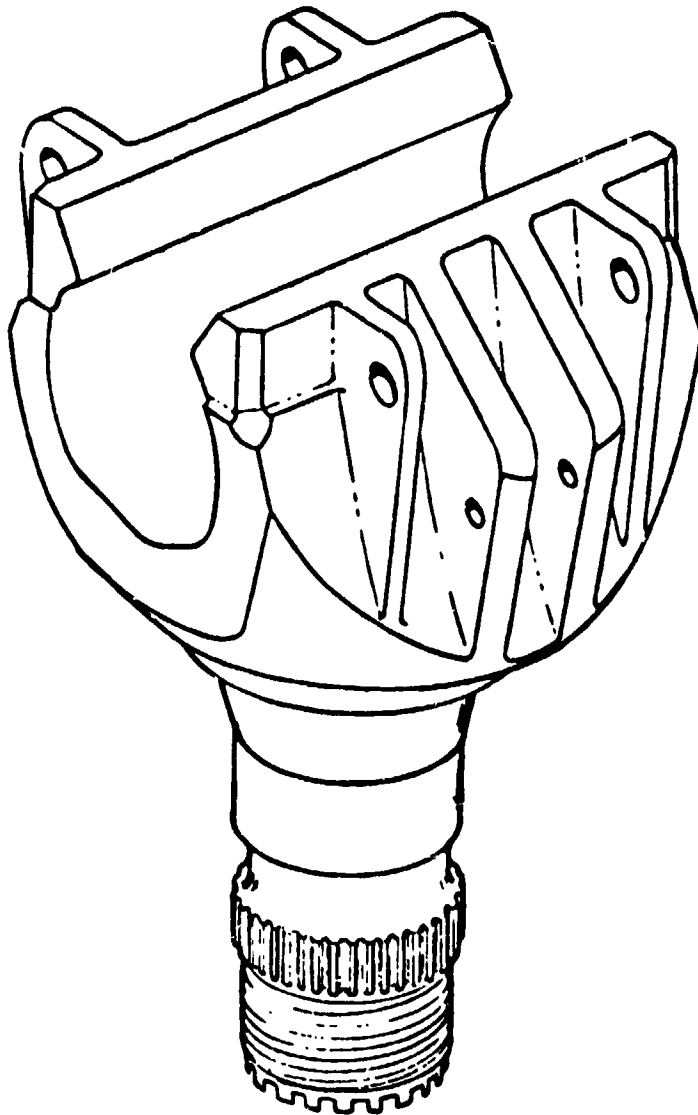
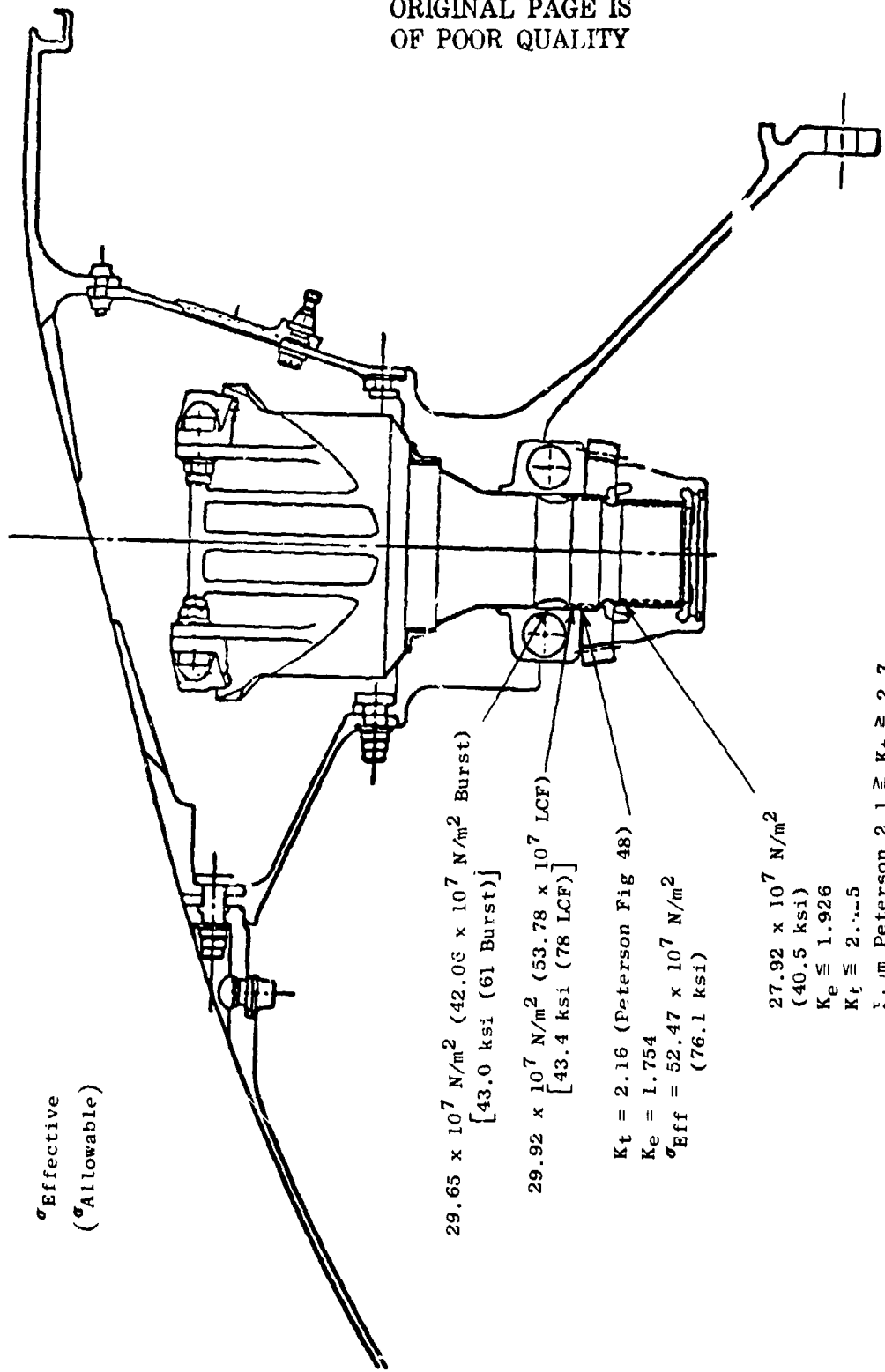


Figure 68. Blade Trunnion.

ORIGINAL PAGE IS
OF POOR QUALITY

ORIGINAL PAGE IS
OF POOR QUALITY



σ Effective
(σ Allowable)

$29.65 \times 10^7 \text{ N/m}^2$ ($42.03 \times 10^7 \text{ N/m}^2$ Burst)
[43.0 ksi (61 Burst)]

$29.92 \times 10^7 \text{ N/m}^2$ ($53.78 \times 10^7 \text{ LCF}$)
[43.4 ksi (78 LCF)]

$K_t = 2.16$ (Peterson Fig 48)

$K_e = 1.754$

$\sigma_{\text{Eff}} = 52.47 \times 10^7 \text{ N/m}^2$
(76.1 ksi)

$27.92 \times 10^7 \text{ N/m}^2$
(40.5 ksi)

$K_e \leq 1.926$

$K_t \leq 2.115$

From Peterson $2.1 \geq K_t \geq 2.7$

Figure 69. UTW Blade Trunnion Stresses.

Table 14. Trunnion Retainer (Nut).

• Load - 306,912 N (69,000 lb) at 3326 rpm			
• Stress Summary			
Hoop Stress	18,158 N/cm ² (26,335 psi)	67,571 N/cm ² (98,000 psi) (LCF)	
Shear Stress on Threads	23,074 N/cm ² (33,465 psi)	38,612 N/cm ² (56,000 psi) (LCF)	
Bearing Design Criteria	16,096 N/cm ² (23,345 psi)	27,580 N/cm ² (40,000 psi) (Fretting)	
• Limiting Design Criteria - Local Retainer Stresses Due To Ring Roll.			

- Threat Stresses In Trunnion.

ORIGINAL PAGE IS
OF POOR QUALITY

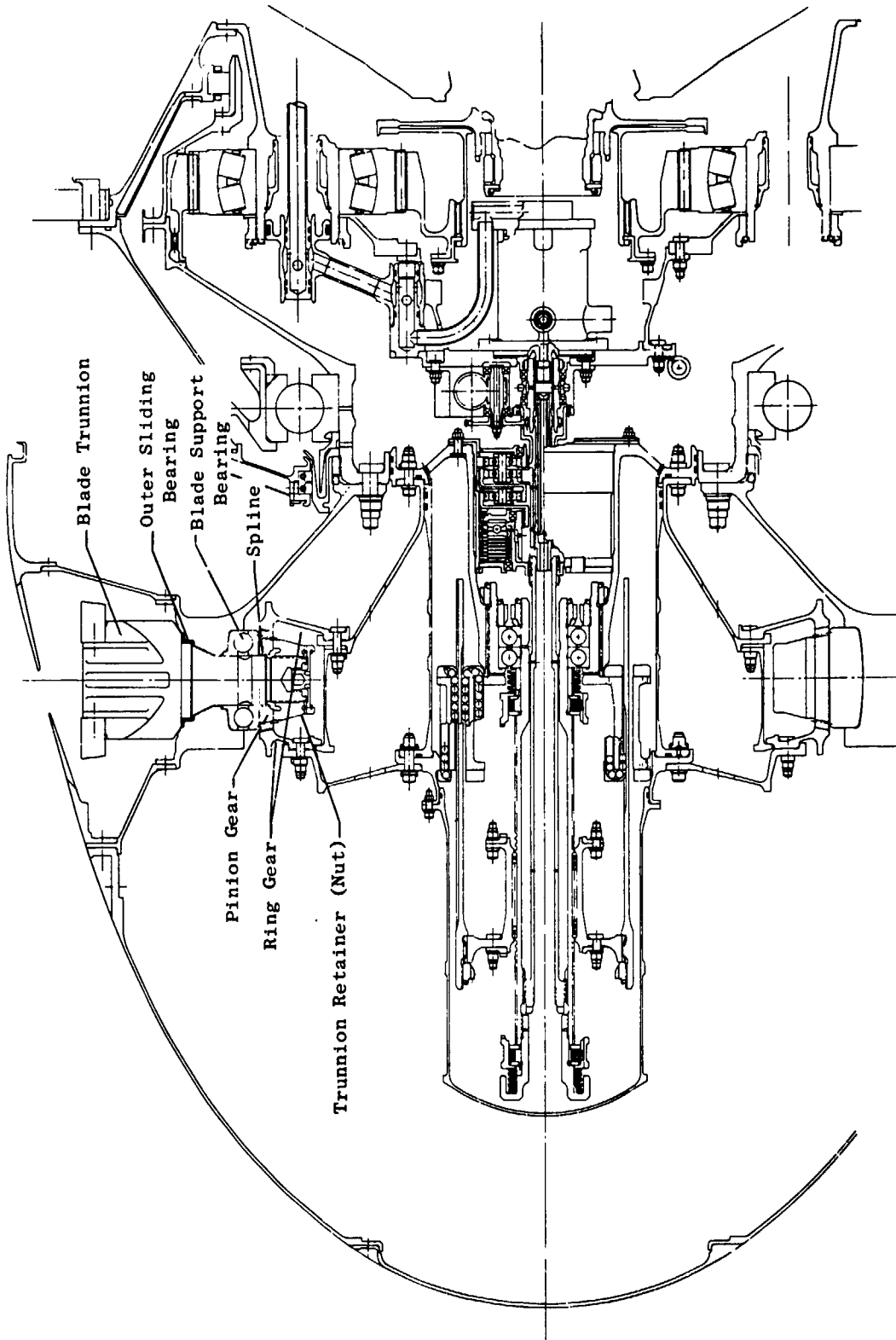


Figure 70. GE Ball Spline Actuation System.

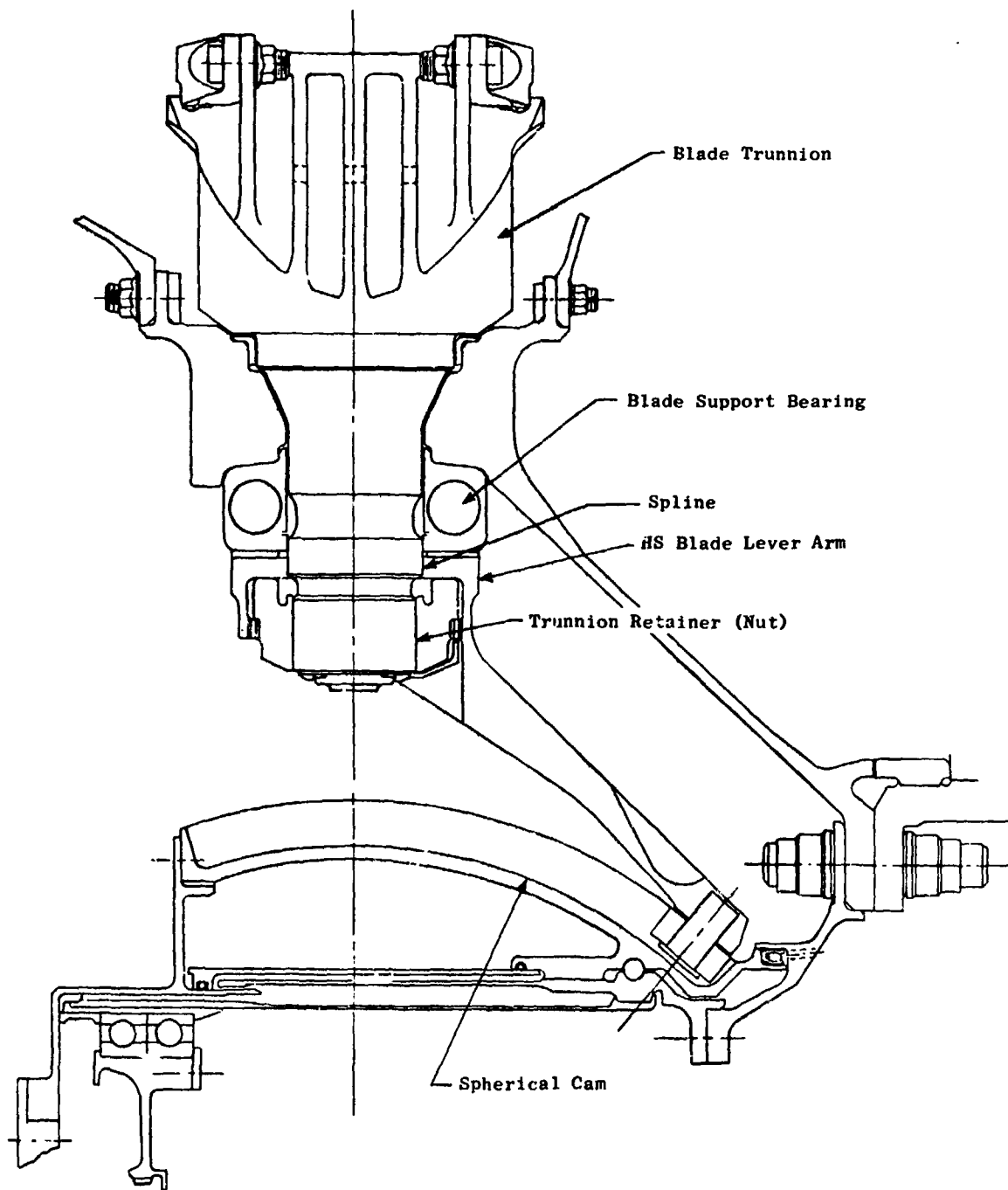


Figure 71. HS Variable Pitch Interface.

ORIGINAL PAGE IS
OF POOR QUALITY

Two sources, the sliding bearing and thrust bearing, produce friction torques which resist rotation of the trunnion during blade pitch change. The sliding bearing's friction torque results from the steel retainer's clamping load and is relieved at speed by the centrifugal load of the blade and trunnion. The thrust bearing friction torque results from the centrifugal load of the blade and trunnion. A tandem bearing component test has determined the thrust bearing friction torque to be 56.5-61 N-M (500-540 lb-in.) at the calculated centrifugal load of the trunnion and blade at 3326 rpm.

3.6 FAN SPINNER

The UTW fan has both a rotating forward spinner and flowpath adapters as shown in Figures 36 and 63. These parts attach to flanges on the fan disk. Both fore and aft rotating flowpath adapters are scalloped where they meet to provide round holes for the blade platforms. Together they provide the inner flowpath for the fan. The spinner and flowpath adapters are fabricated from 6061 aluminum. This material has good section stiffness-to-weight and has the good welded properties needed for fabricating development hardware.

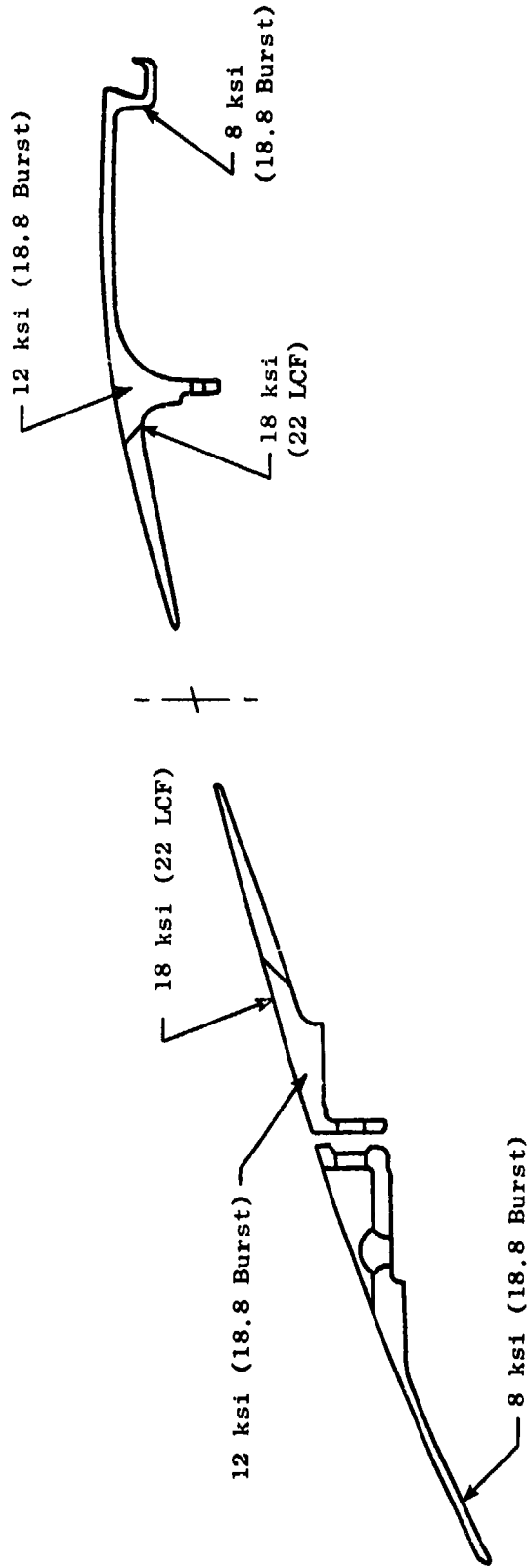
The forward spinner also has a spinner cap for inspection and access to the interior of the fan assembly and the slipping hardware. After removal of the fan spinner, all of the rotating hardware and sump regions forward of the fan frame are easily accessible. Blades may be individually replaced, and the blade actuator or the actuator and disk assembly may be removed as a package. This permits removal of the fan disk assembly, blade actuator, and main reduction gear as a complete module.

Radial fan balance screw bosses are provided in the spinner. This will permit field balance of the engine without removal of the spinner. The concept has been developed and used successfully on General Electric's CF6-50 engine.

The aft flowpath adapter continues the inner flowpath back to the fan core OGV's. A flow discourager seal inhibits air recirculation at this point. There are access holes in the flange of the aft spinner which, with the forward spinner removed, permit access to the fan frame flange which retains the main reduction gear. Critical spinner and adapter stresses are shown in Figure 72. As shown, all stresses fall well within the allowable limits.

3.7 FAN ATTACHMENT HARDWARE

All bolted joints in the fan rotor use Inco 718 bolts and dry-film-lubricant coated A286 nuts. The main rotor joint to the fan stub shaft is held with 18 MP159 1.27 cm (1/2 in.) - 20 bolts. MP159 was chosen for its high strength. Bolt preload has been set to assure that total torque in the joint can be carried in friction. A summary of the disk cone flange bolt design characteristics is presented in Table 15.



Material 6061 T6 Aluminum
Limiting Criteria-Deflection Matching with Blade
 σ Effective
(σ Allowable)

Figure 72. Fan Flowpath Adapters.

Table 15. Disk Cone Flange Bolts.

- Number 18 bolts
- Size - 1.27 cm (1/2 in.) - 20
- Material - MP159
- Torque 217-271 mN (160 - 200 ft-lb)
- Min. Preload - 82,288 N (18,500 lb) per bolt
- Total Preload - 1,481 kN (33,000 lb)
- Percent Torque Carried by Friction -125% At = 0.15
- Bladeout (5 blades) Stress $64,124 \text{ N/cm}^2$ (93,000 psi)
- Min. Preload Stress in bolts - $76,672 \text{ N/cm}^2$ (111,200 psi)